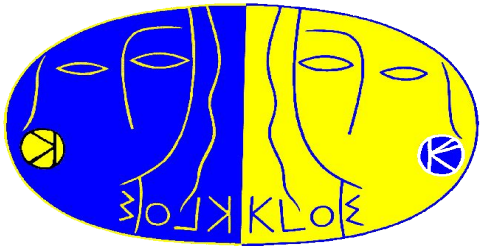

“Determination of the hadronic vacuum polarization contribution to the muon anomalous magnetic moment with KLOE Experiment”

Supervisors: Graziano Venanzoni, Thomas Teubner

With help from: Paolo Beltrame

First Year Presentation

Alka Kumari

DAPHNE(Double Annular phi-factory for Nice Experiments)

- DAPHNE collider located in the National Laboratory of Frascati (INFN) in Italy.
- e+e− collisions at the energy of 1.02 GeV (energy of the phi meson).

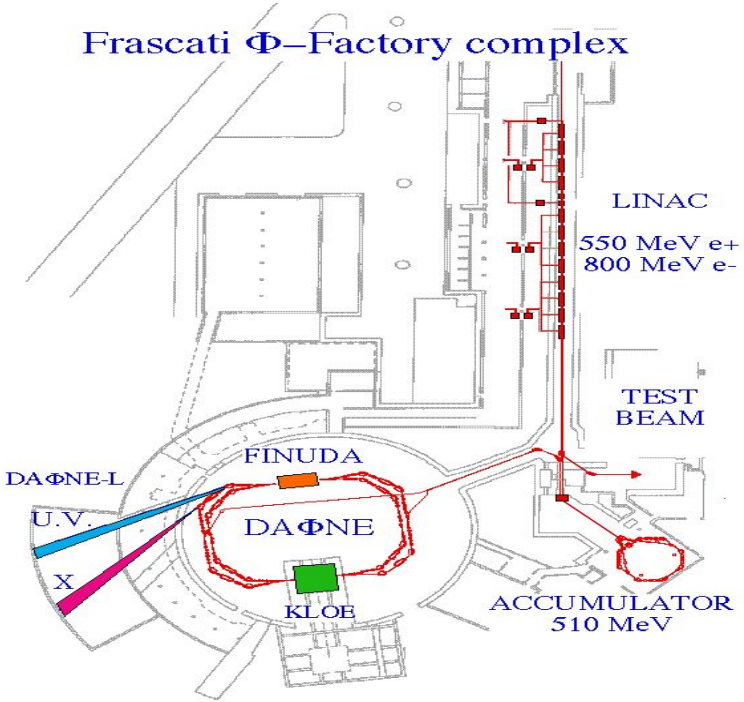

Schematic view of the KLOE at DAPHNE

The KLOE detector

- The KLOE detector mainly consist of DC(Drift Chamber) and EMC(Electromagnetic Calorimeter).
- Where DC tracks charged particles and measures their momenta.
- And EMC measures the energy and position of the photons and electrons, and detects interactions from other charged particles too.

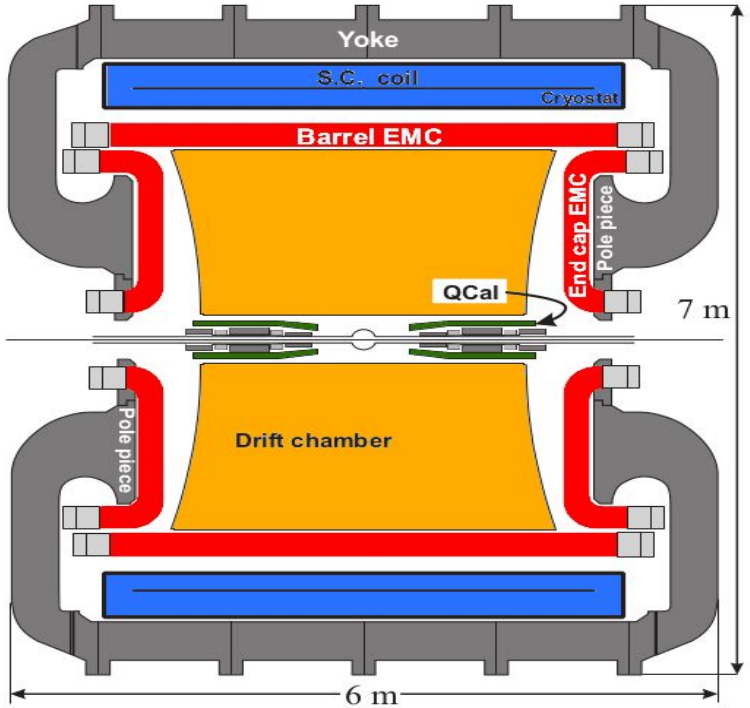

The KLOE Detector (Vertical Cross-Section)

The muon Anomaly

The Muon anomalous magnetic moment:

$$a_\mu = \frac{g_\mu - 2}{2}$$

where, gμ is the gyromagnetic ratio of the muon. The value is expected to be 2 but quantum corrections causes deviation, leading to aμ.

The muon anomaly(aμ) can be expressed as the sum of contributions from the strong force, weak force, and quantum electrodynamics (QED):

$$a_\mu^{\mathrm{SM}} = a_\mu^{\mathrm{QED}} + a_\mu^{\mathrm{weak}} + a_\mu^{\mathrm{had}}$$

The hadronic contribution is the most uncertain part of the SM prediction.

Hadronic cross section measurement(σhad)

- At the DAΦNE collider, the KLOE detector measures collisions at the Φ resonance (approximately 1.02 GeV). The detector is designed to capture the final states of these collisions, particularly focusing on hadronic events like $e^+e^- \rightarrow \pi^+\pi^-$
- The accurate measurement of the hadronic cross section is fundamental for calculating the hadronic vacuum Polarization (HVP) contribution to the muon anomalous magnetic moment.
- The HVP contribution to aμ, is given by an integral over the hadronic cross-section:

$$a_\mu^{\mathrm{HVP}} \propto \int_{4m_\pi^2}^{\infty} \frac{R(s)}{s} K(s) ds$$

Where:

S is the square of the center-of-mass energy of the collision.

K(s) is a kernel function that decreases with increasing s.

R(s) is the ratio of the cross-section for hadron production to the cross-section for muon pair production.

Initial State Radiation(ISR)

- In some of the annihilation process, where one of the incoming particle emit photon before collision termed as Initial State Radiation(ISR). This radiation reduces the center-of-mass energy of the collision.
- This radiation is helpful in the KLOE experiment to measure low energy cross section.
- The photon can be detected by the conservation of the momentum of the system.

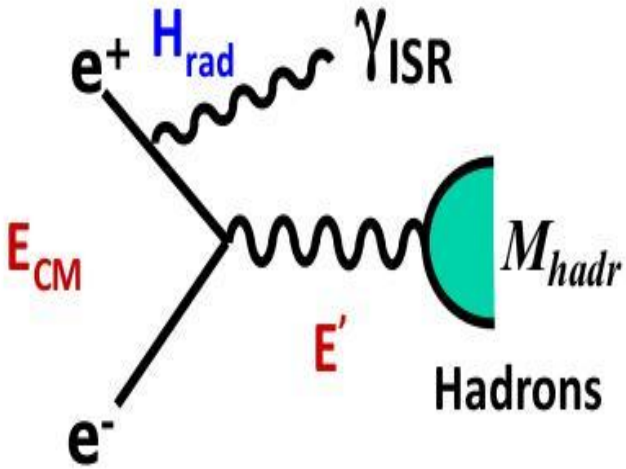

Luminosity (Current Work)

- For an accurate measurement of the cross section of an annihilation process, precise knowledge of the collider luminosity is required.
- Luminosity is defined as the number of particles per unit area per unit time.
- Luminosity measurement with KLOE detector using Large Angle Bhabha events can be represented as:

$$\int \mathcal{L}\,\mathrm{d}t = \frac{N_{\mathrm{obs}} - N_{\mathrm{bkg}}}{\sigma_{\mathrm{eff}}} \ .$$

Advantage of this method

- The high theoretical accuracy
- The clear event topology of the signal
- The cross section for LAB scattering is relatively large

Results

Momentum of the selected tracks

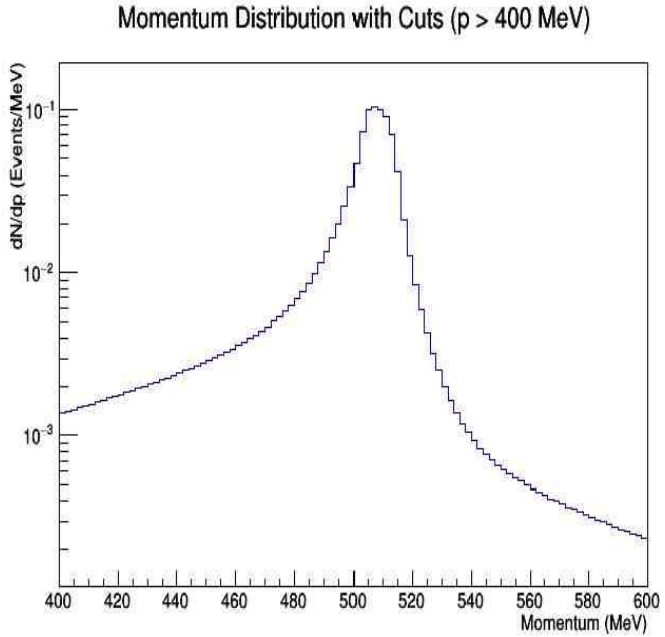

Polar angle of the selected tracks

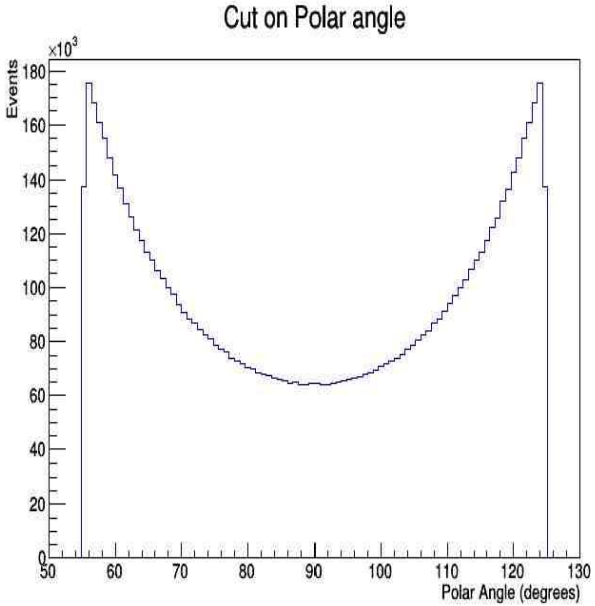

Acollinearity

Acollinearity is the angular separation between the final state particles produced in the collision process. if the particles are not aligned and scatter off each other at some angle then they are acollinear to each other.

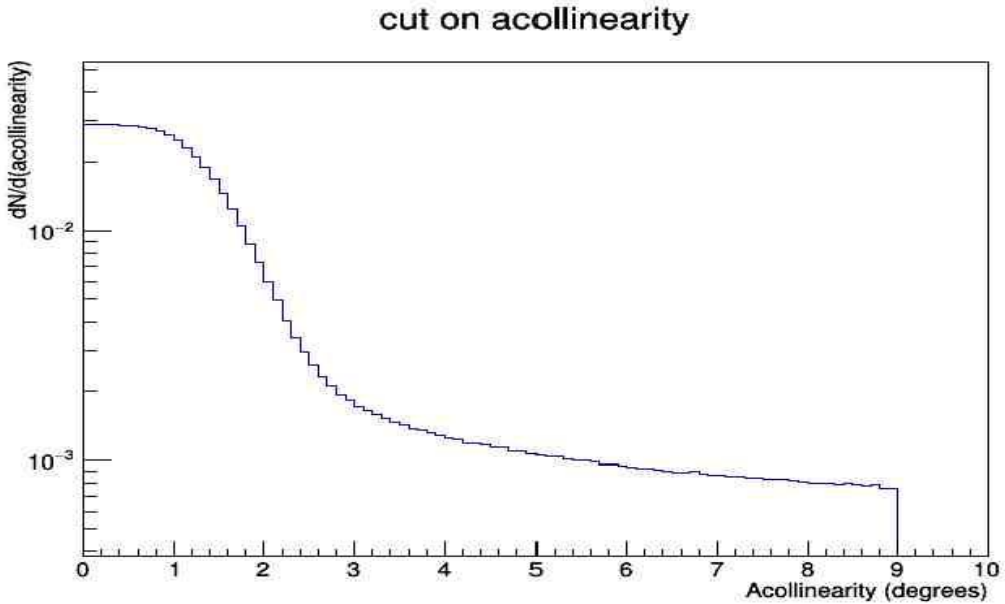

Conclusion:

- Measuring the Luminosity of the KLOE detector using Large angle Bhabha events, give us the events free from background noise by using the different acceptance cuts on angle, momentum and energy.
- This can help in the measurement of the hadronic cross section for the evaluation of the hadronic contribution to the anomalous magnetic moment of the muon.
- The experiment contributes to the measurement of the hadronic cross section at low energies through its use of ISR techniques.

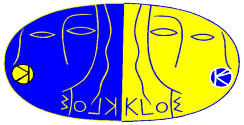

Thank you!

Quantum Computing For Neutrino Scattering

Towards Qudit Implementations of Effective Field Theories

Marina Maneyro
Year 1 Particle Physics PGR presentations
University of Liverpool
Supervisors: Costas Andreopoulos, Gabriel Perdue, Doga Kürkçüoglu

June 21st, 2024

Motivation

- High Energy Physics
  - Computationally intensive: data processing, lattice simulations, Monte Carlo event generation
- Quantum Computing:
  - could provide results out of reach for classical computers
  - well suited for representing strongly correlated systems
- Could quantum computing improve neutrino simulations?

Quantum Computing Fundamentals

- Leverages quantum superposition, entanglement
- Qubit: $|0\rangle$, $|1\rangle$ superposition
- Qubit states manipulated using quantum gates (unitary operations)
- Current hardware: $\sim$100 qubits, prone to noise, rapidly improving
- Quantum error correction: key to a new era of quantum computing
- Qudits: quantum harmonic oscillators, more states in one hardware element

Quantum Error Correction

- Algorithms and error mitigation strategies distinct from classical computing
- Classical approach: enabled by making copies of a bit
- No cloning theorem forbids this for quantum states
- QEC also uses additional qubits/resources (larger Hilbert space)
- Qubit state protected by entanglement with ancilla qubits, which get measured without modifying the state we wish to preserve

Quantum Error Correction

- Goal: reduce the error rate, allowing to perform increasingly complex reliable computation
- Introducing ancilla qubits initially increases likelihood of errors
- Break-even point: error-corrected qubit information preserved longer than a single, uncorrected qubit

Quantum Error Correction

- Due to the importance of QEC it has been at the center of the PhD activities so far (literature review and quantum circuit simulations)
- Surface code:
  - Lattice of qubits, some store data, others measure to detect errors

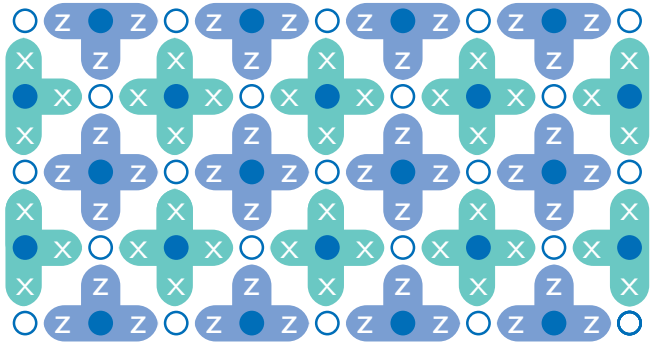

Quantum Error Correction

- Surface code:
  - Changes in measurement outcomes indicate errors
  - Entanglement and measurement cycles are applied at intervals to preserve the state over time
  - Implemented for seven qubits

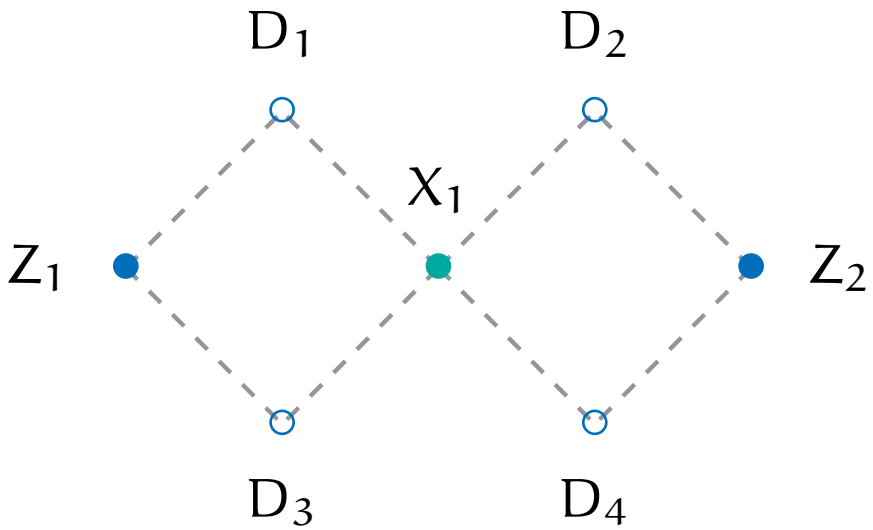

Quantum Error Correction

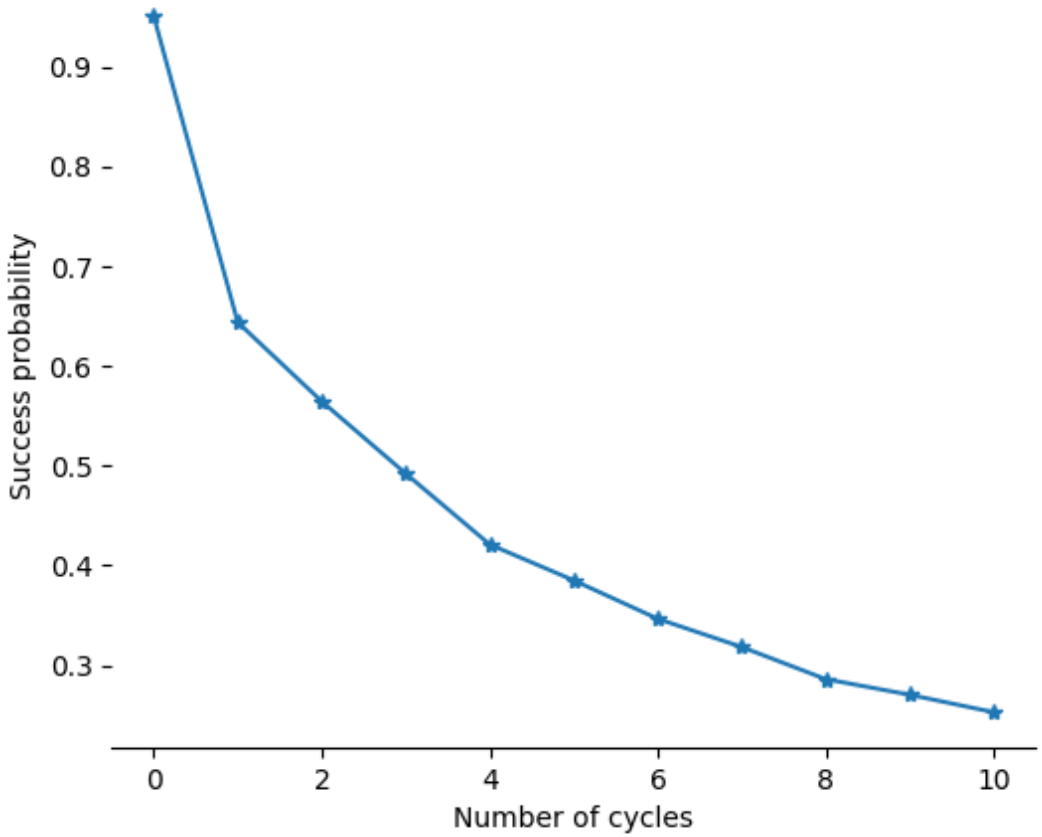

Figure: Success rate of the seven-qubit surface code over several cycles

Quantum Error Correction

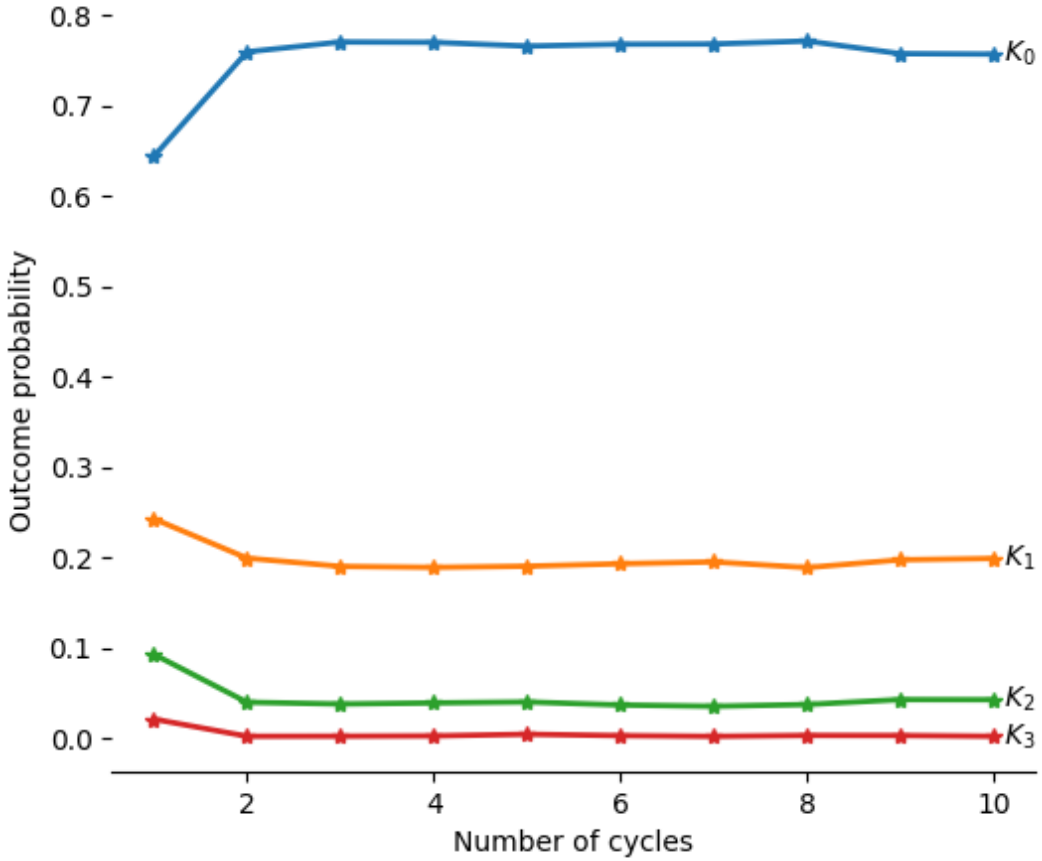

Figure: Probability of different syndromes for seven-qubit surface code over several cycles. Results enforce that no errors took place in previous cycle applications

Neutrino Event Generatiors

- Necessary for experimental design and data interpretation
- Upcoming experiments such as DUNE and Hyper-Kamiokande will increase precision needs
- Limited kinematic information, reliance on different models covering different energy ranges
- Measured interactions: neutrino-nucleus $\rightarrow$ need for nuclear models. Could this aspect benefit from Quantum Computing?
- One approach: nuclear Effective Field Theories

Future Goals

- Precedent of nuclear (and other) EFTs implemented in qubit-based computers $\rightarrow$ How could this be realized using qudits?
- What would be the best approach to error correction, ensuring reliable computation?
- What could be carried out using current and near-future hardware? What resources are needed for useful results?
- How do different implemented EFTs compare?

Correlated $D^0\overline{D}^0$ systems in $B^+ \to D^0\overline{D}^0 K^+$ amplitude analysis

Ho Sang Lee

University of Liverpool

21st June 2024

QCD and Hadron Spectroscopy

- The discovery of the J/ψ $c\bar{c}$ states implied an entire spectrum of excited states governed by QCD
- Hadron spectroscopy aims to study the strong interaction at low energies by searching for expected and exotic hadrons (e.g. tetraquarks, pentaquarks...) and measuring their properties

  $\Longrightarrow$ Experimental inputs to non-perturbative QCD

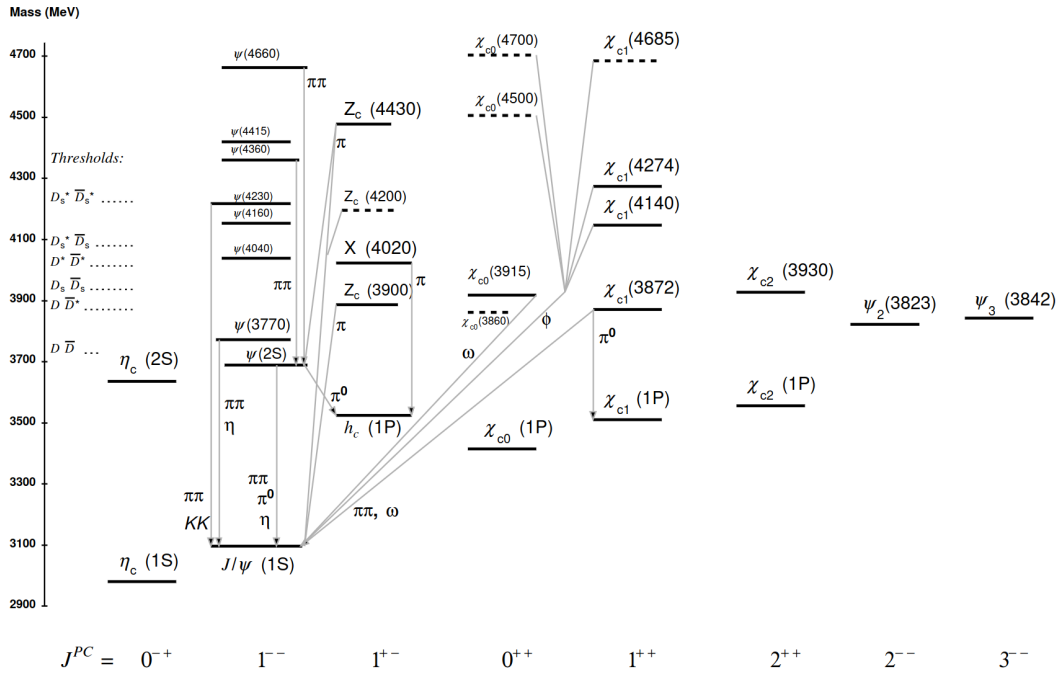

Figure 1: Map of known charmonia states. Figure from PDG 2023.

Dalitz plots and coherent $D^0\overline{D}^0$ systems

- Decay dynamics in $B^+ \to D^0\overline{D}^0 K^+$ decays described by the isobar model — Amplitude written as a coherent sum of interfering components:

$$\mathcal{A}(m^2_{D^0\overline{D}^0}, m^2_{D^0K^+}) = \sum_j c_j F_j(m^2_{D^0\overline{D}^0}, m^2_{D^0K^+}) \quad (1)$$

- Reconstructing $D^0/\overline{D}^0$ in CP final states enhance/suppress certain resonances — Want to quantify effects on amplitude fit
- See arXiv:2102.07729 or Paras's seminar for more on coherent $D^0\overline{D}^0$ systems

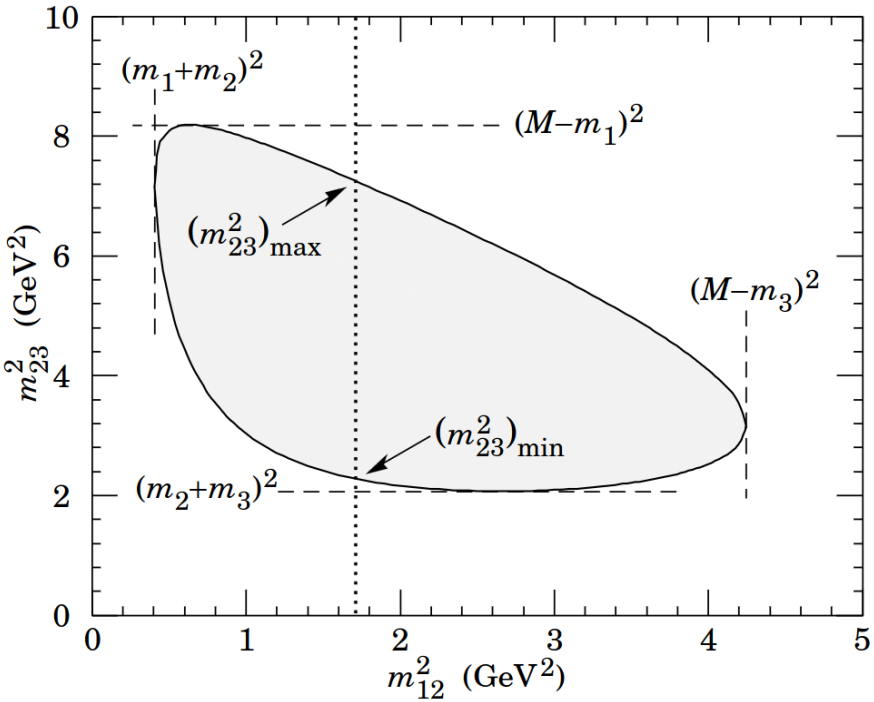

Figure 2: Dalitz plot showing the phase space of a $D^0 \to \pi^+\overline{K}^0 p$ decay. Figure from PDG 2022.

Toy Generation - Model Composition

- Results of previous $B^+ \to D^0\overline{D}^0 K^+$ (BaBar) and $B^+ \to D^+D^-K^+$ (LHCb) analyses used to construct a toy amplitude model
- $D^0\overline{D}^0$ resonant contributions: $\psi(3770)$, $\psi(4040)$, $\psi(4160)$. $\psi(4415)$, $\chi_{c0}(3915)$, $\chi_{c2}(3930)$ - $B^+ \to XK^+$, $X \to D^+D^-$ decay observed at LHCb, also known to decay to $D^0\overline{D}^0$ final state
- D^0K^+ resonant contributions: $D_{s1}^{*+}(2700)$, $D_{s2}^{*+}(2573)$ - observed in BaBar $B^+ \to D^0\overline{D}^0K^+$ analysis

Resonance	J^P	Mass (MeV/c^2)	Width (MeV/c^2)
$\psi(3770)$	1^-	3773.3 ± 0.4	27.2 ± 1.0
$\psi(4040)$	1^-	4039 ± 1	80 ± 10
$\psi(4160)$	1^-	4191 ± 5	70 ± 10
$\psi(4415)$	1^-	4421 ± 4	62 ± 20
$\chi_{c0}(2P)$	0^+	3921.7 ± 1.8	18.8 ± 3.5
$\chi_{c2}(2P)$	2^+	3922.5 ± 1.0	35.2 ± 2.2
$D_{s1}^{*+}(2700)$	1^-	2714 ± 5	122 ± 10
$D_{s2}^{*+}(2573)$	2^+	2569.1 ± 0.8	16.9 ± 0.7

Table 1: Table of resonances included in toy model. Masses and widths from PDG 2023.

Toy Generations - Quantum Correlations

- Effects of correlated $D^0\overline{D}^0$ systems accounted for by scaling the amplitudes of resonances:
  - Enhanced $D^0\overline{D}^0$ resonances - Unscaled
  - Suppressed $D^0\overline{D}^0$ resonances - Scaled by factor of 0 (Effectively removed)
  - Non-$D^0\overline{D}^0$ resonances - Scaled by factor of $1/\sqrt{2}$

$\Longrightarrow$ Simpler resonance model in *CP*-tagged sample

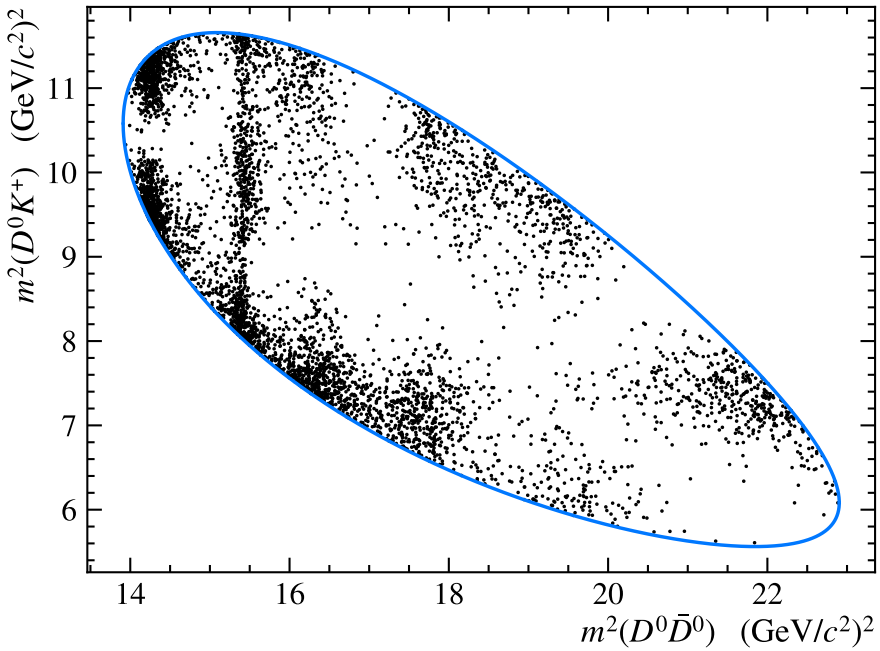

(a) Flavour-tagged

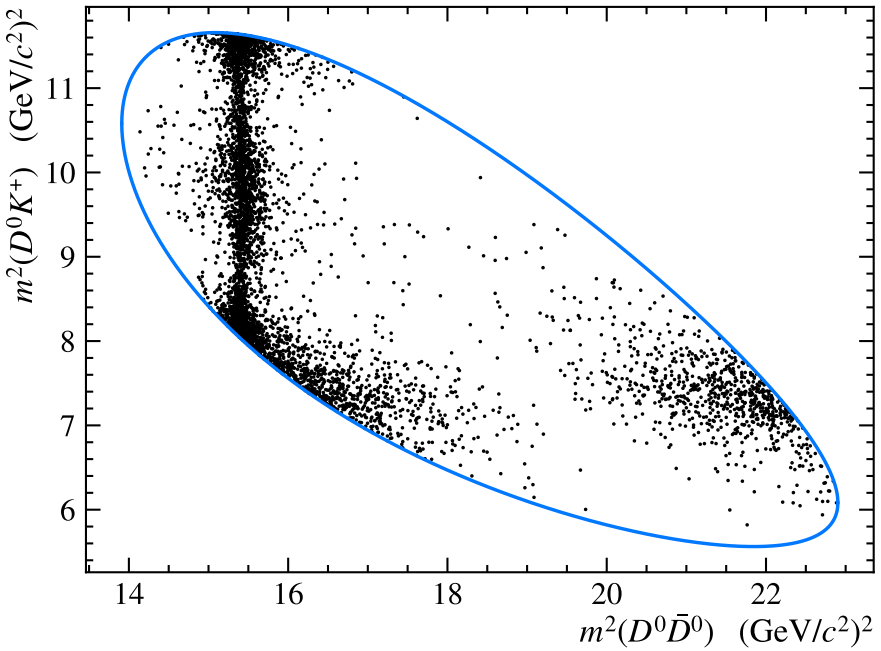

(b) *CP* double-tagged

Figure 3: Toy Dalitz plot with 5×10^3 events, generated with the flavour-tagged (left) and *CP* double-tagged (right) amplitude models.

Fit Model Composition - Methodology

- Interested in sensitivity to new resonances - Need data-driven way to determine model composition prior to fit
- Fit different configurations to data - Baseline with $\psi(3770)$ and $\chi_{c2}(2P)$ and alternative configuration with additional resonances

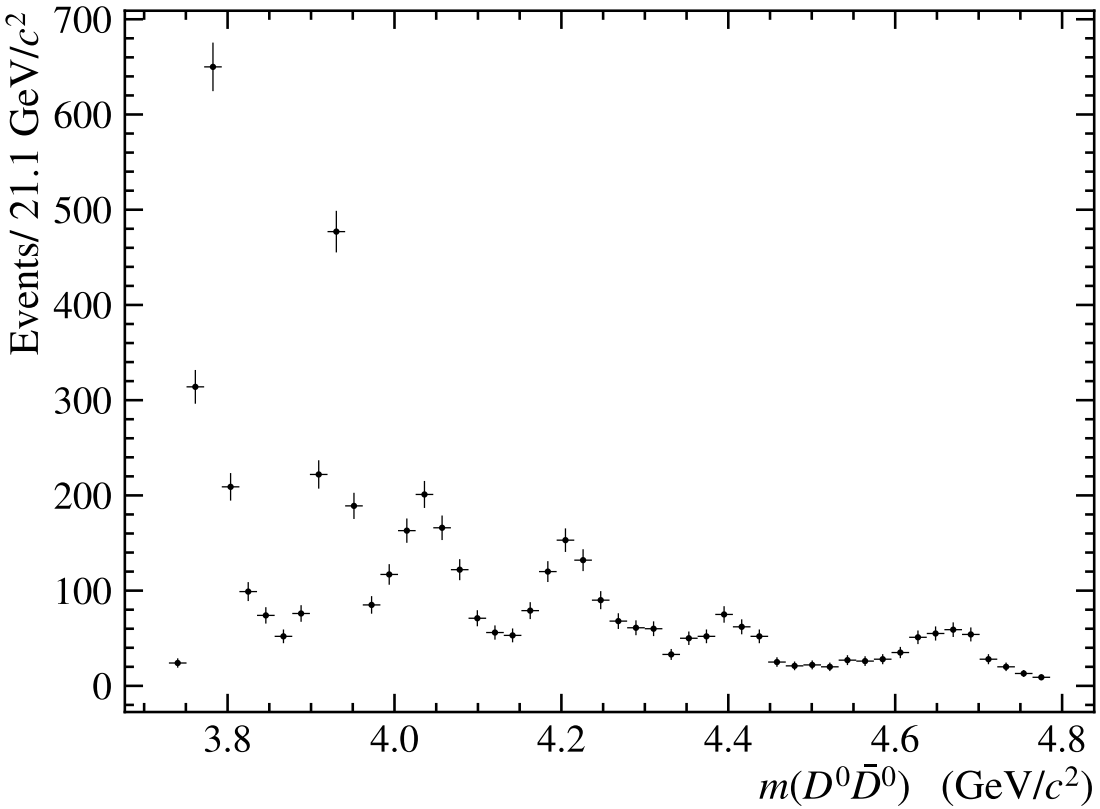

Figure 4: $m_{D^0\overline{D}^0}$ distribution of the flavour-tagged toy.

Fit Model Composition - NLL Distribution

- Generate ensemble of toys from fit results with baseline configuration
- Fit ensemble with baseline and alternative configurations, compute test statistic $t = -2\Delta\text{NLL}$
- Compute t_{data}, compare to distribution from toy ensemble
- Iterate; resonance with largest change in NLL added to baseline configuration if t_{data} over threshold, process repeated

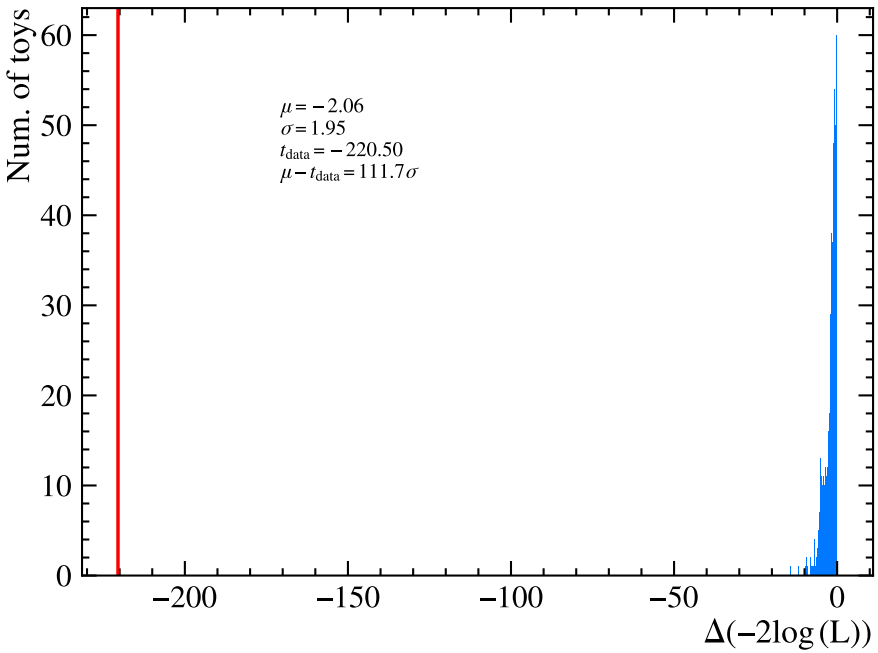

(a) Flavour-tagged sample

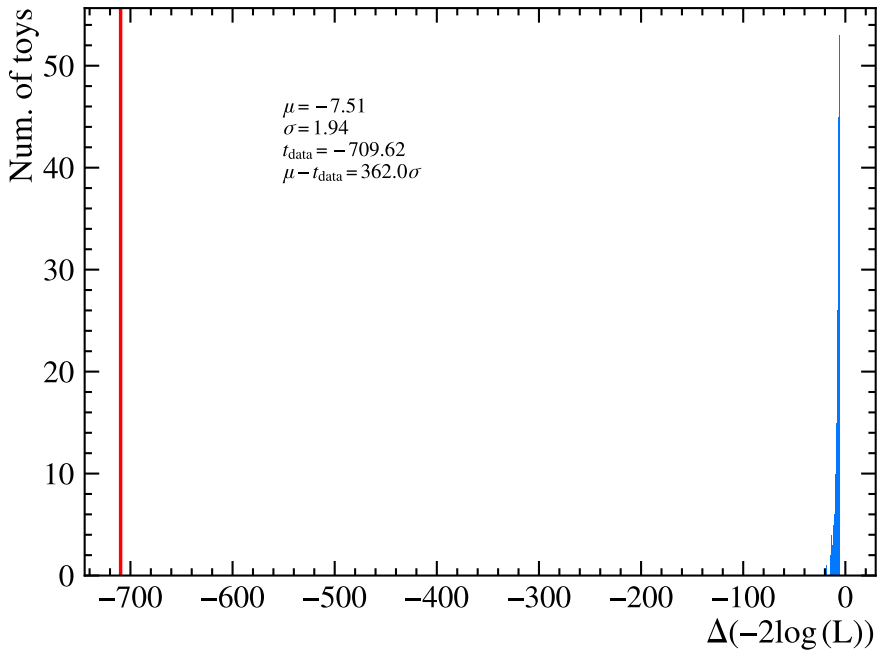

(b) *CP* double-tagged sample

Figure 5: Test statistic distribution for the inclusion of the χ_{c0} resonance from fits to 5×10^3 flavour-tagged toy ensemble along with t_{data}.

Fit Results

- *CP* double-tagged toy can be fit with a simplified amplitude model, reducing the statistical errors on fit and potential systematics from mismodelling the resonance structure

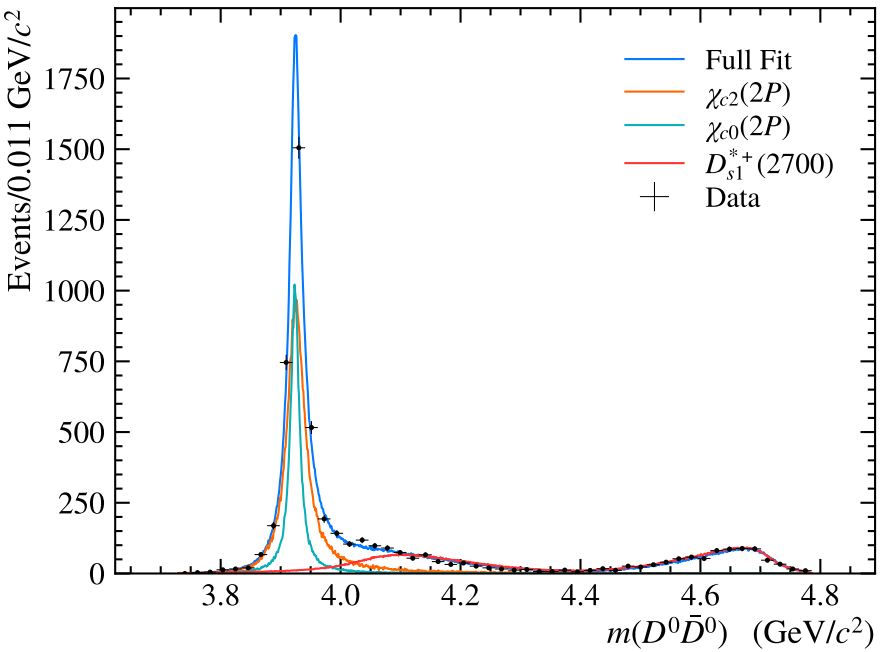

(a) *CP* double-tagged

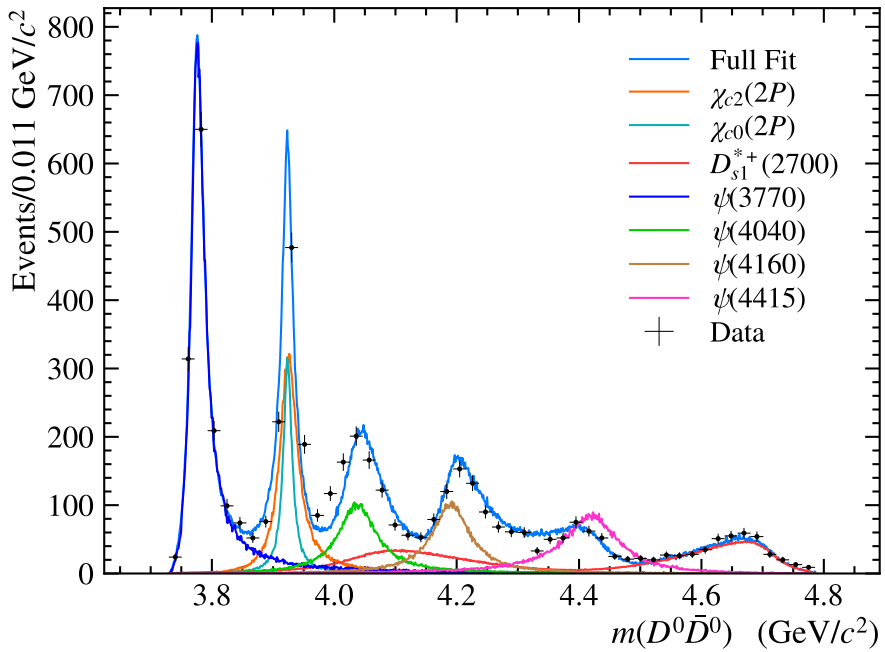

(b) Flavour-tagged

Figure 6: Projection of fit results onto $m_{D^0\overline{D}^0}$. PDFs represented by a high-statistics toy.

Summary and Future Work

- Demonstrated that *CP* double-tagging can provide greater sensitivity to the underlying resonant structure in $B^+ \to D^0\overline{D}^0 K^+$ decays on a per-event basis
  - In reality, $D^0 \to S_\pm$ branching fraction much lower than pseudo flavour-tag — Expect to have much smaller *CP*-tagged sample $\implies$ Need simultaneous fit
- Effect on fit highly model dependent; need to look further into the $B^+ \to D^0\overline{D}^0 K^+$ amplitude model:
  - Including non-resonant decays
  - Look at different plausible amplitude models (e.g. different composition of $D^0\overline{D}^0/DK$ resonances)
  - Consider potential backgrounds - K/π misidentification particularly dangerous
- Isobar formalism not the only approach to amplitude analysis; consider other approaches such as MIPWA/K-matrix....etc?
- Expect to have enough *CP* double-tagged $B^+ \to D^0\overline{D}^0 K^+$ events by the end of LHCb run 3; much of the work in the toy study is applicable to real data

Questions?

Backup Slides

Neutral D Decays

- D mesons evolve in time as CP (mass) eigenstates, corresponding to superpositions of flavour eigenstates, given by (neglecting CP violation):

$$|D_+\rangle = \frac{1}{\sqrt{2}}\left(|D^0\rangle + |\overline{D}^0\rangle\right)$$
$$|D_-\rangle = \frac{1}{\sqrt{2}}\left(|D^0\rangle - |\overline{D}^0\rangle\right)$$

- Can decay to either (pseudo) flavour-tag final states such as $K^-\pi^+/K^+\pi^-$ or CP-tag final states such as $K^+K^-/\pi^+\pi^-$ ($C=+1$) and $K^0_S\pi^0$ ($C=-1$).

Coherent $D^0\overline{D}^0$ systems

- Coherent $D^0\overline{D}^0$ systems refer to pairs of entangled D^0 and $\overline{D}^0$ mesons which exist in an overall C/P eigenstate depending on the relative orbital angular momentum:

$$C = P = (-1)^{L_{D^0\overline{D}^0}} \tag{2}$$

- Hence, the permitted quantum states of coherent $D^0\overline{D}^0$ systems can be written as:

$$|D\overline{D}\rangle_{C=+1} = \frac{1}{\sqrt{2}}\left(|D^0\overline{D}^0\rangle + |\overline{D}^0 D^0\rangle\right) = \frac{1}{\sqrt{2}}\left(|D_+ D_+\rangle - |D_- D_-\rangle\right)$$
$$|D\overline{D}\rangle_{C=-1} = \frac{1}{\sqrt{2}}\left(|D^0\overline{D}^0\rangle - |\overline{D}^0 D^0\rangle\right) = \frac{1}{\sqrt{2}}\left(|D_- D_+\rangle - |D_+ D_-\rangle\right)$$

- Key consequence of quantum correlations - **tagging (measuring) one D meson in a state projects the other D meson into a particular state**

Fit Parameters - Flavour-tagged

Resonance	Magnitude.	Phase (rad)	Fit Frac.
$\psi(3770)$	1.562 ± 0.053	-0.955 ± 0.073	0.302
$\psi(4040)$	0.833 ± 0.042	0.601 ± 0.078	0.085
$\psi(4160)$	0.894 ± 0.045	-0.078 ± 0.096	0.099
$\psi(4415)$	1.089 ± 0.042	-2.469 ± 0.096	0.147
$\chi_{c0}(2P)$	0.709 ± 0.049	1.331 ± 0.044	0.073
$\chi_{c2}(2P)$	1.0	0	0.121
$D_{s1}^{*+}(2700)$	1.191 ± 0.042	0.463 ± 0.079	0.176

Table 2: Fit fractions, phases and magnitudes with statistical uncertainties from `MINUIT` obtained from the nominal fit to the flavour-tagged sample.

Fit Parameters - *CP* double-tagged

Resonance	Magnitude	Magnitude (Scaled)	Phase (rad)	Fit Frac.
$\chi_{c0}(2P)$	0.724 ± 0.027	0.724 ± 0.027	1.389 ± 0.024	0.229
$\chi_{c2}(2P)$	1.0	1.0	0	0.437
$D_{s1}^{*+}(2700)$	0.823 ± 0.019	1.164 ± 0.027	0.596 ± 0.060	0.285

Table 3: Fit fractions, phases and magnitudes with statistical uncertainties from `MINUIT` obtained from the nominal fit to the *CP* double-tagged samples.

Fit Model Composition - $D_{s2}^{*+}(2573)$

- $D_{s2}^{*+}(2573)$ excluded due to small fit frac; $< \mathcal{O}(1)$ events expected in both toy datasets

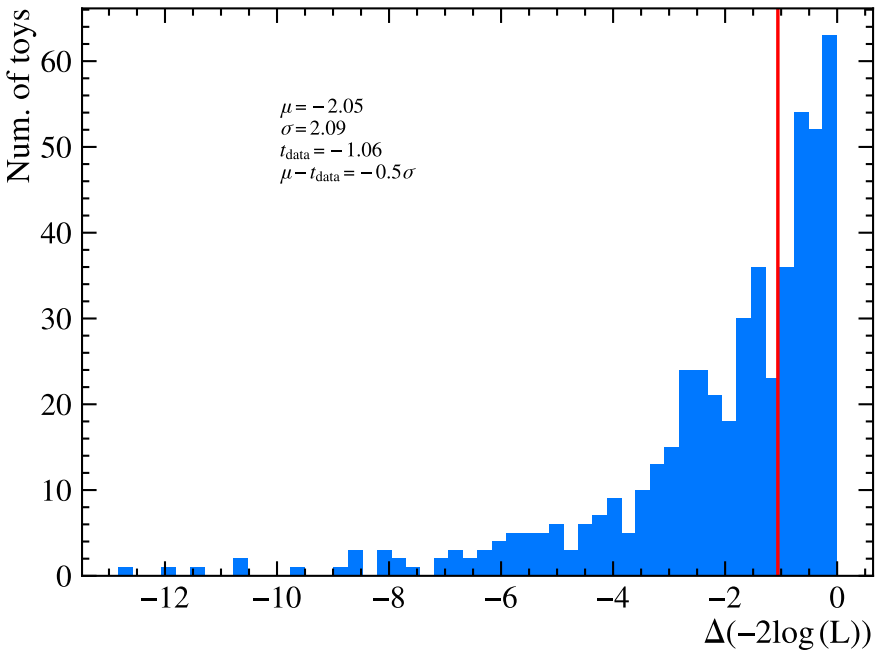

(a) Flavour-tagged

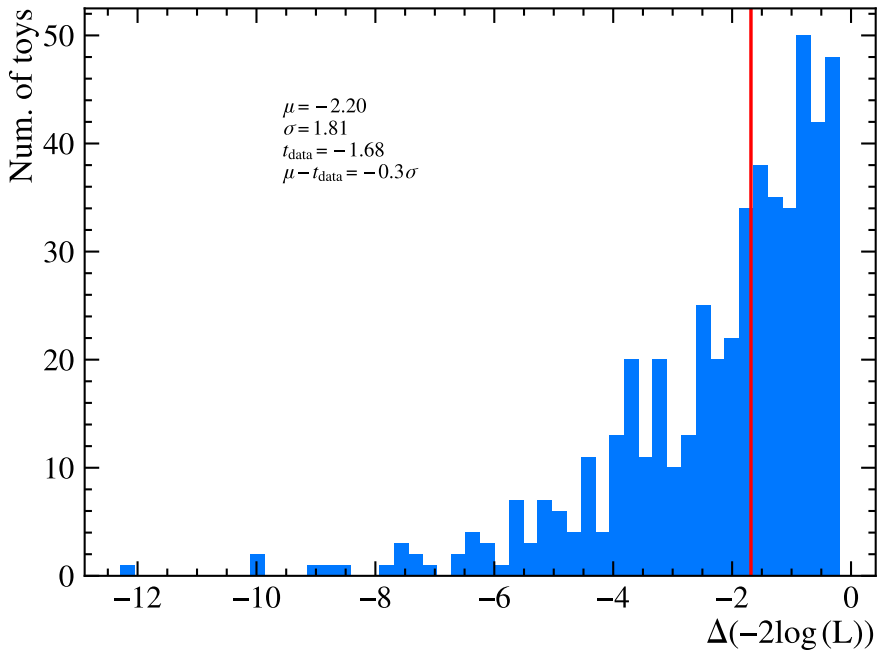

(b) *CP* double-tagged

Figure 7: Test statistic distribution for resolution of χ_{cJ} peak into two separate resonances along with t_{data}.

UNIVERSITY OF LIVERPOOL

Tau Reconstruction and Leptoquarks at the ATLAS Detector

Mehul Gunvant Depala

Supervisors: Prof Andrew Mehta (P), Prof Monica D'Onofrio (S) and Dr Nikolaos Rompotis

The τ –lepton Introduction

Basic Properties:

- Mass – 1777 MeV
- Lifetime – 2.9 x 10^-13 s
- 65 % decay hadronically
- Prongs are defined by the number of charged hadrons in decay.

Important physics analyses involving the τ lepton:

- DiHiggs
- MSSM Heavy Higgs
- H → ττ

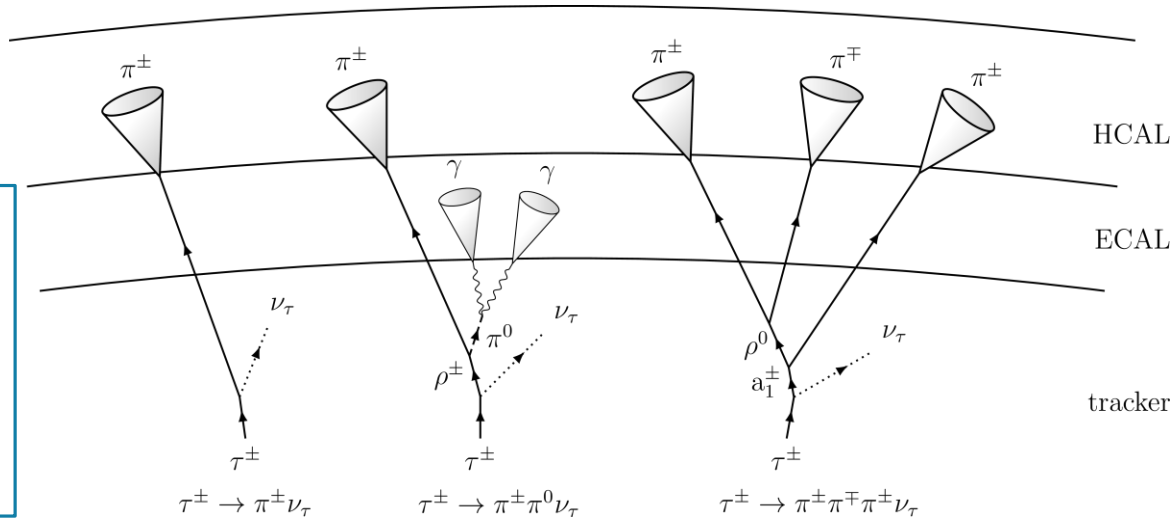

Decay modes of τ - lepton	Number of Prong	Number of neutral hadrons
1p0n	1	n = 0
1p1n	1	n = 1
1pxn	1	n ≥ 2
3p0n	3	n = 0
3pxn	3	n ≥ 1

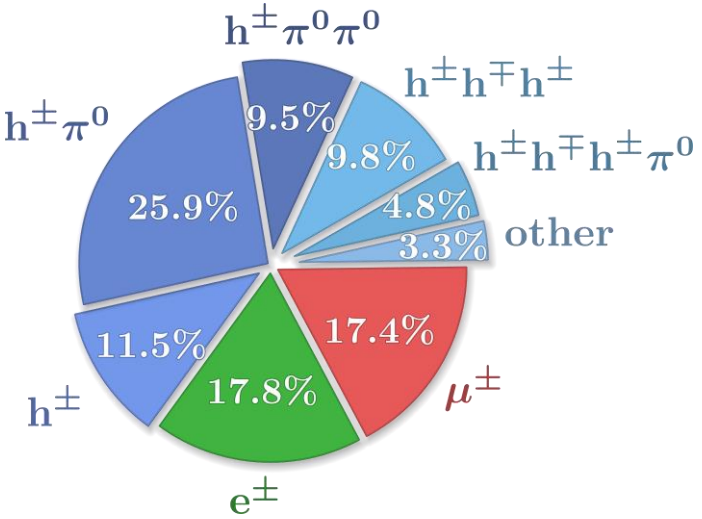

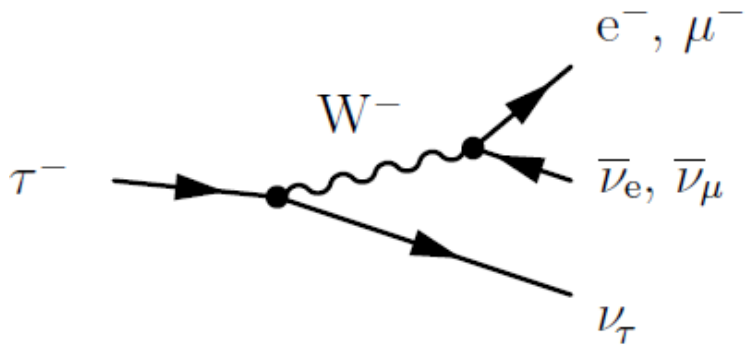

Current Reconstruction, ID and Classification

1. Jet seeding and Vertex Association:
   - Finding the seed of the τ jet and associating a vertex

2. Track Classification:
   - Classifies the tracks associated with the jet using RNN
   - Four categories: Tau tracks, conversion tracks, isolation tracks and fake tracks

3. Tau ID:
   - Discriminates against tau candidates and QCD dijet background using RNN.

4. Decay Mode Classification:
   - Classifies the Tau candidates into 5 categories based on the number of prongs and neutral hadrons
   - DeepSet Neural Network

5.Energy Calibration:
   - Calibration of the final energy of tau candidate
   - Boosted regression tree

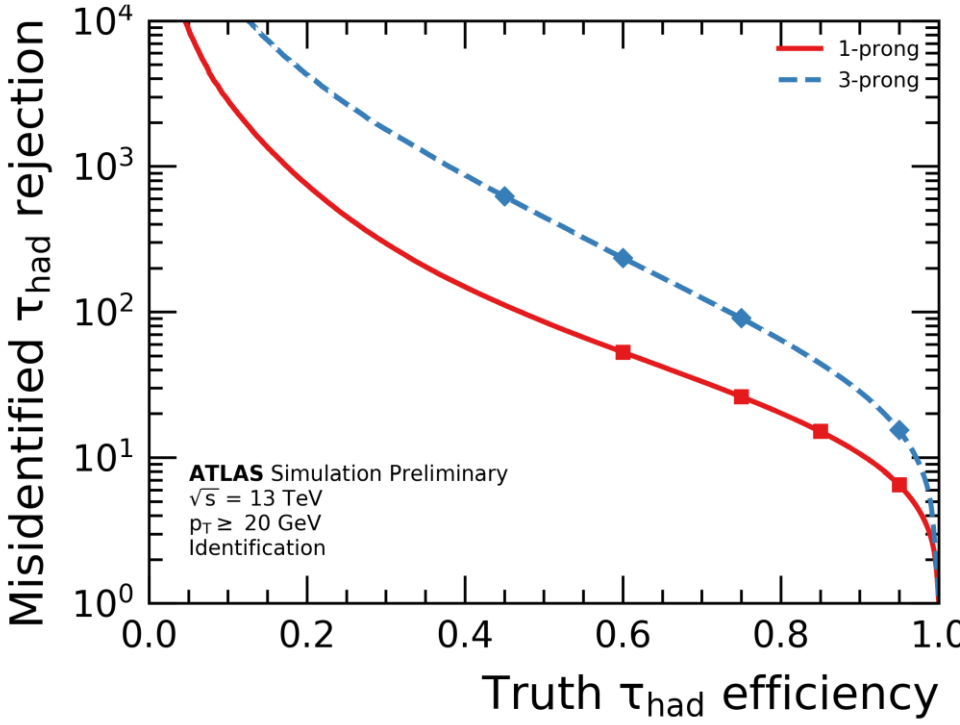

ROC Curve demonstrating performance of Tau ID RNN

ATL-PUB-2022-044

Unified Approach with GNN and Liverpool Group Work

Unified approach being implemented at ATLAS for Tau ID. Two approaches:

- GNTau (Tel Aviv University): Tau ID + Track Classification
- TauJetGraphs (Liverpool group): Tau ID + Decay mode classification

Liverpool group consists of: Prof Monica D'Onfofrio, Dr Nikolaos Rompotis, Dr Joe Carmignani, Robert McNulty, Jordy Degens and Mehul Depala

- Graph Neural Network algorithm being implemented
- Graphs are nodes connected by edges.

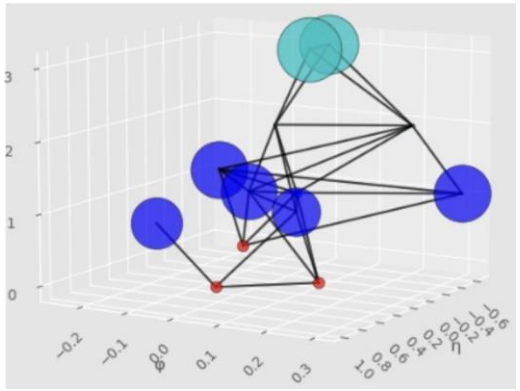

Layers of graph contain:

- Track variables
- PFO Objects
- Conversion tracks
- Clusters

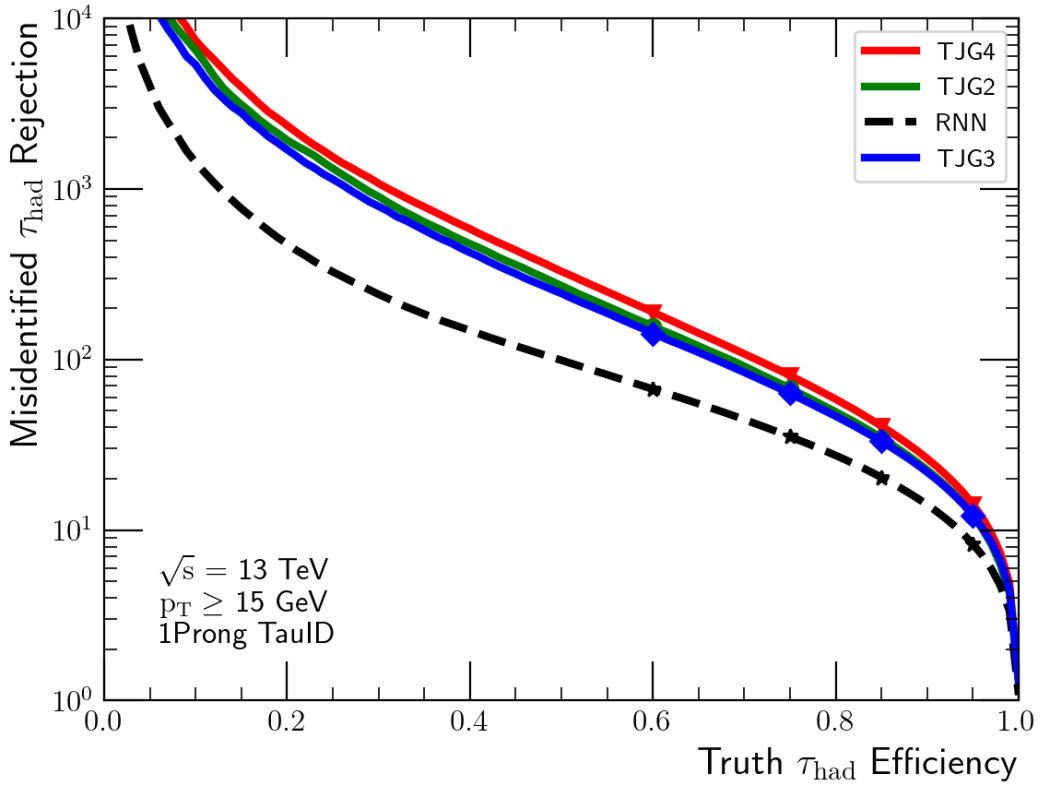

Courtesy: Dr Joe Carmignani

My Involvement and Isolation Track Investigation

Main task for ATLAS Authorship:

- Goal is to compare two approaches by performing tests and comparing differences.
- Validate of data once algorithm implemented.

Initial work:

- Studying input variables
- Isolation track investigation.
- Experimenting with code and understanding application to physics analyses.

- Studying the variables and their properties used by the training is important to check the relative discriminating power.
- Isolation tracks belong to quark and gluon initiated jets.
- Typically expect true τ's to have fewer isolation tracks vs QCD events.
- Looked at the transverse momentum; plot shows QCD Dijets carry a larger percentage of the jet transverse momentum relative to true true τ's.

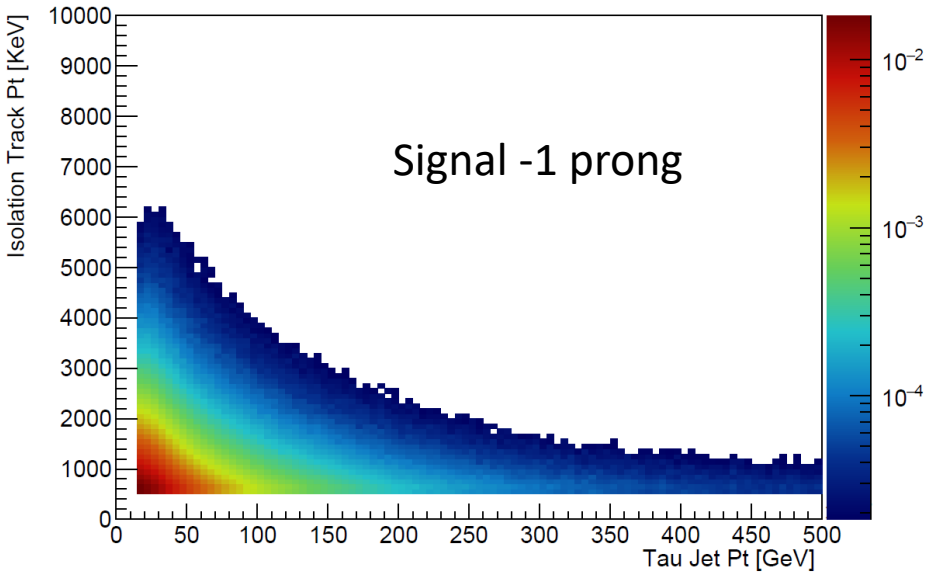

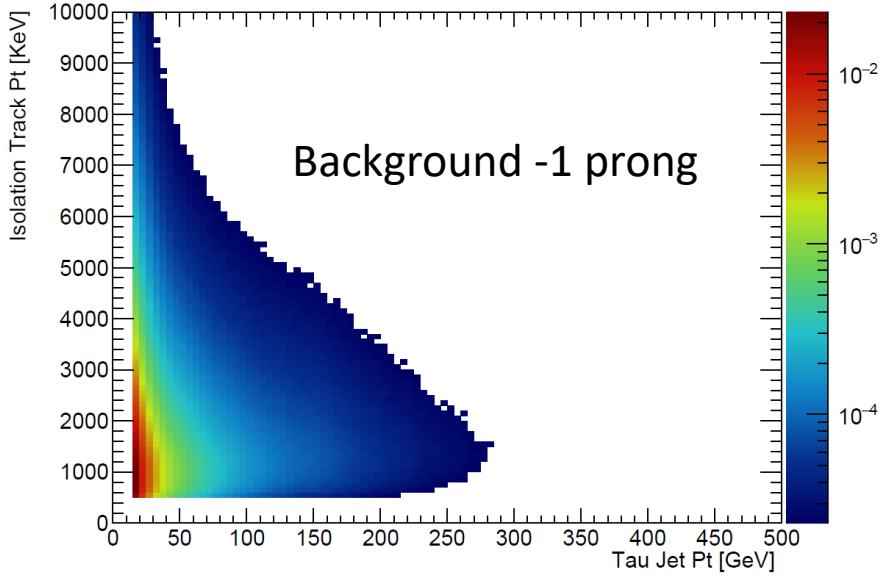

Isolation tracks analysis

Method of investigation:

- Check distribution before and after Tau ID RNN score cut.
- Residual differences indicate potential discriminating power for GNN.

- Impact parameters show interesting differences for isolation tracks.
- Signal have wider distribution due to presence of Tau tracks.
- Discrimination is disappears after RNN cut. No residual discriminating power

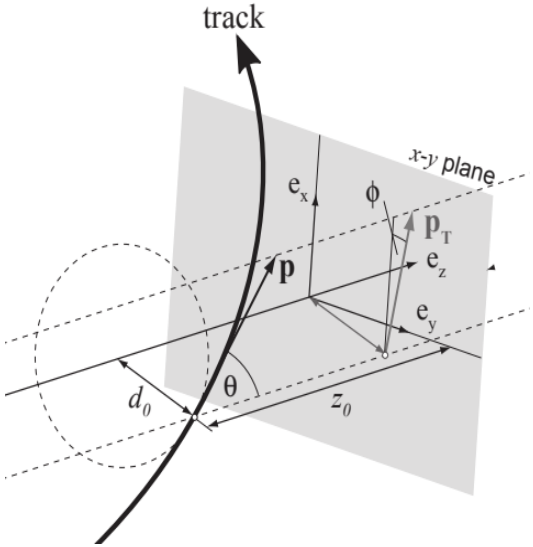

d0: Transverse impact parameter relative to Tau vertex.

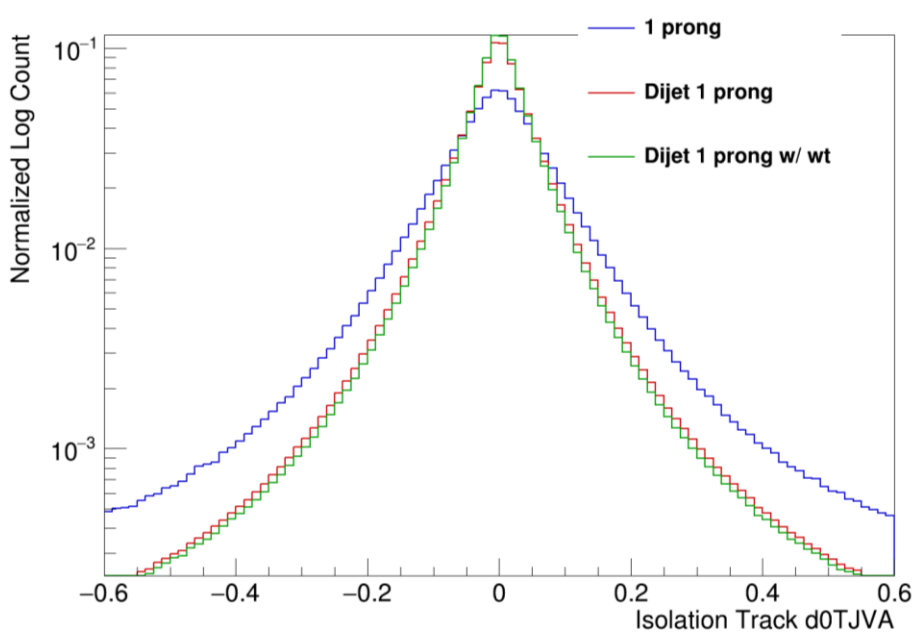

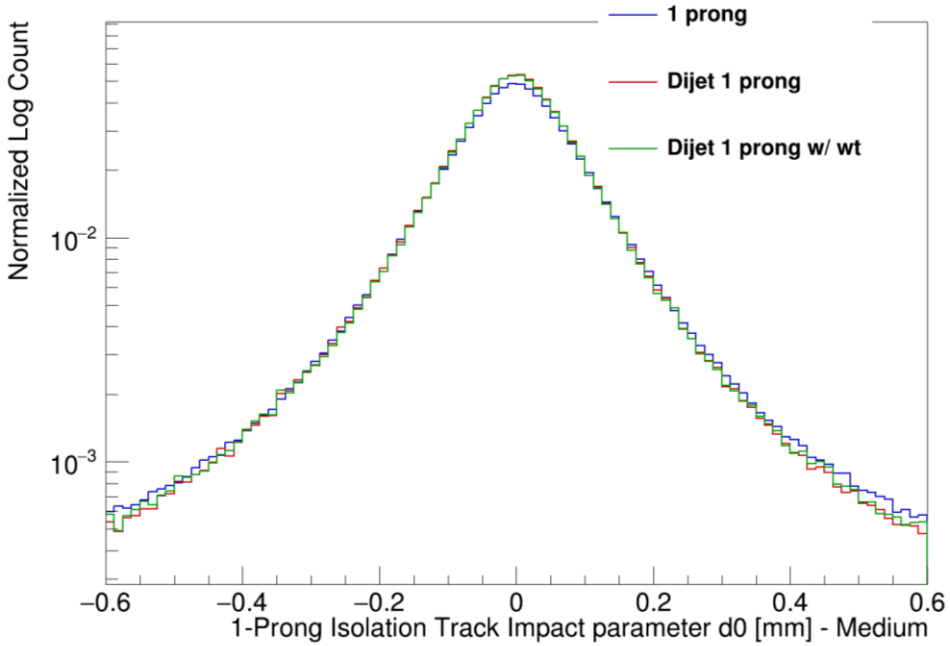

Number of isolation tracks

- Distribution of number of isolation tracks with cuts on the Tau ID RNN Score.
- Distributions of signal and background become closer - showing RNN is using number of isolation tracks.
- Residual differences indicating isolation tracks still hold discriminating power for GNN to utilize.

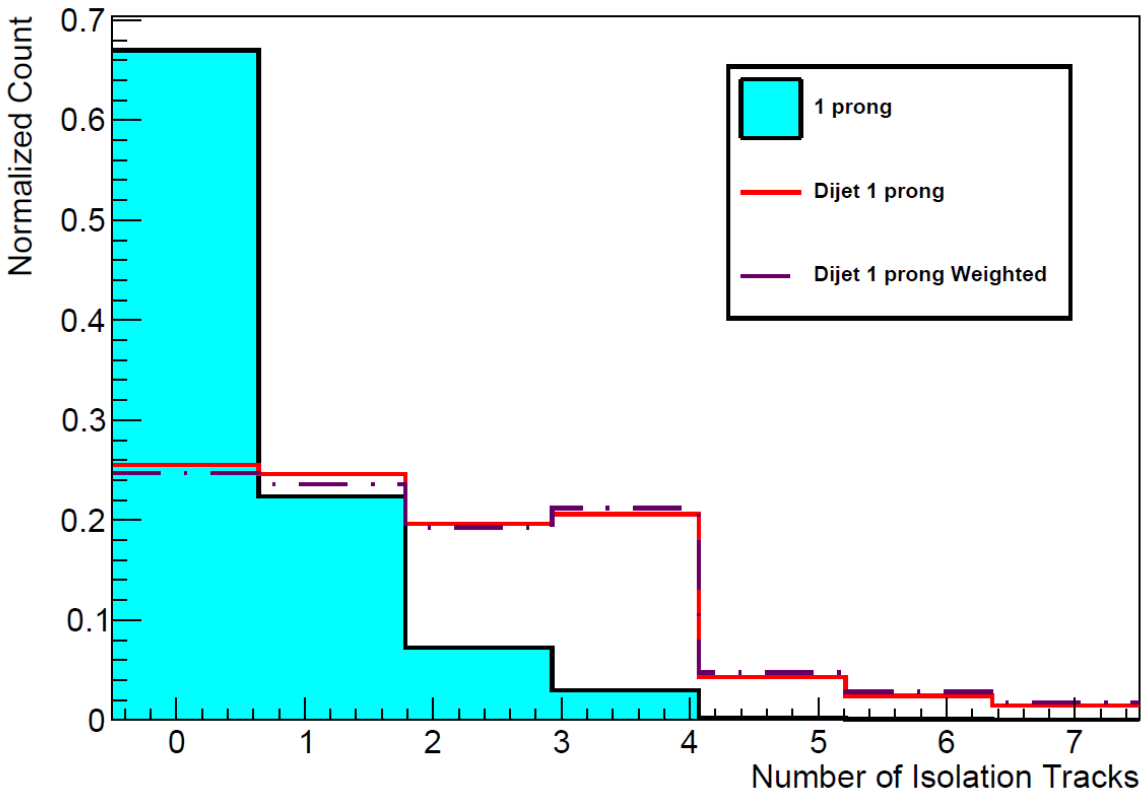

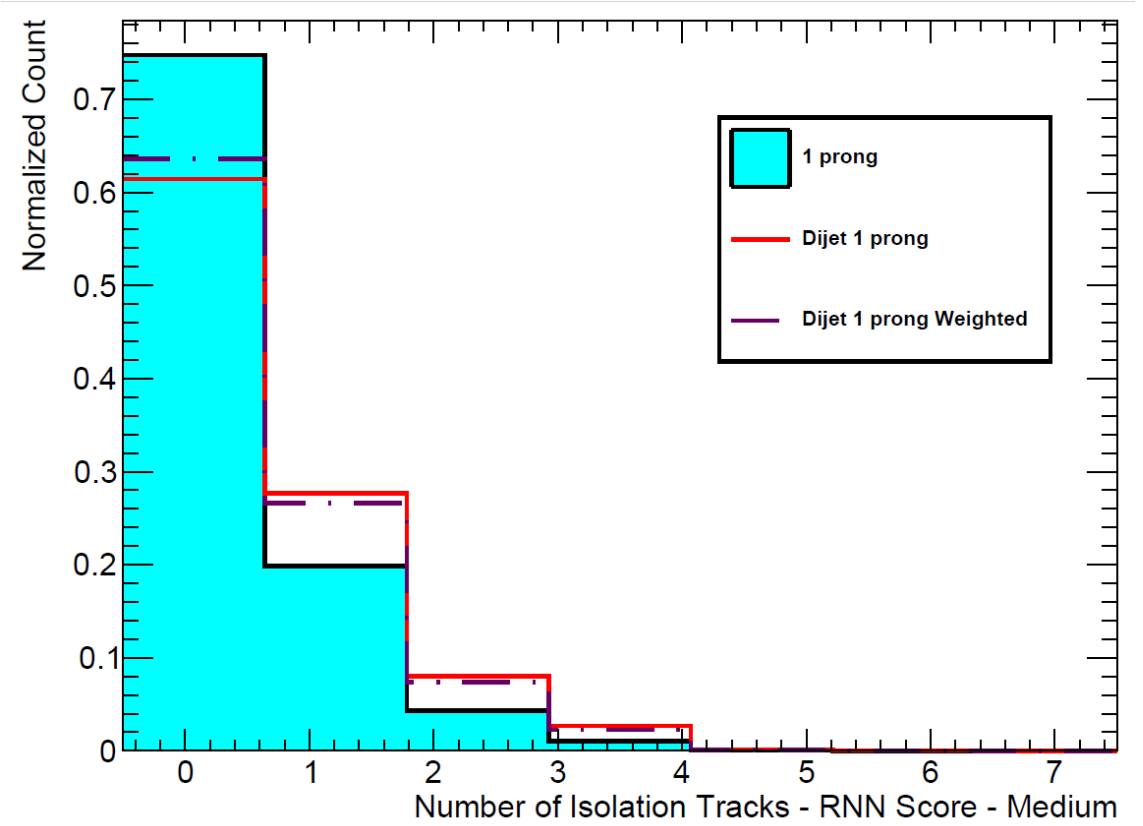

Leptoquarks Introduction

Particle properties and motivation:

- Hypothetical particles carrying quantum numbers for baryons and leptons.
- Provide a link for similarities in lepton and quark family structure.

Experimental motivation:

- Explanation for potential non-lepton flavour universality observed at LHCb.
- g-2 discrepancy
- Neutrino masses

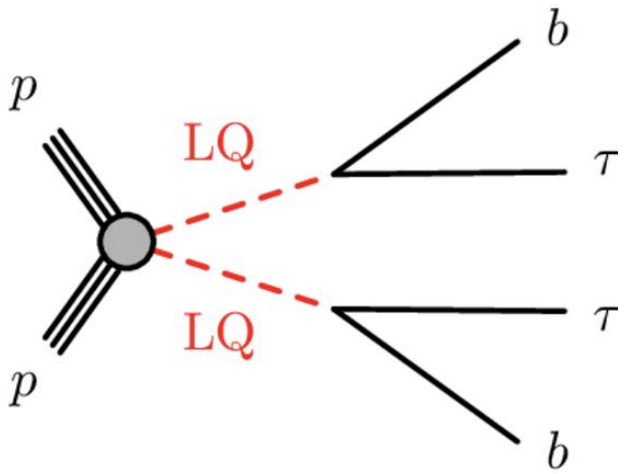

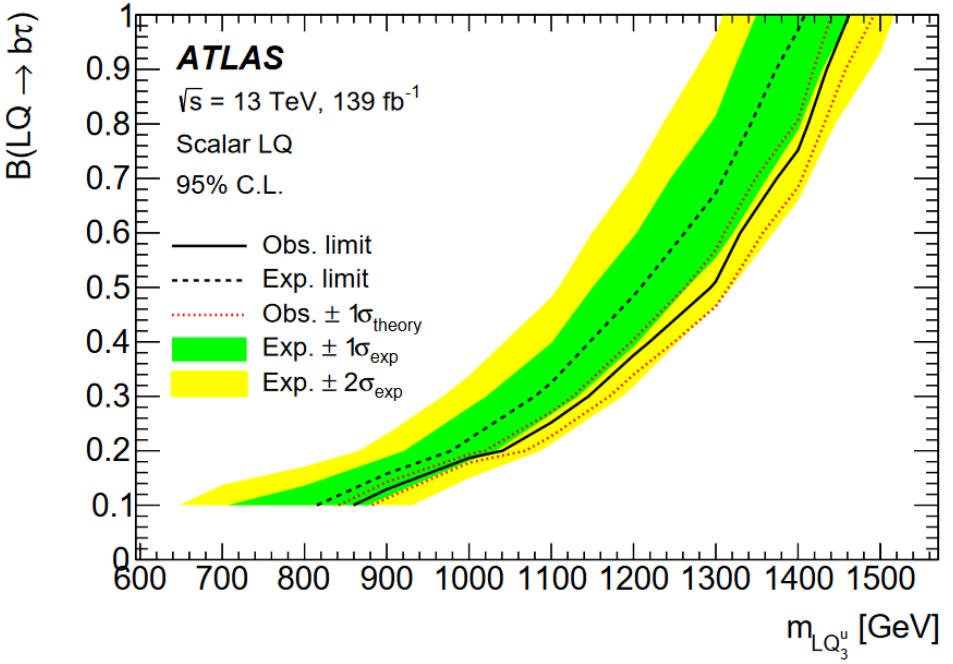

Arxiv: 2303.01294

- Search into LQs decaying into pair produced bτ final state.
- Showing no deviation from SM upto a mass of 1500 GeV.
- This is for scalar LQ, there is also study for vector LQ.

Outlook for Leptoquark Analysis

- Begun the LQ analysis – currently looking at background MC samples
- Plot showing invariant mass of bτ systems in ttbar background.
- Waiting for signal MC sample from ATLAS collaborators.

Long term outlook:

- Analysis in bτ bτ, bτ bν and bν bν channel.
- Extending limit with higher CoM energy, more data and better b-tagging and τ –ID performance.

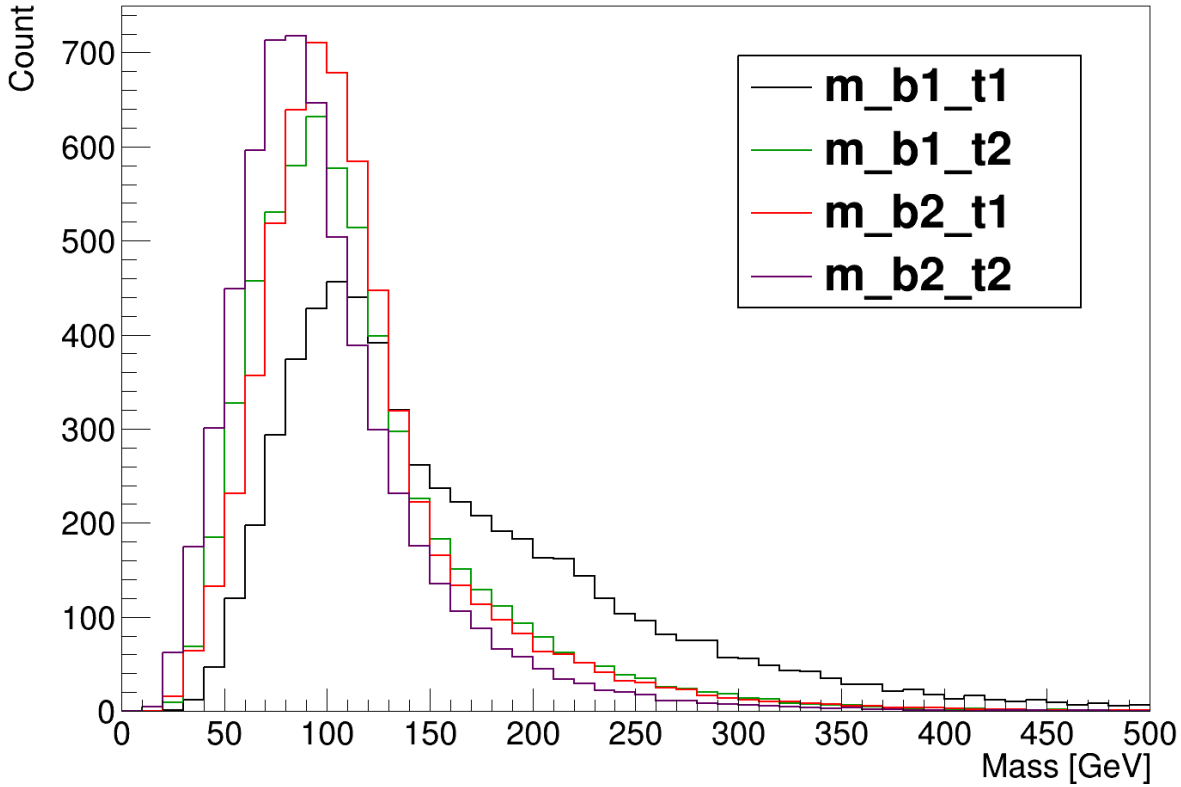

Summary and Outlook for the Future

Tau ID Outlook:

- Complete a 1-prong training on the GNN using a reduced dataset.
- Perform training on GNTau algorithm and reproduce results demonstrated in the reduce dataset.
- Validate on data with “tag and probe” analysis once the algorithm is implemented in official ATLAS software.

Leptoquark Outlook:

- Look at the other backgrounds (Drell-Yan, Diboson, etc) in the LQ analysis.
- Work on the LQ analysis.
- Aim to do LTA at CERN where I will undertake Control shifts and collaborate with experts on the LQ analysis.

Thank you for listening!
Any questions?

Development of Position Reconstruction Methods in the LUX-ZEPLIN Outer Detector

Tea Hall

Supervised by:

Prof. Sergey Burdin & Dr. Ewan Fraser

(+ thanks to the Liverpool LZ/XLZD group!)

Year 1 Particle Physics PhD Presentations

June 21st 2024

UNIVERSITY OF LIVERPOOL

LUX-ZEPLIN - Introduction

LUX-ZEPLIN (LZ) is a direct dark matter detection experiment, located 1 mile underground at Sanford Underground Research Facility (SURF) in South Dakota, USA.

LZ's primary search focuses on the detection of Weakly Interacting Massive Particles (WIMPs).

LZ is the world leader in sensitivity to both spin-independent and spin-dependent WIMP-nucleon scattering interactions.

The experiment employs a 7t dual-phase liquid xenon (LXe) time-projection chamber, and two anti-coincidence veto detectors, the Xe Skin and Outer Detector (OD).

The OD is filled with 17t of Gd loaded liquid scintillator (GdLS), split across 10 acrylic tanks of varying geometry.

OD scintillation light is detected by the 120 OD PMTs.

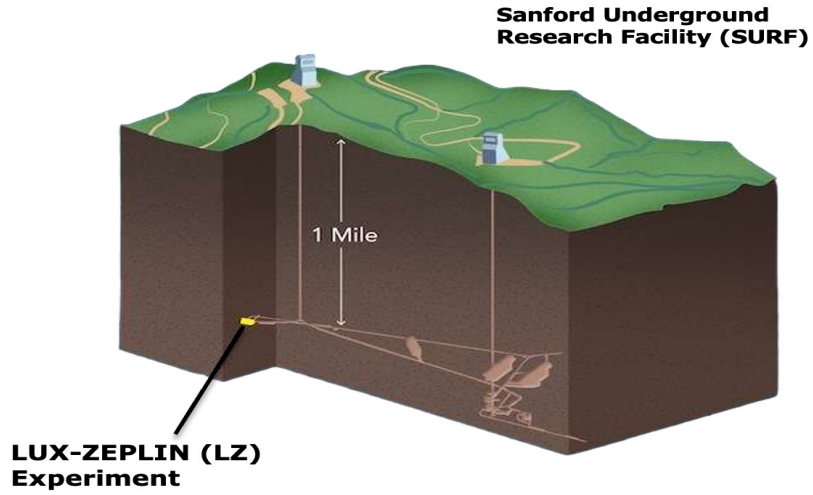

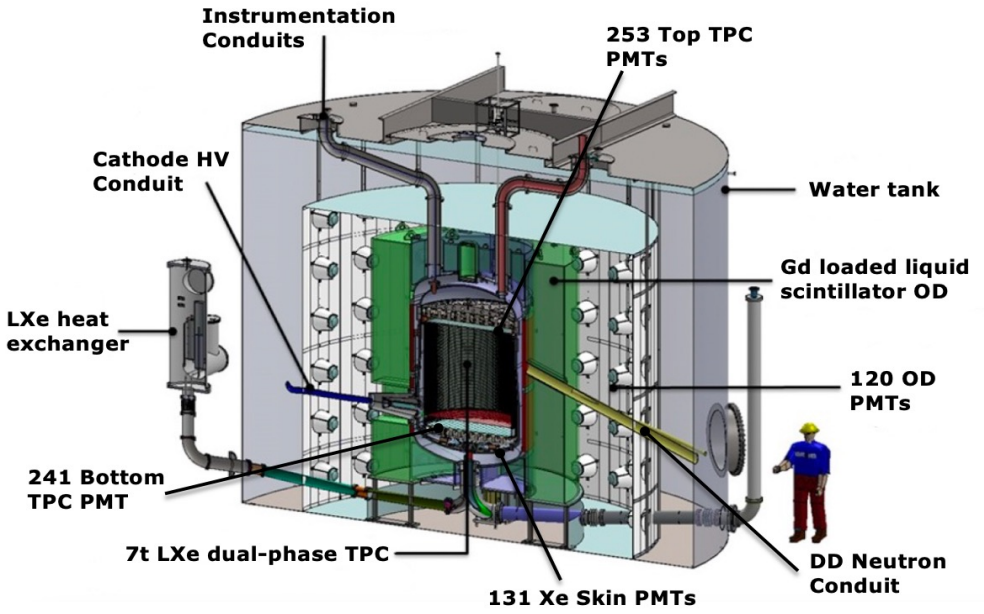

LUX-ZEPLIN - Interactions

Particle interactions upon the LXe atoms in the TPC result in the emission of primary scintillation (S1) light and ionisation electrons.

The E field drifts the electrons to the top of the TPC, then they are accelerated into the GXe phase, producing secondary scintillation (S2) photons.

The TPC possesses O(mm) precision event position reconstruction capabilities.

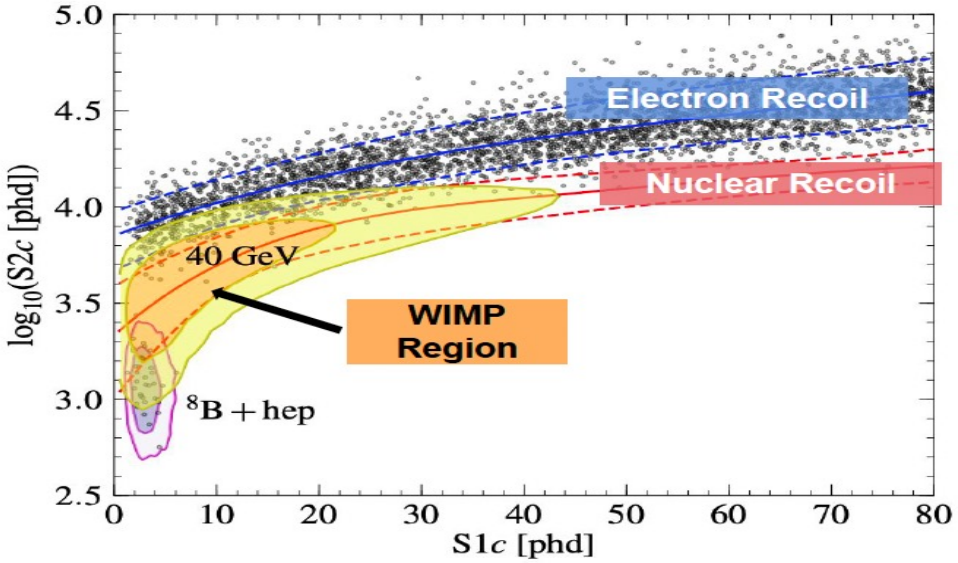

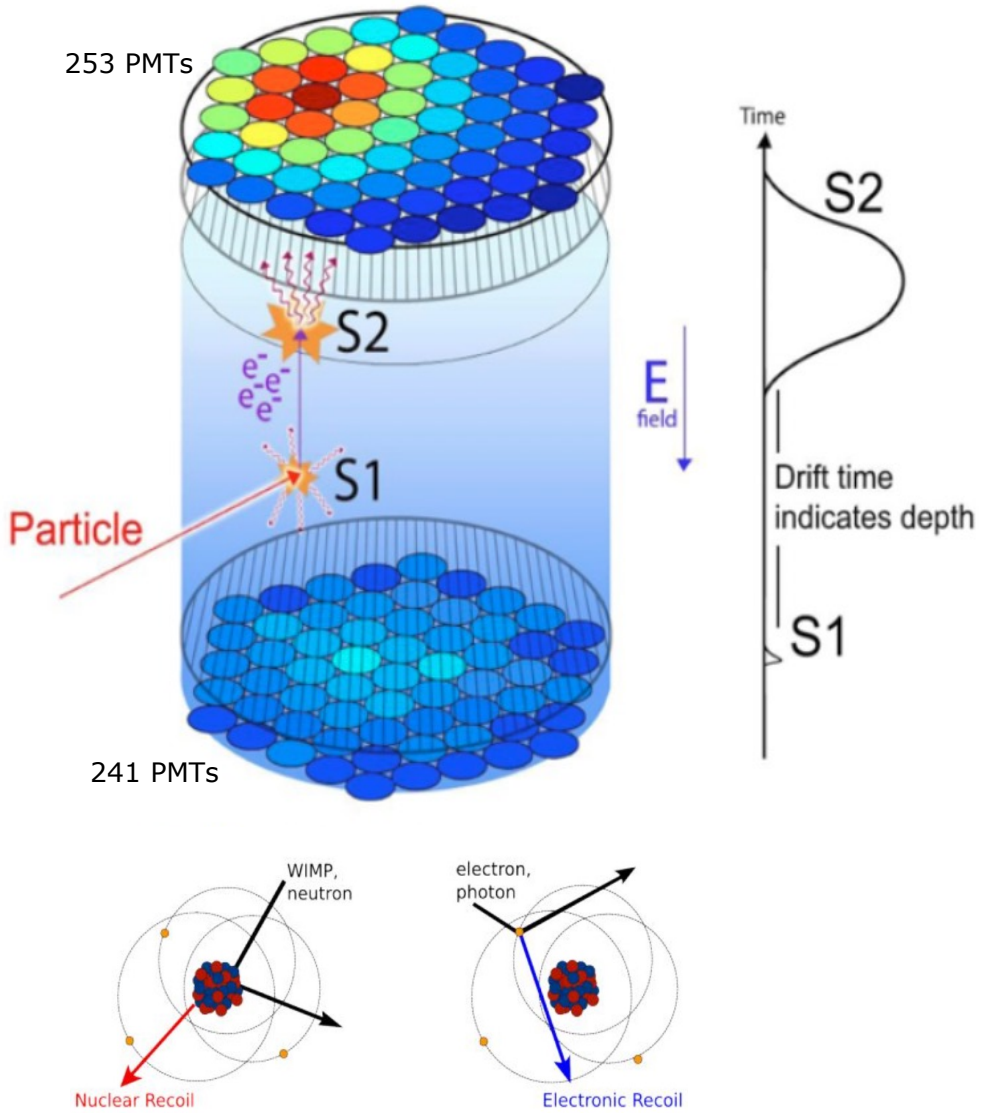

OD Position Reconstruction - Motivation

The currently implemented position reconstruction uses a centroid/centre of gravity method.

$$PA = \sum_{PMT=800}^{919} |chPA_{PMT}|$$

$$x_{cm} = cos_{Sum} = \frac{1}{PA} \sum_{PMT=800}^{919} chPA_{PMT} \times x_{PMT}$$

$$y_{cm} = sin_{Sum} = \frac{1}{PA} \sum_{PMT=800}^{919} chPA_{PMT} \times y_{PMT}$$

This method is poor, places OD events in unphysical regions:

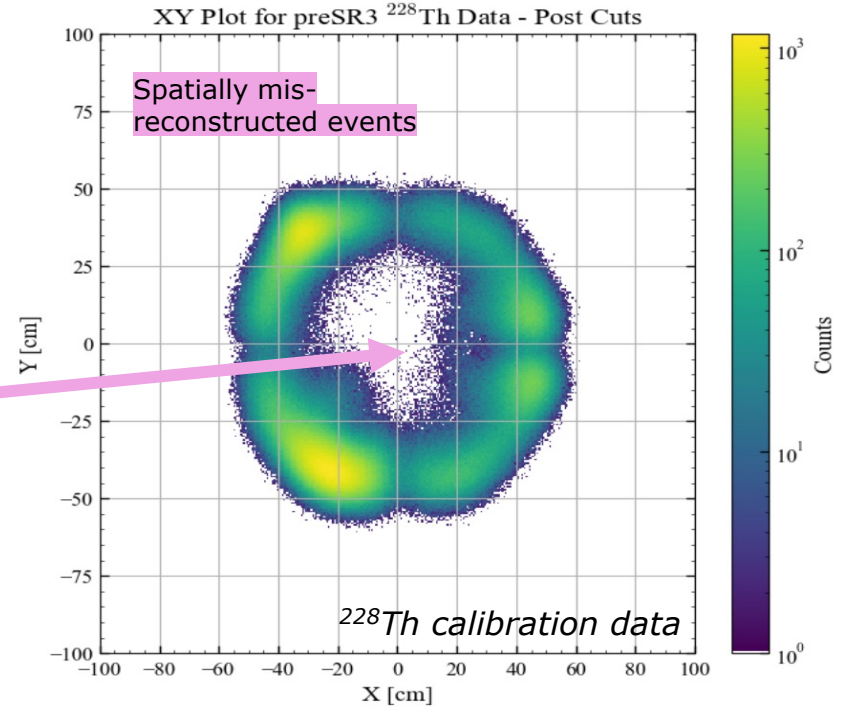

- TPC and Skin regions.
- Beyond the OD acrylic and water tanks.

Accurate (X,Y,Z) position reconstruction within the OD would prove to be important for various reasons:

- Ultimate spatial correlation between single scatter neutron signals in the TPC and neutron capture signals in the OD.
- Improved OD background discrimination.
- Full mapping of light collection efficiencies across the OD.
- Equivalent energy resolutions and thresholds across the OD.

→ Maintain high neutron veto efficiency and reduced dead time.

OD Position Reconstruction - Methods

Two approaches were investigated:

- Light response function method.
- Machine learning method.

Light Response Functions

Light response functions (LRFs) characterise a PMTs response to scintillation light, as a function of an events distance from said PMT.

The light response function method aims to use similar methods as used in the TPC, which was also used by LZ's predecessors, LUX and ZEPLIN-III.

While this method is used only for (X,Y) position reconstruction within the LZ TPC, the method in development for the OD extends to (X,Y,Z).

Machine Learning

Another novel approach to (X,Y,Z) position reconstruction within the LZ OD.

Two multi-layer perceptron neural networks were developed, each with varying input variables, as to make predictions of (X,Y,Z) positions of events within the OD.

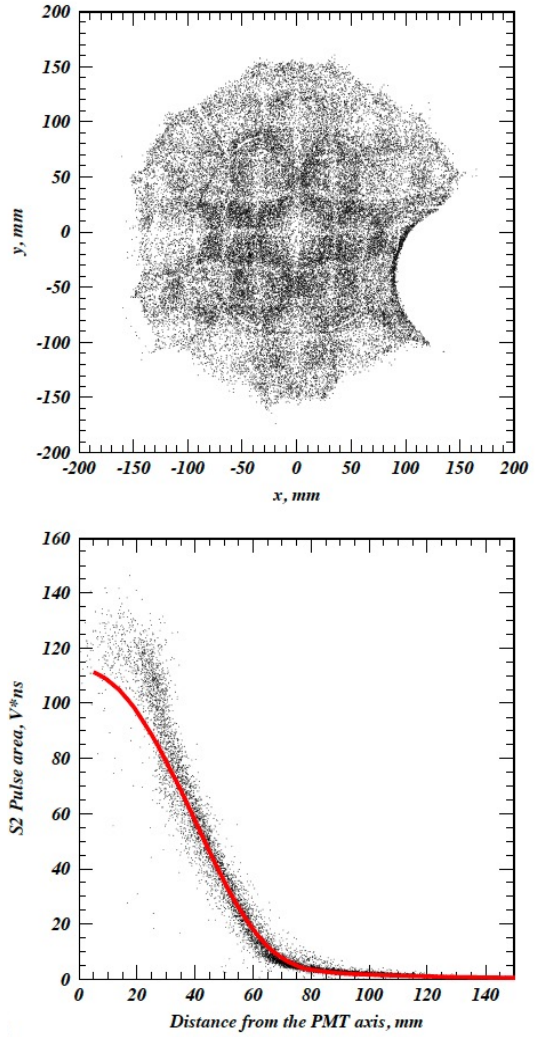

ZEPLIN-III TPC Initial Guess LRF

LRFs – Overview

This analysis used preSR3 ^{228}Th data and two types of simulations, photon bomb simulations (PB) and OD gamma simulations (ODγ), simulation photons constrained to the OD scintillator tanks.

Each simulation type was created with three energies:

- 511 keV.
- 1022 keV.
- 2615 keV.

Data initial (X,Y,Z) event positions were provided by the centroid method.

Simulation initial (X,Y,Z) event positions were provided by the parent particle position RQs.

The 2615 keV gamma peak was selected from the preSR3 ^{228}Th data.

Also ensuring gamma peak selection, pulse area cuts were also placed upon the simulation data.

Energy [keV]	PB PA Selection [phd]	OD γ PA Selection [phd]
511	30–110	25–55
1022	70–210	70–120
2615	200–500	220–340

LRFs – Data and Simulation Comparison

The 2615 keV simulation LRFs are largely discrepant with the data LRFs.

Differences between data and sims are likely arising from:

- The alternative definitions of positions.
- Potential mismatch in OD geometry between physical data and simulations.

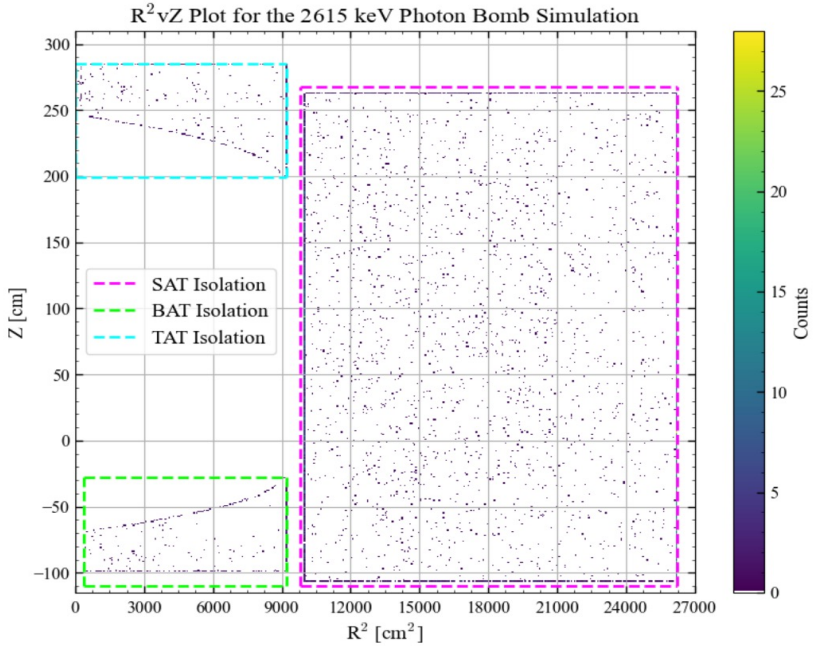

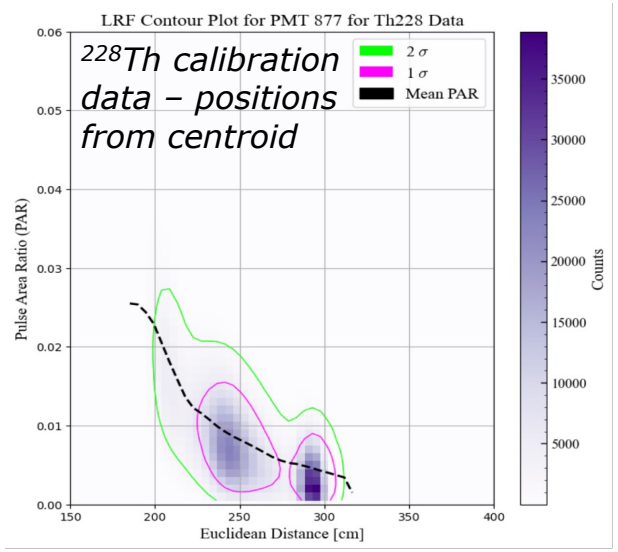

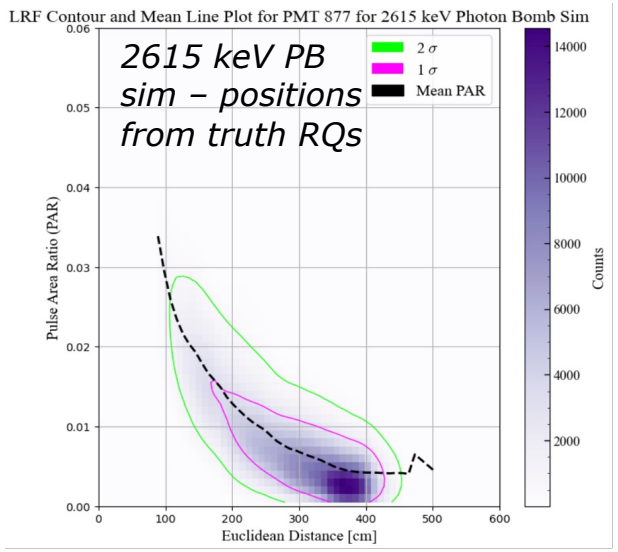

More detailed consideration of the OD (X,Y,Z) position reconstruction is required.

Individual acrylic tanks have been isolated to investigate their LRFs.

Geometry of top and bottom tanks complex, analysis focuses on side acrylic tanks only.

LRFs – Simulation Mean PAR Comparison

Numerator of pulse area ratio limited to 1 phd:

Higher energy γ

↓

Larger energy deposit

↓

Larger pulse area

↓

Smaller minimum PAR

These results indicate an energy dependence in the OD.

Analysis must be extended to incorporate a wider range of energies within the OD, ~27 keV to 8.5 MeV.

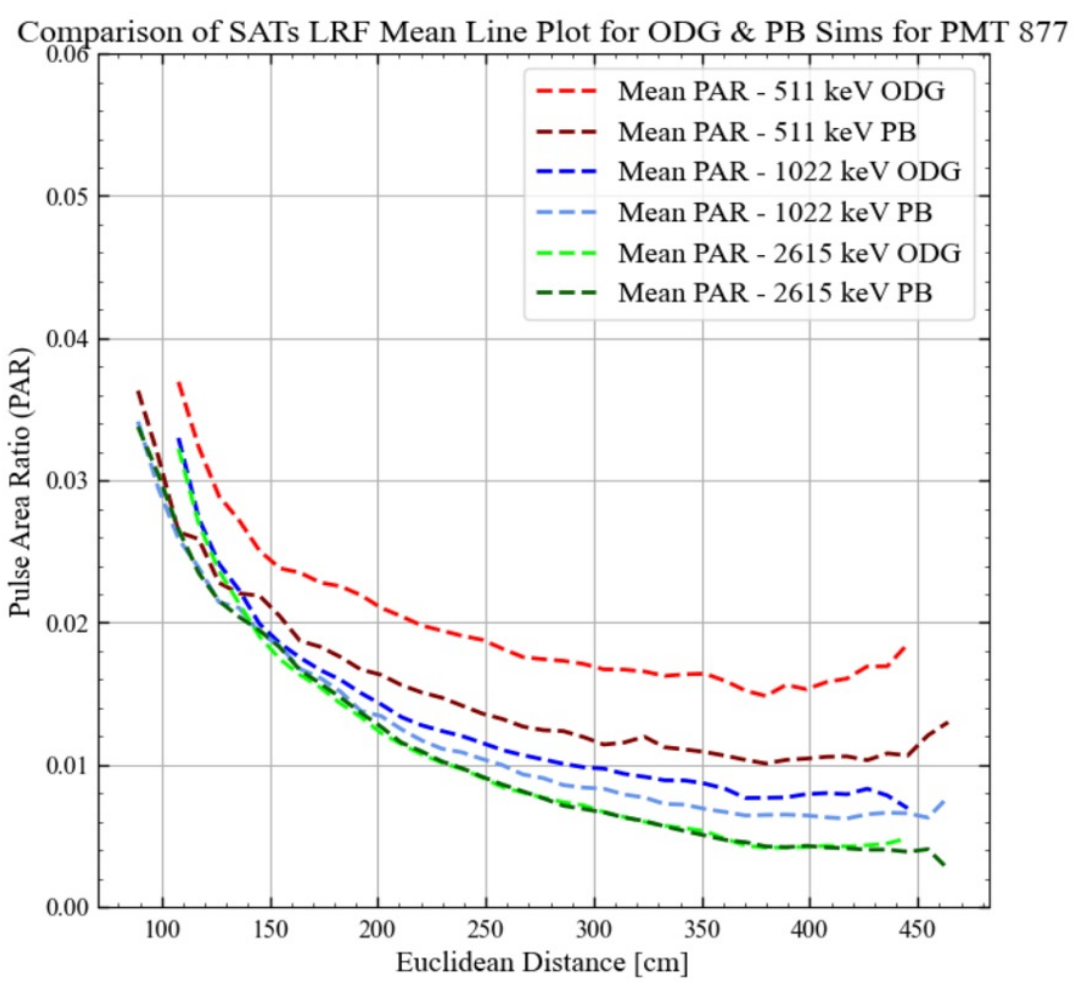

Machine Learning - Overview

Two multi-layer perceptron (MLP) neural networks were created to make predictions of (X,Y,Z) positions in the OD.

One MLP used only the largest pulse area observed by each PMT (MLP1), while the other used this and the respective timing information (MLP2).

Activation function: Leaky ReLU.

Optimiser: Adam.

Loss function: custom Euclidean distance.

$$Loss_{Euclidean} = \sqrt{(\Delta x)^2 + (\Delta y)^2 + (\Delta z)^2}$$

MLP1 had an input shape of (120,) and MLP2 (240,).

Each MLP had the same layer arrangement:

Input → 240 nodes → 120 nodes → 60 nodes → 30 nodes → (X,Y,Z) output.

MLP1 & MLP2

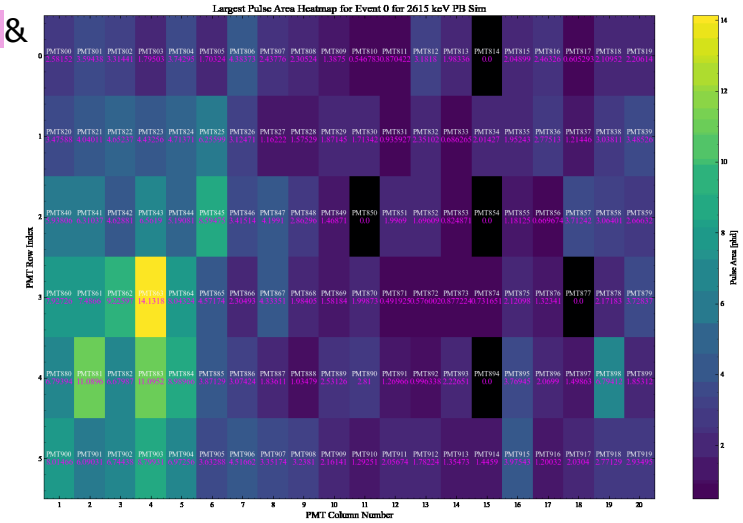

MLP2

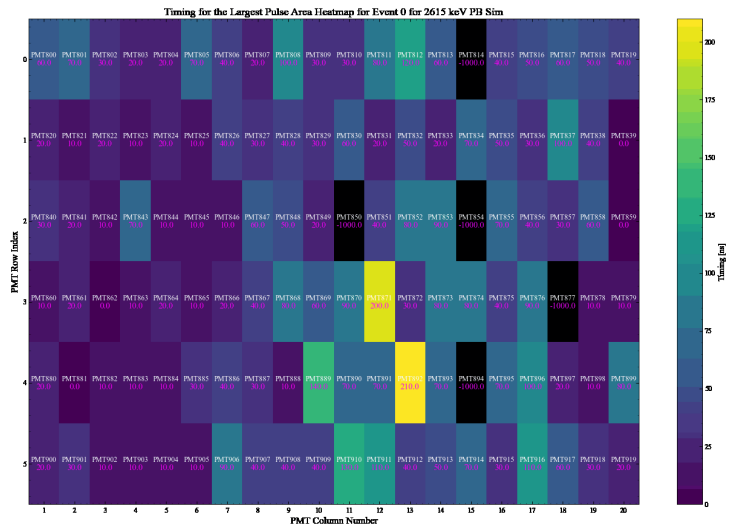

Blacked PMTs saw no pulse.

Machine Learning – Loss Curves

Losses for both model trend downward rapidly in the first 5 epochs.

Both models converge at ~25 epochs.

MLP1 has much higher initial losses, with large fluctuations present in the validation losses.

- Model is overfitting?

MLP2 has lower initial losses, validation loss fluctuations are also smaller in contrast.

- Performs and generalises better to unseen data.

MLP1

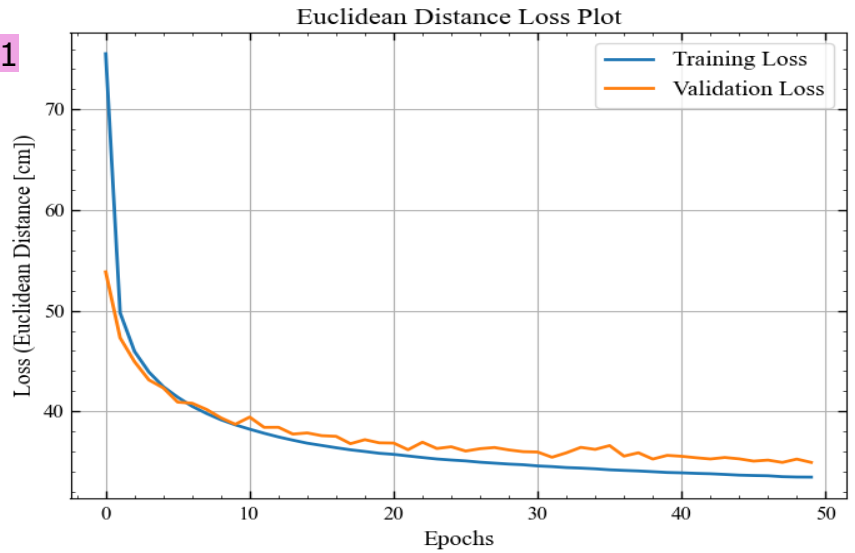

MLP2

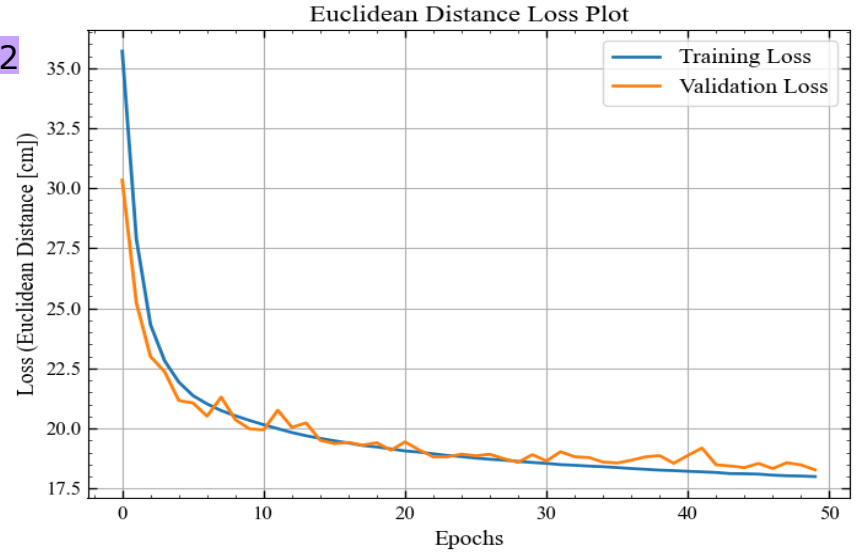

Machine Learning - Position Resolution

Neither models are suitable for accurate OD position reconstruction in their current state:

- MLP1 prediction positions are constrained to the OD, while MLP2 predicts events outside the OD.
- Both model's predictions show a position bias in the top and bottom of the OD.
- MLP1 does not predict events along the inner or outer boundary of the SATs.
- MLP2 is also poor at predicting events along the outer boundary of the SATs.

MLP1 achieved a superior position resolution of 9.78cm (X), 9.53cm (Y) and 15.39cm (Z).

MLP2 achieved a position resolution of 18.75cm (X), 19.44cm (Y), and 27.52cm (Z).

MLP1

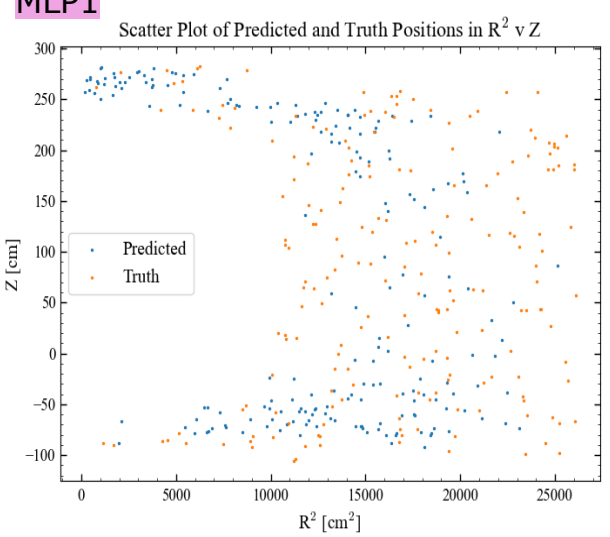

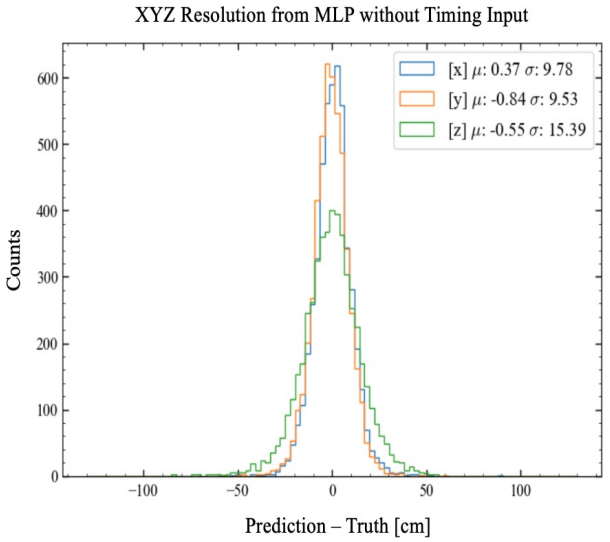

MLP2

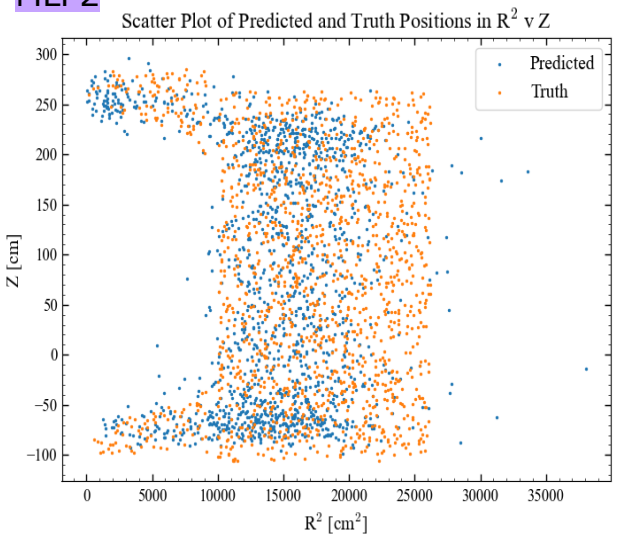

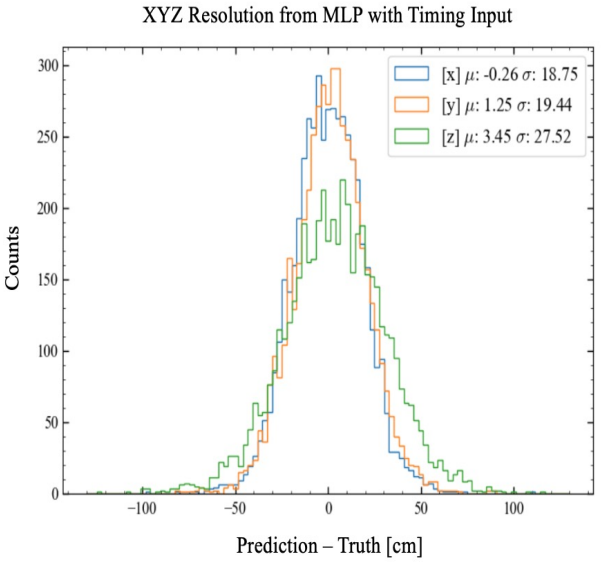

Conclusions and Future Work

Summary:

- Two methods were investigated in the development of OD (X,Y,Z) position reconstruction.
- Discrepancies were evident between the initial guess LRFs from preSR3 ^{228}Th data and simulations, likely arising due to geometry and initial position definition differences.
- For a more detailed consideration of OD position reconstruction, the acrylic tanks were isolated for individual analysis of their LRFs.
- Both MLP models require further work, neither produce desirable predictions to be utilised in OD position reconstruction.
- MLP2 excels in loss reduction but is poor at accurately predicting events within the physical regions of the OD.

Future Work:

- Extend the simulation LRF analysis to incorporate a wider range of energies, capturing all physics within the OD.
- Correct the timing input for the MLPs, the -1000ns inputs are likely unhelpful to the model and are causing issues.
- Fix the synchronicity issues between the largest pulse inputs and their respective timing information.
- Investigate the use of convolutional neural networks (CNNs) for predicting (X,Y,Z) events within the OD.

Thank You!

Back up slides

Light Response Functions Overview

Light response functions (LRFs) characterise a PMTs response to scintillation light, as a function of an events distance from said PMT.

The light response functions of all active PMTs within the detector comprises a light response model (LRM).

LRFs can be measured in various ways in both physical data and Monte Carlo simulation data:

- Collimated mono-energetic gamma sources.
- Detector geometry.

This LRF method utilised both physical and simulation data:

- preSR3 ^{228}Th data, strict cuts to isolate the ^{208}Tl 2615 keV gamma peak.
- Photon bomb simulations.
- OD gamma simulations.

This approach aims to extend the method used in the TPC and extend it to develop precise position reconstruction in the OD.

Tea Hall | sgthall2@liverpool.ac.uk

LRFs – TPC Method and MERCURY

(X,Y) positions are reconstructed from the S2 light pattern on the top PMT array hit pattern using MERCURY.

MERCURY performs event reconstruction through identifying the best estimate of a scintillation vertex, given the distribution of photons across the PMTs.

Initial position estimates from centroids are provided.

A first approximation is obtained through fitting the measured PMT responses with a smooth function.

Less biased position estimates are then obtained from a similarity function, which comprises of a statistical method:

- Maximum likelihood
- Weighted least squares

Process is repeated until a convergence criterion is met.

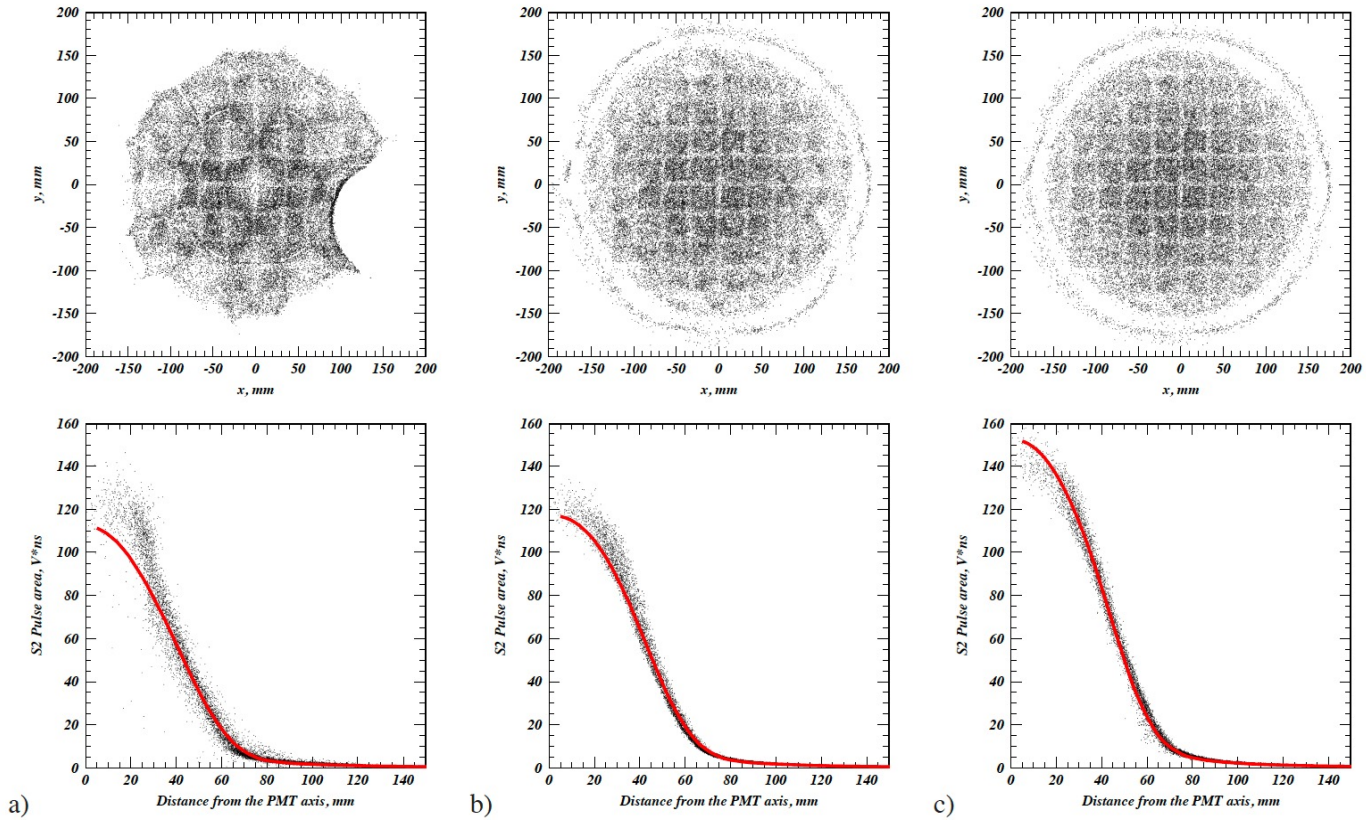

LRFs – preSR3 ^{228}Th Data

Strict cuts were placed to isolate the ^{208}Tl 2615 keV gamma peak, in addition to coincidence and burst noise cuts.

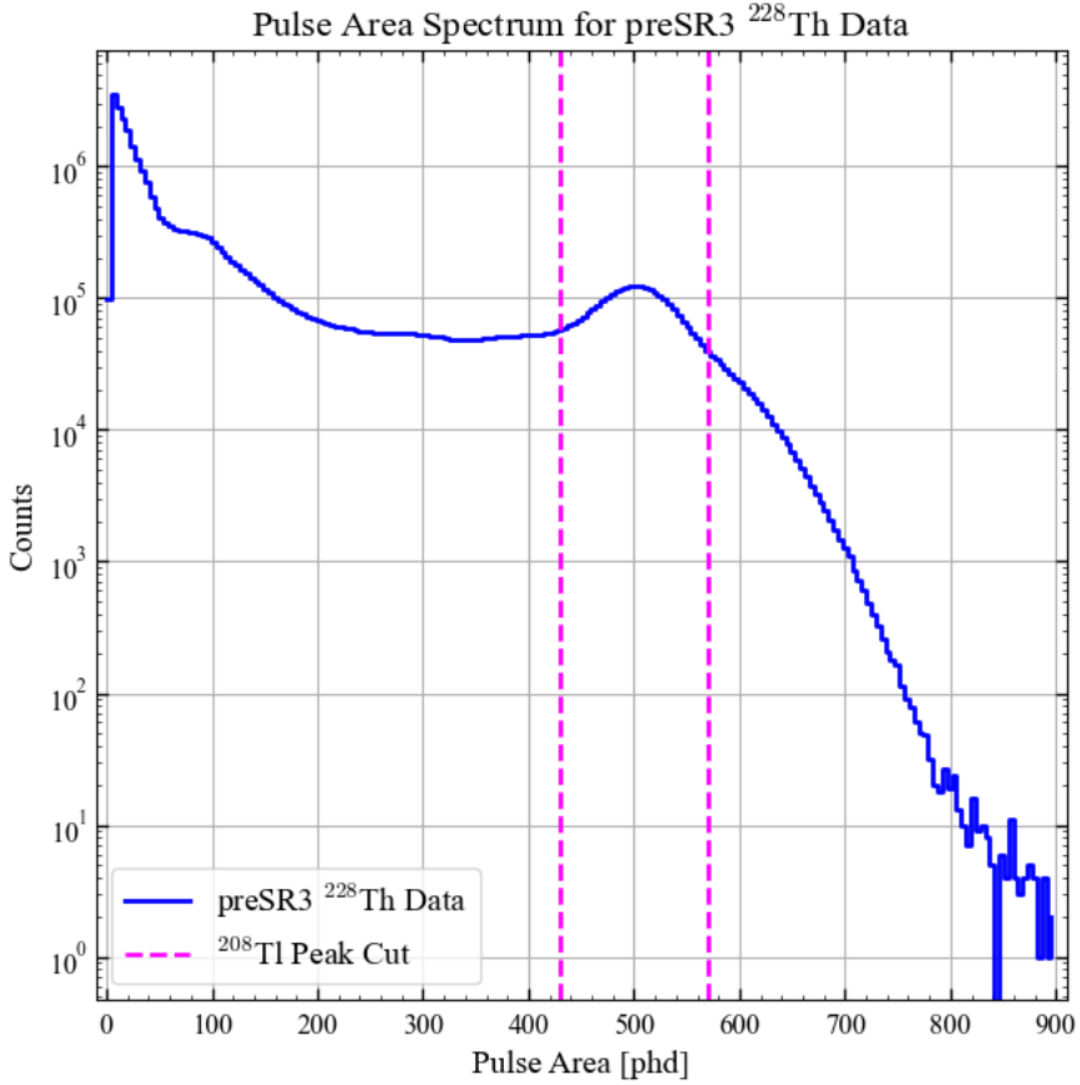

LRFs – preSR3 ^{228}Th Data

Each PMTs response is given as a pulse area ratio (PAR).

$$PAR = \frac{Pulse\ Observed\ by\ PMT}{Largest\ Observed\ Pulse\ in\ OD}$$

The distance was defined as the Euclidean distance between said PMT and the event, initial guess event positions from centroid method.

Observations:

- **OD LRFs are not a smooth function as expected.**
- Discrepancy in LRF shape for PMTs near BATs likely arising due to the minimal events reconstructed in that region.
- Difference in AT geometry likely a factor.

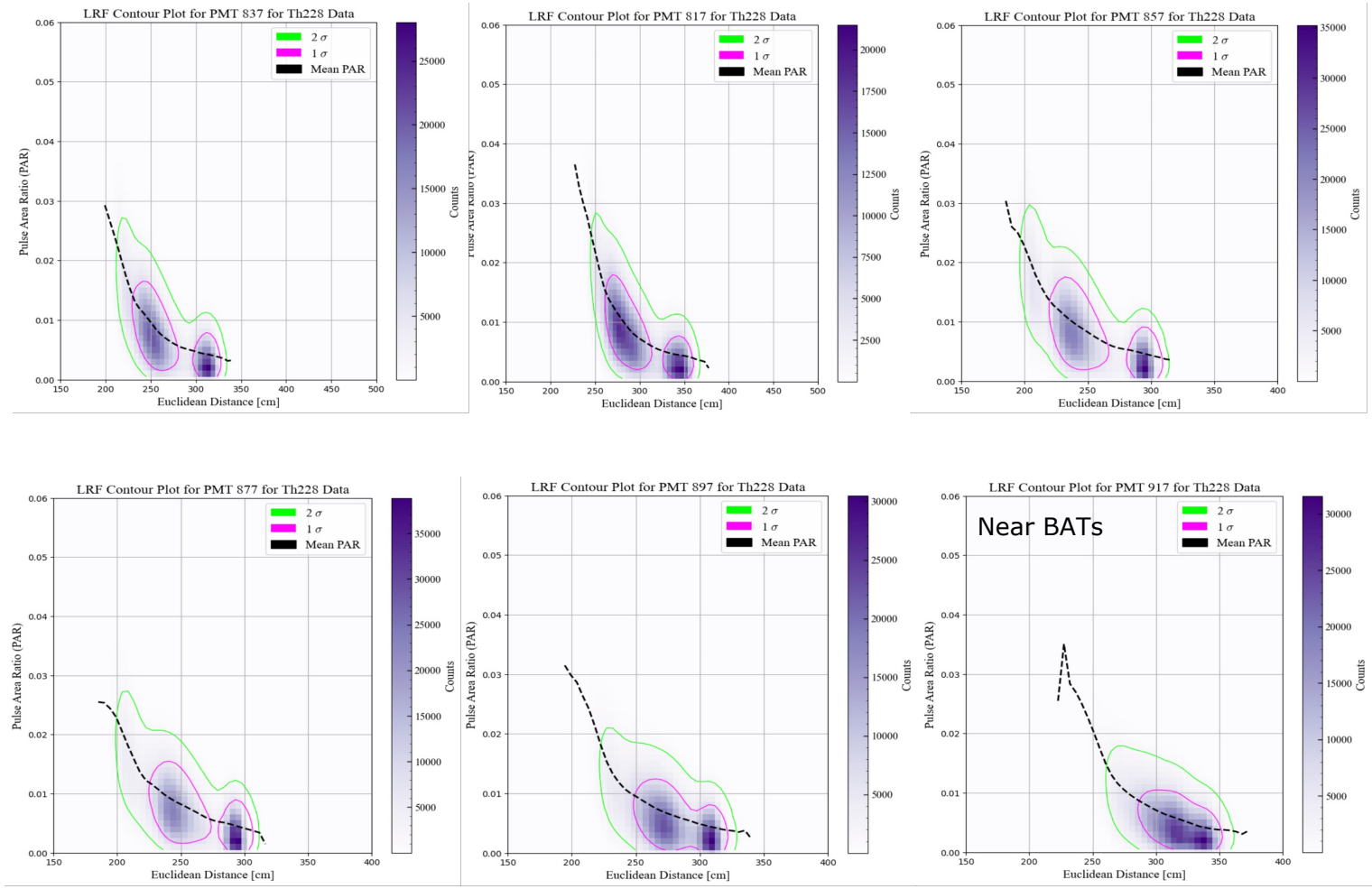

LRFs – Acrylic Tank Isolation Cuts

The isolation of the OD GdLS acrylic tanks was achieved by placing strict cuts in radial and Z space.

TATs Cut [cm]	SATs Cut [cm]	BATs Cut [cm]
$0 > \mathrm{R} > 96$	$99 > \mathrm{R} > 162$	$19 > \mathrm{R} > 96$
$199 > \mathrm{Z} > 285$	$-95 > \mathrm{Z} > 259$	$-95 > \mathrm{Z} > -29$

LRFs – Simulations

The 2615 keV simulation LRFs are discrepant with the data LRFs.

Simulations place events in the BATs; hence the shape may be expected.

Differences between data and sims are likely arising from:

- The alternative definitions of positions.
- Potential mismatch in OD geometry between physical data and simulations.

LRFs from sims will be used to compose the LRM, then have real data tuned on them at the stage of iterative improvement of position reconstruction.

AT geometry resulting in LRF shape changes in PMTs at different heights.

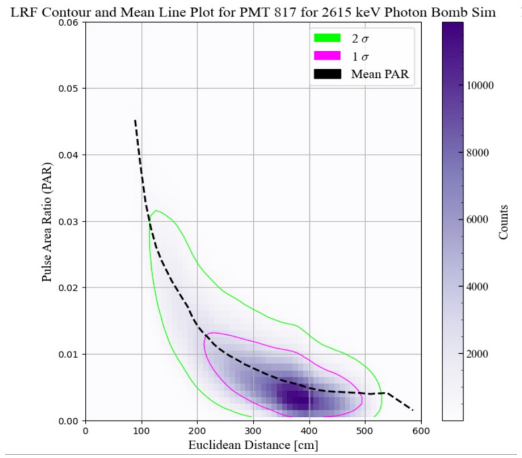

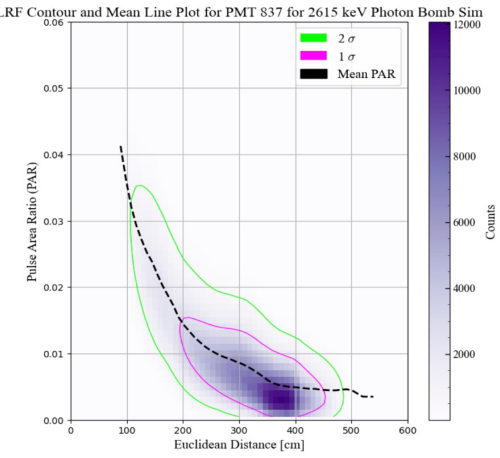

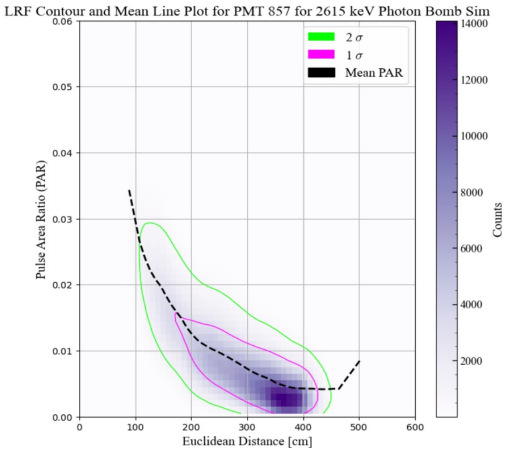

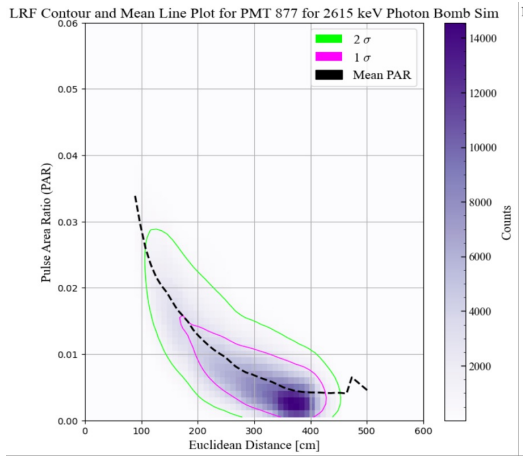

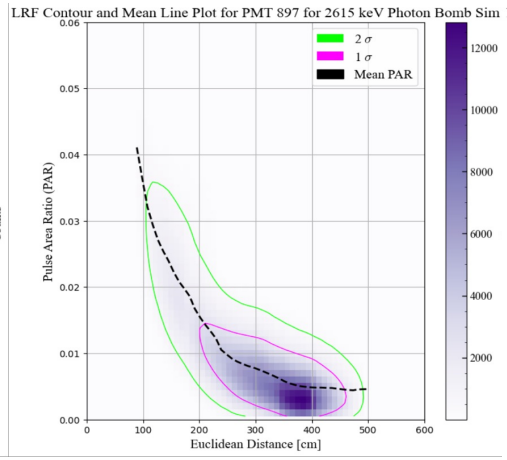

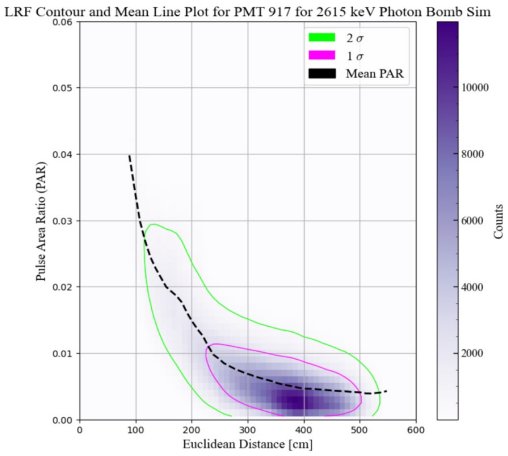

LRFs – Simulations

The PB and ODγ simulations at 2615 keV have LRF mean PARs that match, while the other simulations of equal energy differ from each other.

Numerator of PAR limited to 1 phd:

Higher energy γ

↓

Larger energy deposit

↓

Larger pulse area

↓

Smaller minimum PAR

These results indicate an energy dependence in the OD.

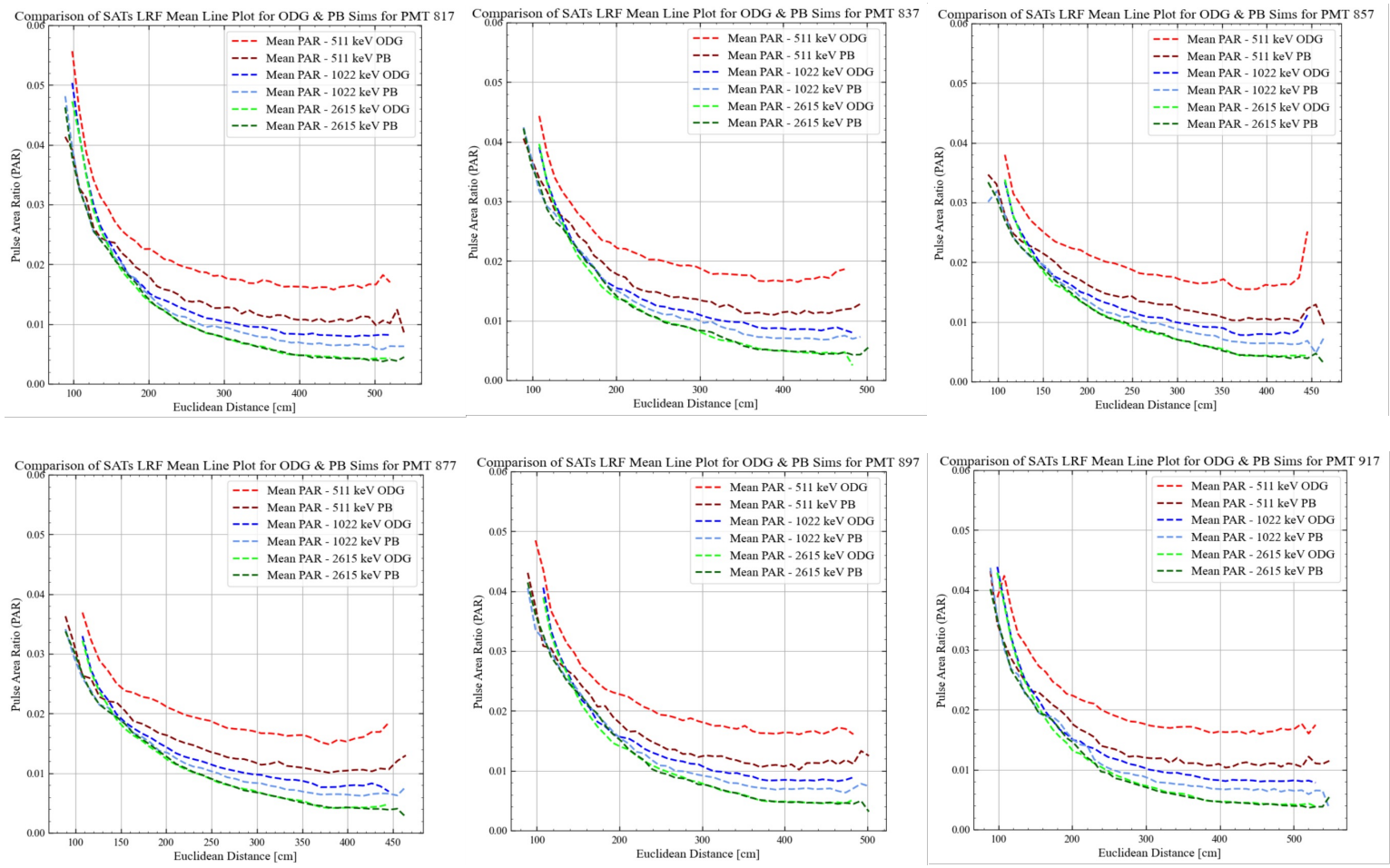

HYPER-KAMIOKANDE LIGHT INJECTION SYSTEM AND DETECTOR SYSTEMATICS

Unik Limbu

Hyper-Kamiokande

- Hyper-K is the next generation water Cherenkov neutrino detector
- Will be instrumented with PMTs in the ID and OD, as well as mPMTs (see picture below) for better timing and spatial resolution

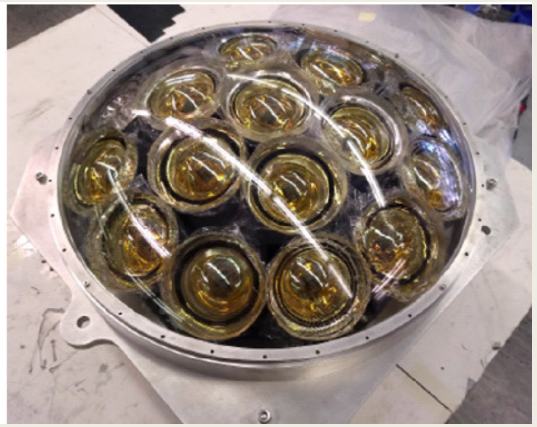

- Physics goals:
  - ➢ Neutrino oscillation measurements
  - ➢ CP violation in leptonic sector
  - ➢ Proton decay

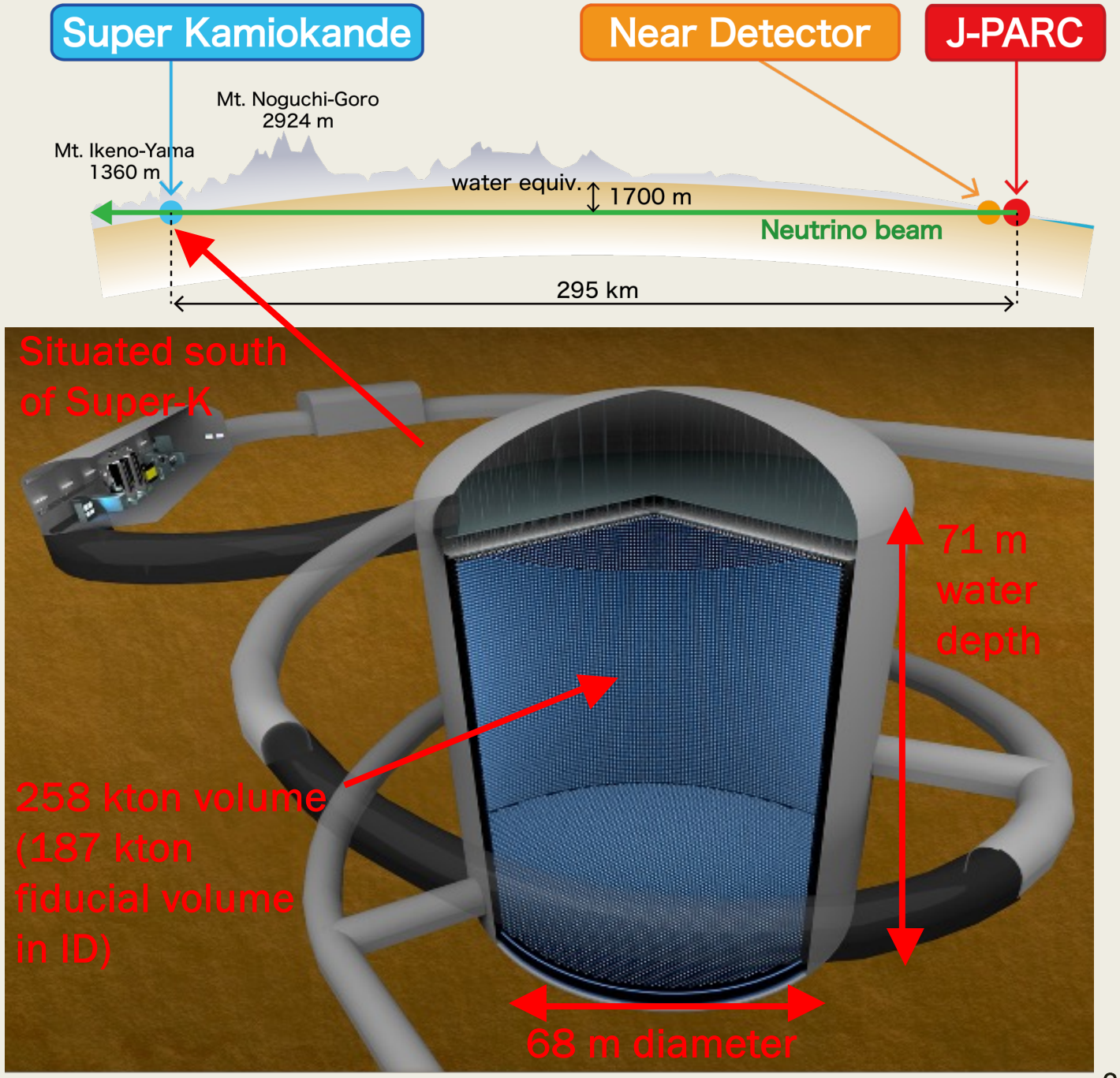

Light injection (LI) system

- LI system will inject known quantities of light into the detector – Collimator (2°opening angle) and diffuser (40° opening angle)
- 33 ID injector positions with both collimator and diffuser - illuminated by pulsed laser
- Characterising optical properties of water (scattering, absorption) along with PMT characteristics
- Worked with WCSim and analyses are based on injector position 12

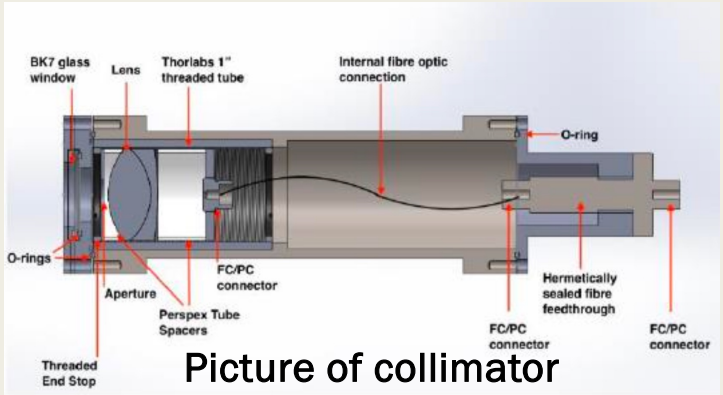

Picture of collimator

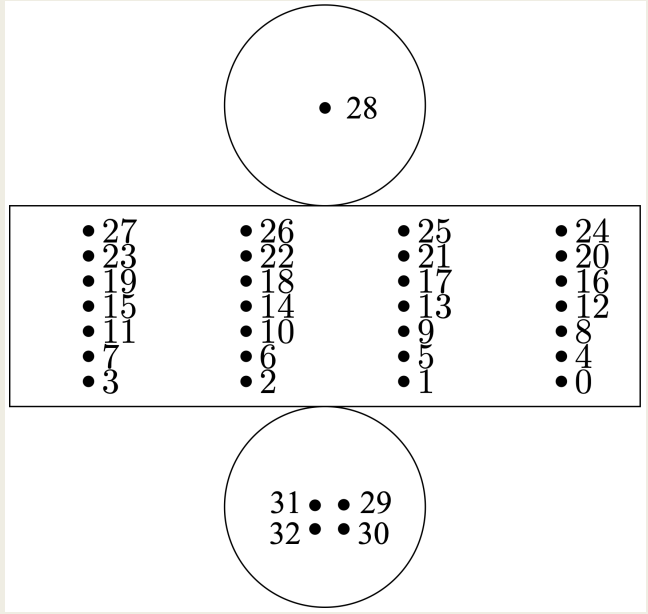

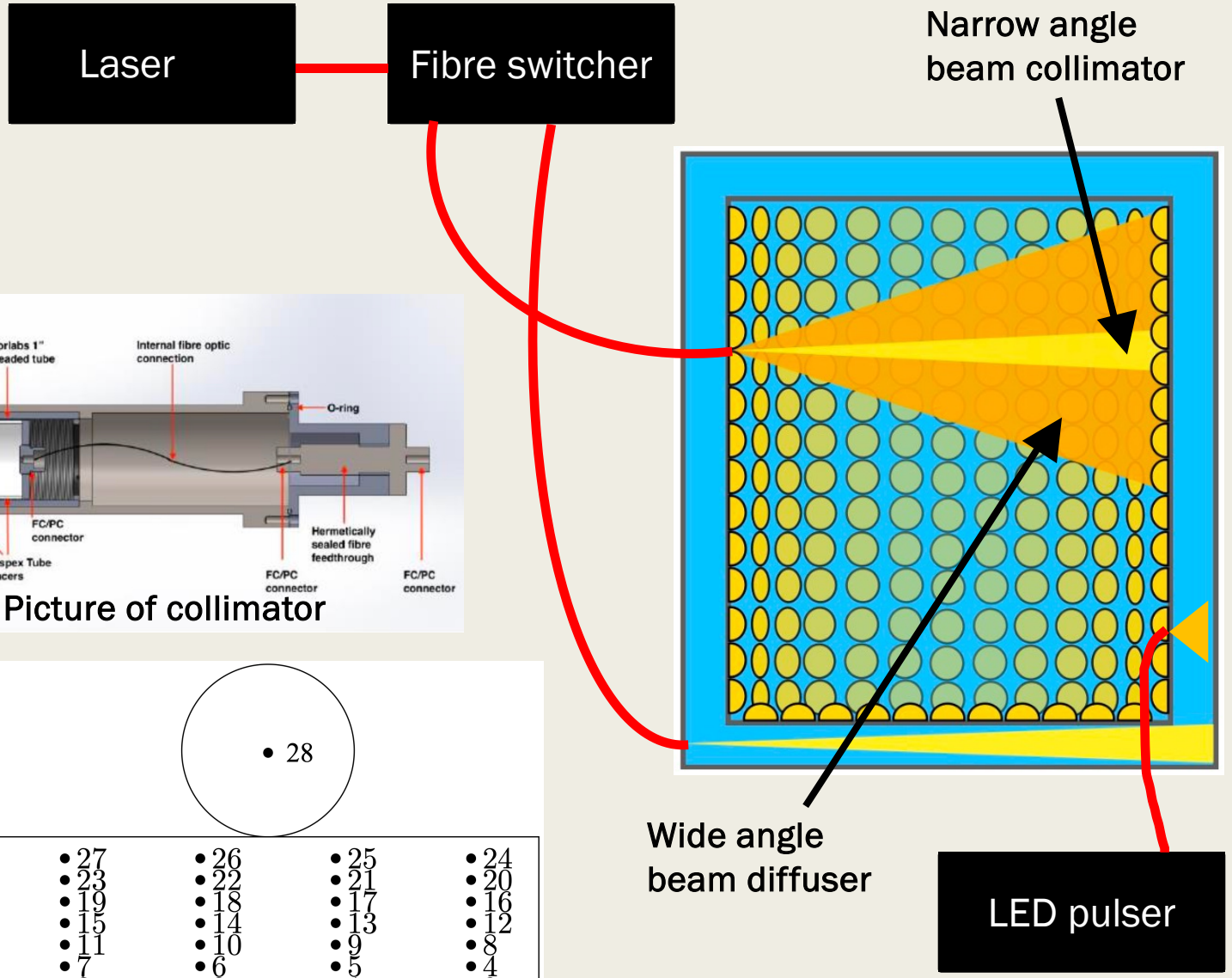

Collimator analysis (1)

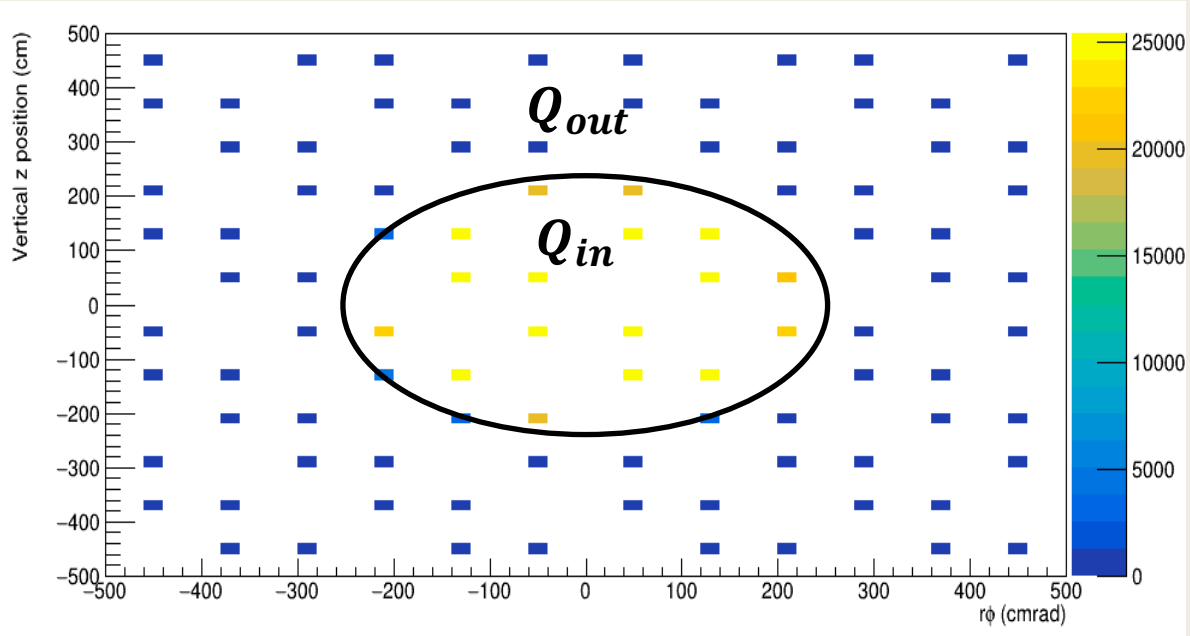

- Charge ratio $\frac{Q_{in}}{Q_{out}}$ - the ratio of total collected charge inside the beam spot to that outside the beam spot of the PMT
- Scattering $\propto \frac{1}{\text{rayff}}$ and Absorption $\propto \frac{1}{\text{abwff}}$

where rayff and abwff are Rayleigh scattering coefficient and absorption coefficient, respectively

- Sensitive to scattering but minimally to absorption

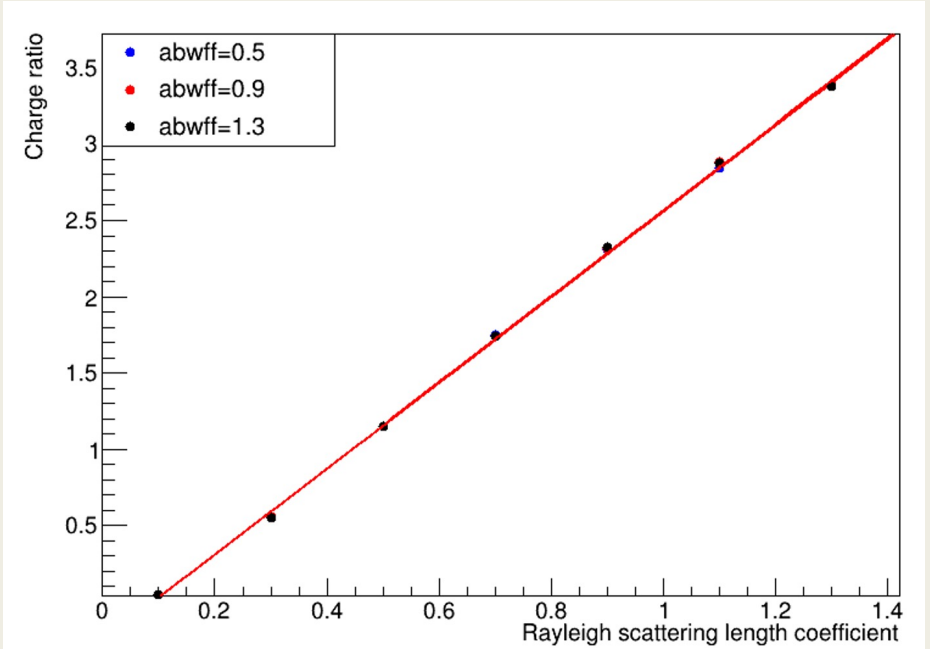

Higher scattering coefficient (lower scattering) increases charge ratio

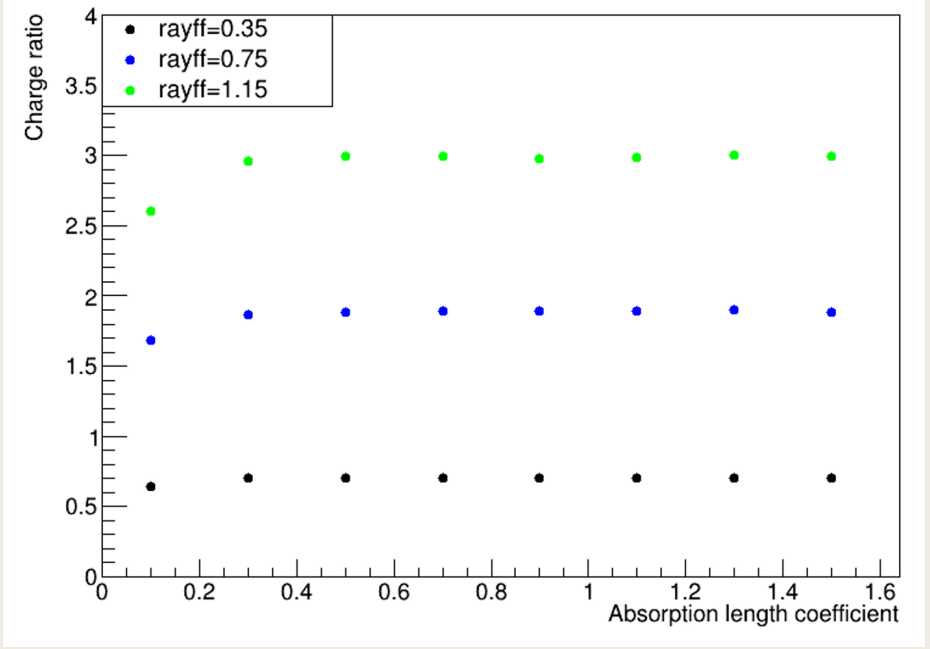

No correlation between absorption and charge ratio

Collimator analysis (2)

Larger scattering coefficient values (low scattering) cause dip

Smaller absorption coefficient values (high absorption) cause significant dip

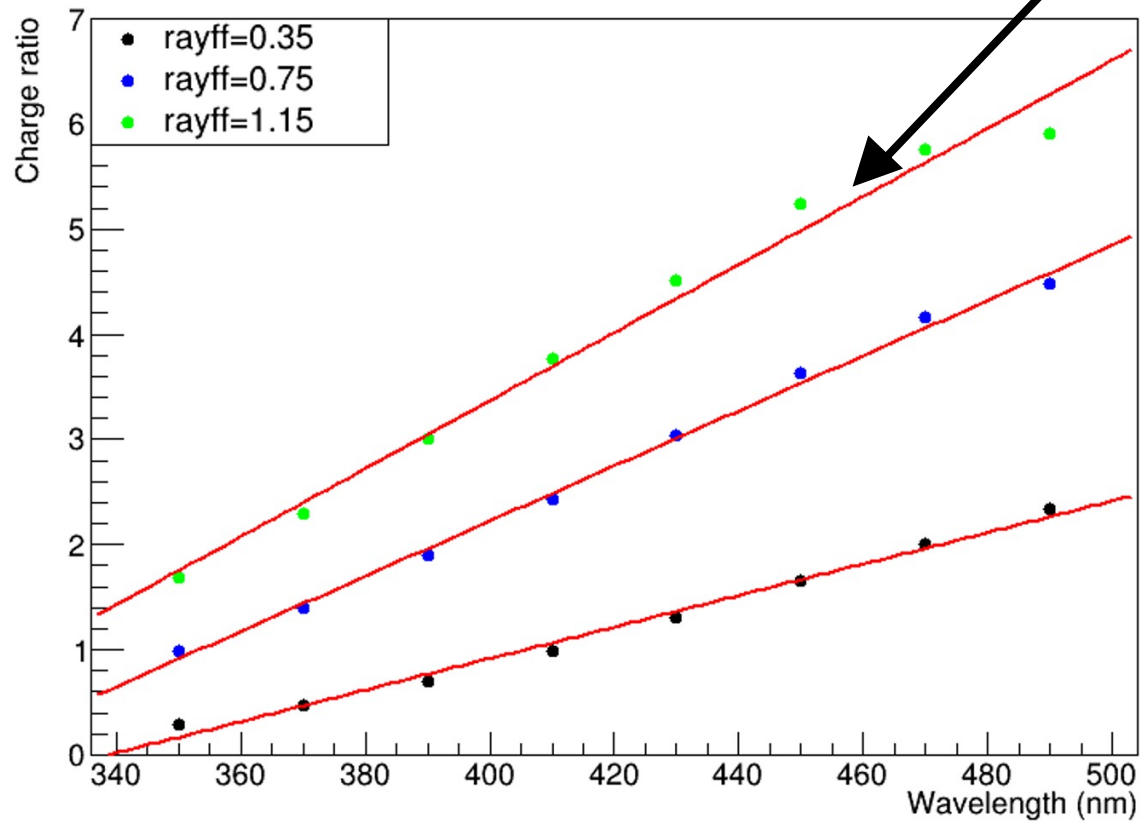

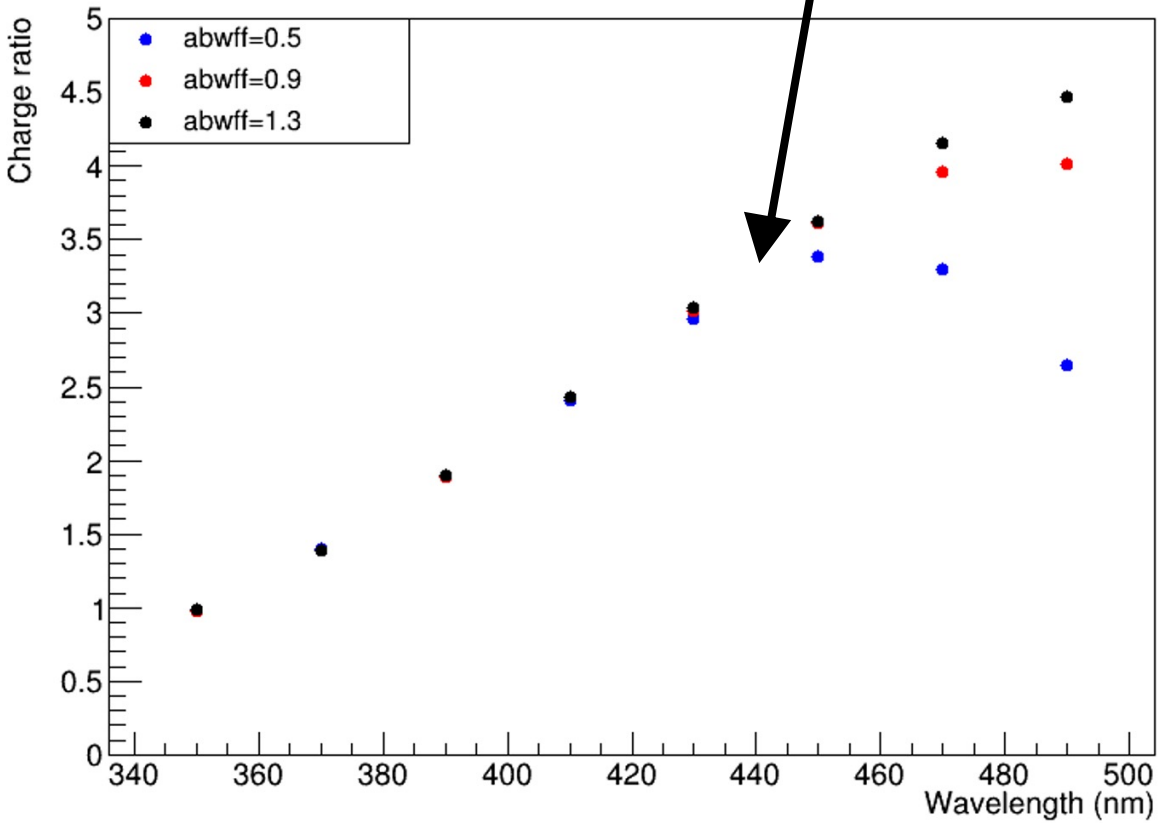

- Charge ratio increases linearly with wavelength
- Results breaks down at low scattering and high absorption

Tail analysis (1)

- Time residual:

$$t_{res} = t - t_{flight}$$

- Fitted the `tail' using a reciprocal function:

$$y = \frac{p_0}{x + p_1} + p_2$$

where p_0, p_1 and p_2 are the fitting parameters

- Right: Example of the fitted residual plot for rayff $= 0.7$ (collimator)
- Examined each fitting parameter as function of water parameters

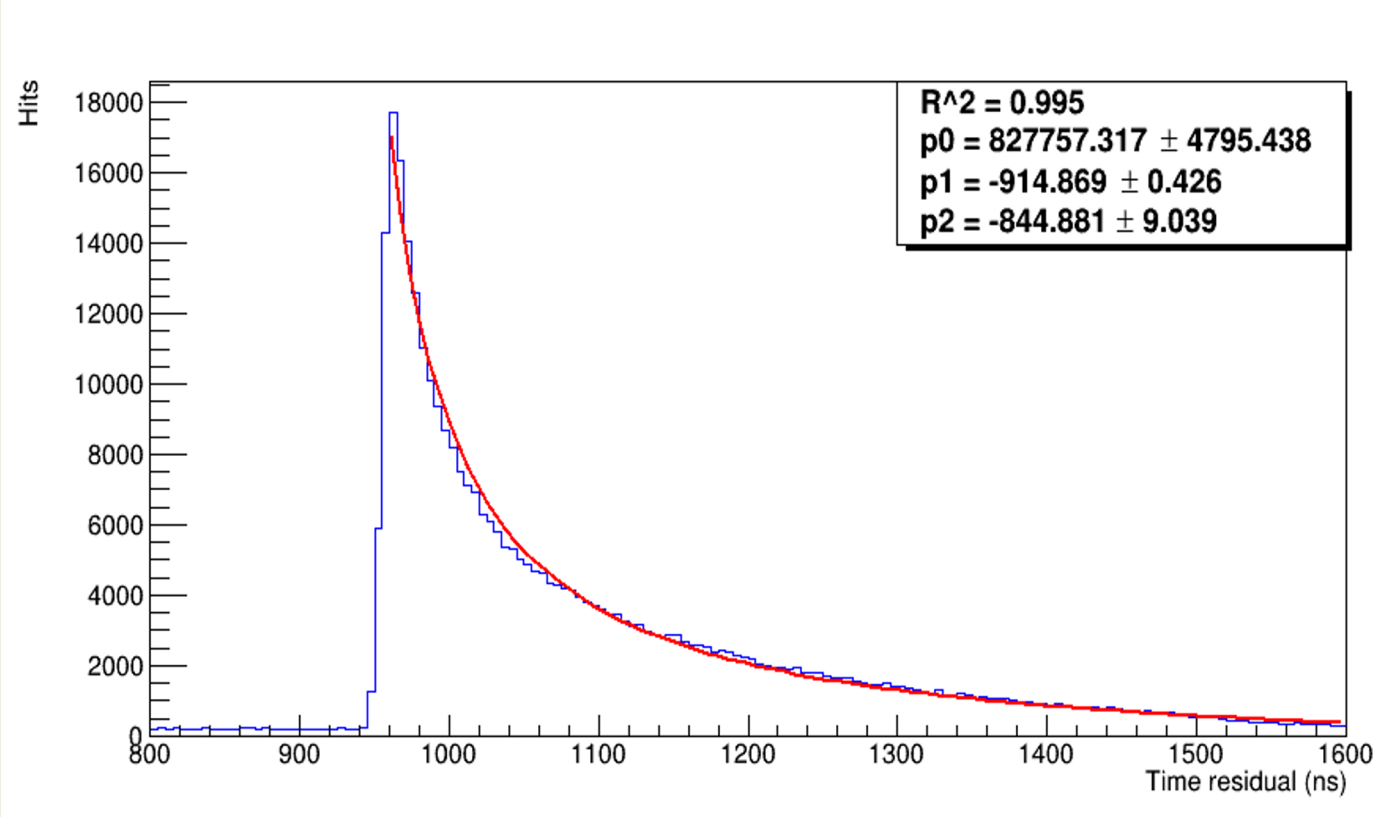

Tail analysis (2)

Have opposite correlation

p_0 - intensity of scattering/absorption

p_1 - shift in time domain

p_2 - baseline noise

➢ Scattering:

- Inverse relationship between p_0 and coefficient
- p_1 shows a decreasing trend, stabilising as the coefficient increases

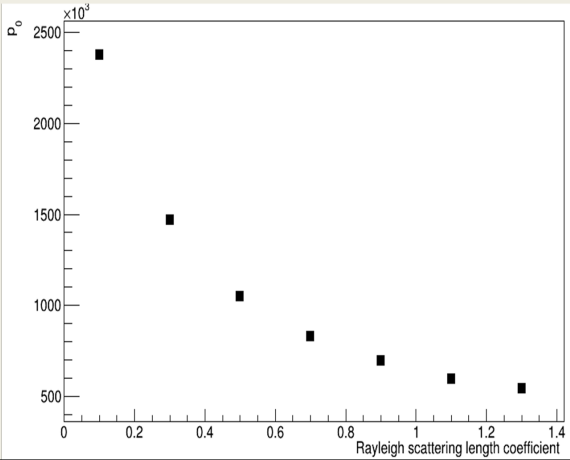

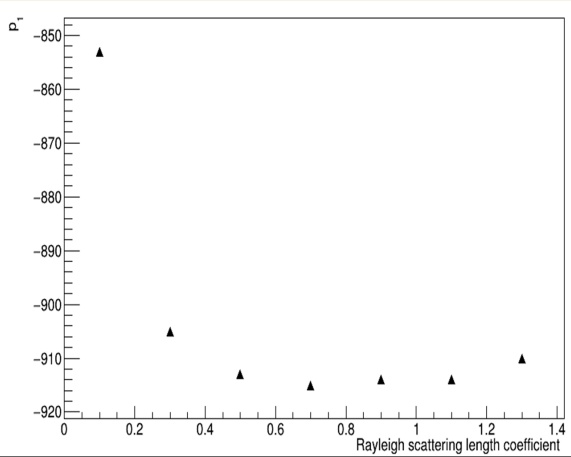

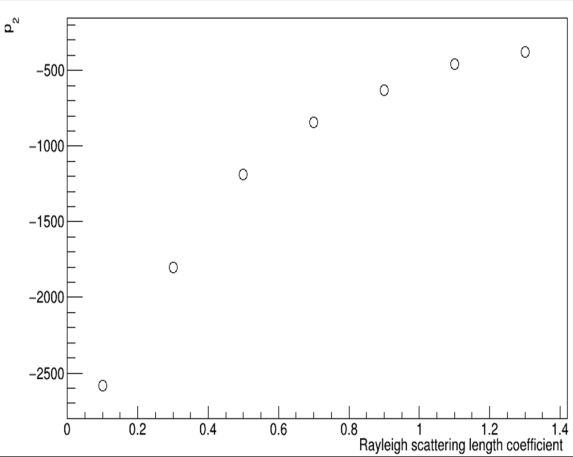

➢ Absorption:

- increasing trend between $p_0$and coefficient
- p_1 also shows an increasing trend

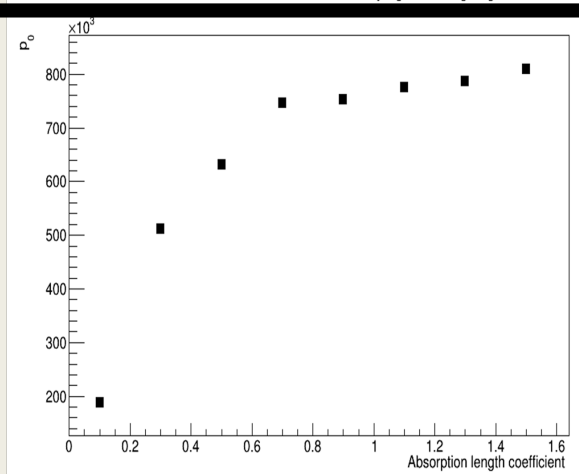

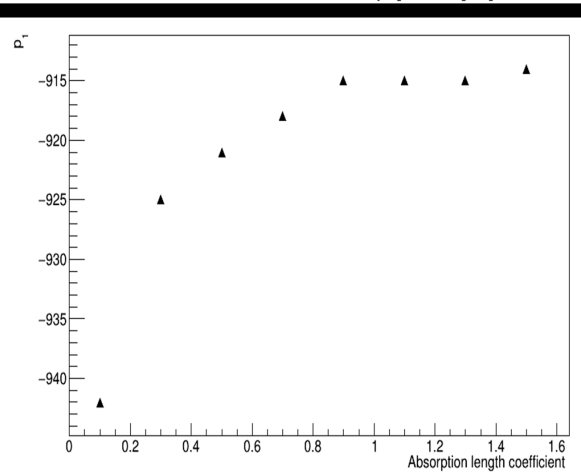

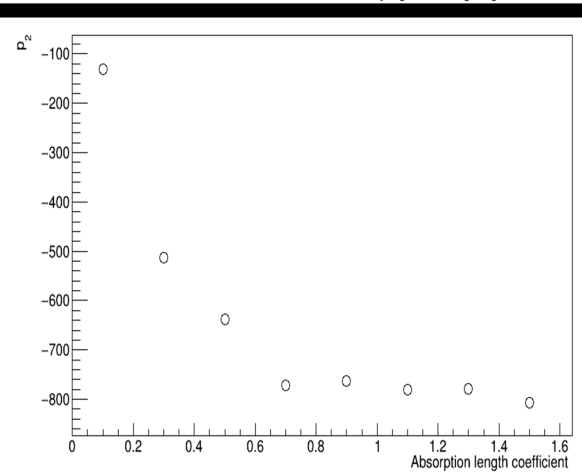

Future work

- Time residuals for diffuser
- LI board R&D (hardware)
- Bottom-up approach for detector systematics:
  - Fewer correlations among nuisance parameters
  - Determine systematics from detector properties such as water quality (scattering, absorption), PMT, etc
  - Better understanding of calibration and detector performance

Summary

- Charge ratio within the beam spot showed good sensitivity to scattering but minimal effect to absorption. Results breaking down at low scattering and high absorption for the wavelength
- Examined the fitting parameters with the scattering and absorption. However, there is still more work to do in order to fully understand which water parameters may be the most useful

Thank you for listening!

Any questions?

UNIVERSITY OF LIVERPOOL

LEVERHULME TRUST

Annual Progress Report presentation

Student: Clément Devanne,

Supervisors: Pr G.Venanzoni, Dr R.Pilato

Motivation for MUonE

Experiment

The g-2 experiment at Fermilab aims to measure the anomalous magnetic moment of the muon aμ

$$a_\mu = \frac{g_\mu - 2}{2}$$

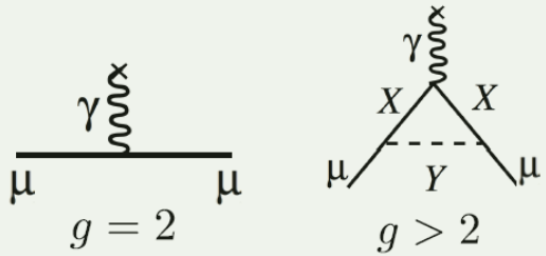

Theory

The different contribution to aμ are:

QED

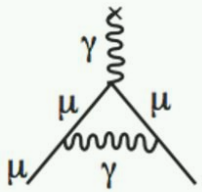

a_μ 99.99%
δa_μ 0.001%

Electroweak

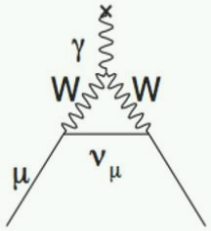

a_μ 1 ppm
δa_μ 0.2%

Hadronic Light-by-Light

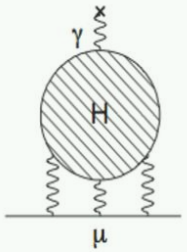

a_μ 1 ppm
δa_μ 16%

Hadronic Vacuum Polarization

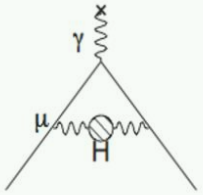

a_μ 59 ppm
δa_μ 84%

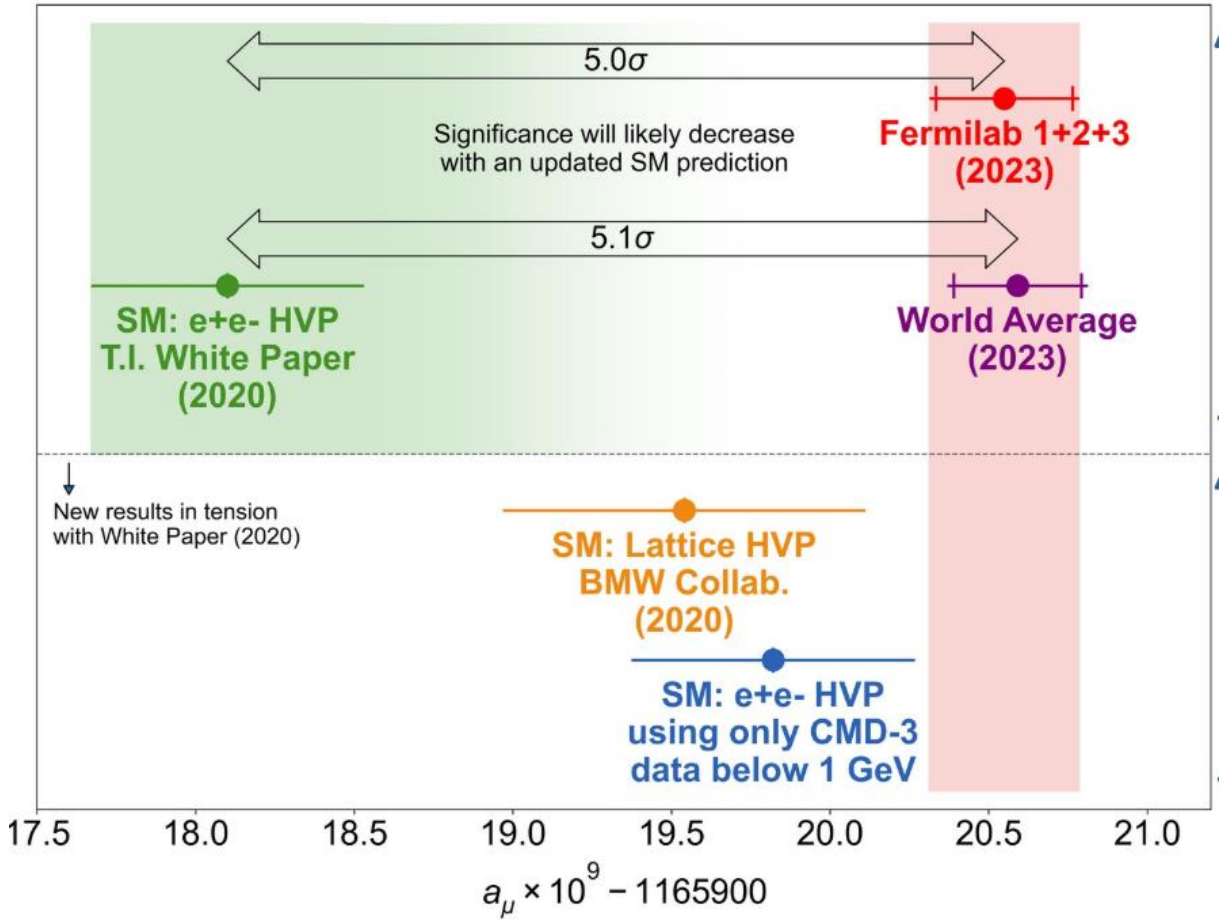

A clarification is needed on the theoretical prediction.

The main source of uncertainty comes from the leading order of the hadronic vacuum polarisation contribution

MUonE

MUonE aims to provide an independent measurement of the contribution from hadronic vacuum polarization at leading order to the muon's anomalous magnetic moment using the scattered angles in a muon-electron elastic interaction.

The running of α is parameterized by $\Delta\alpha$ and can be measured by MUonE, which can be expressed in a leptonic and a hadronic part: $\Delta\alpha = \Delta\alpha_{lep} + \Delta\alpha_{had}$

We then extract the hadronic vacuum polarization leading order using :

$$a_\mu^{HLO} = \frac{\alpha}{\pi}\int_0^1 dx(1-x)\Delta\alpha_{had}$$

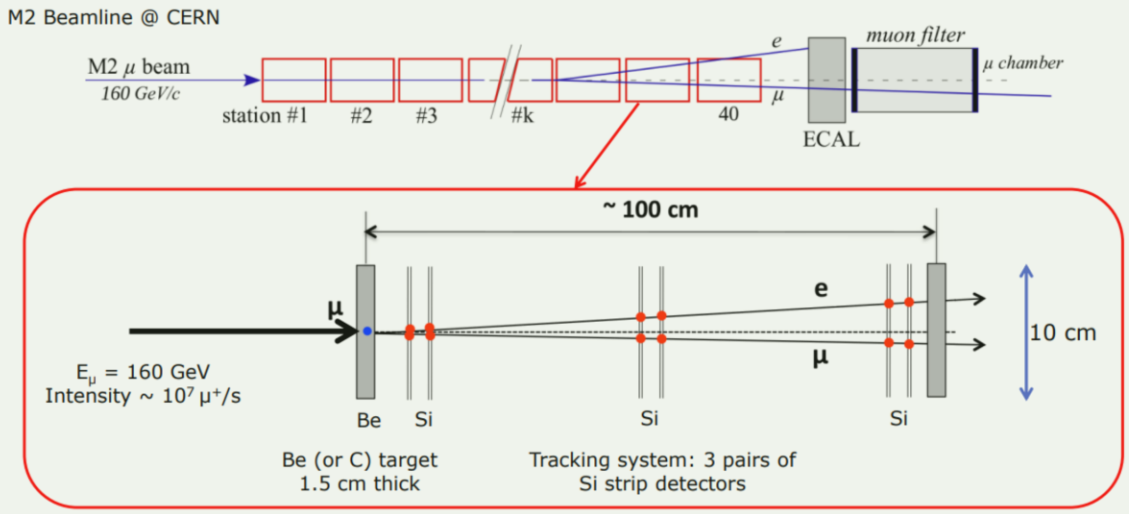

The final goal of MUonE is to get a_μ^{HLO} with ~0.3% statistical error and comparable systematics.

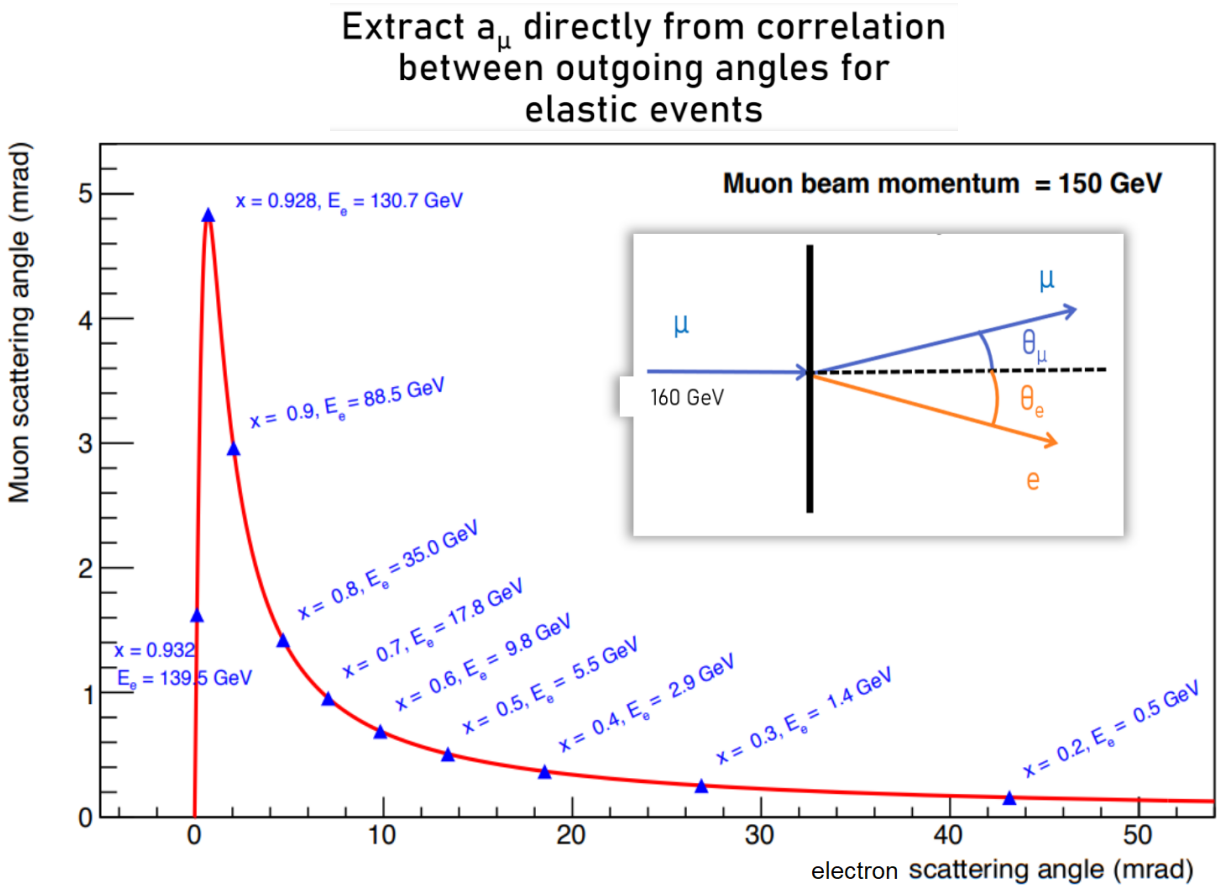

MUonE test run 2023

A three-week test run has been conducted in 2023 with:

- A muon beam provided by the M2 beamline at CERN
- 2 tracking station
- A 2 or 3cm target in Beryllium
- An Electromagnetic Calorimeter

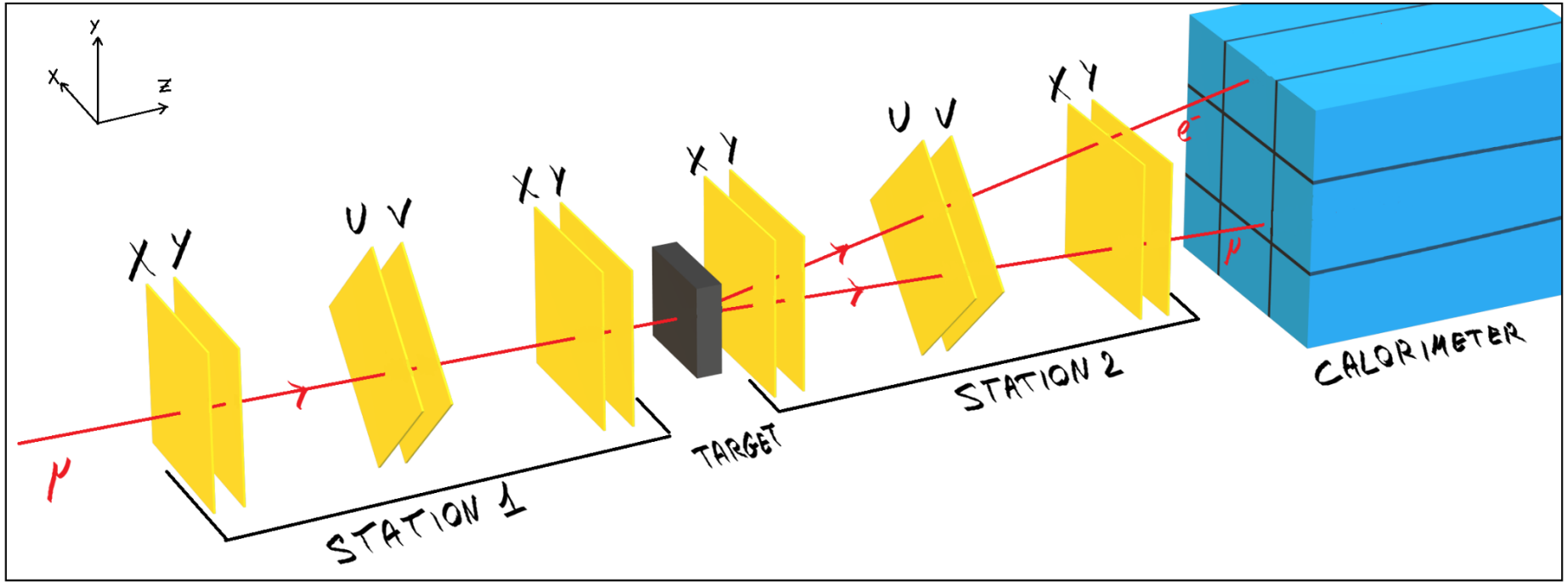

We expect to measure $\Delta\alpha_{lep}$ with O(5%)

Studies of the systematics

Definition of R_{lep}

- $\Delta\alpha_{lep}$ is defined by the equation below, from the theoretical calculation of the leptonic vacuum polarization at 1 loop

$$\Delta\alpha_{lep}(t) = k[f(m_e)+f(m_\mu)+f(m_\tau)]$$

$$f(m) = -\frac{5}{9}-\frac{4}{3}\frac{m^2}{t}+\left(\frac{4}{3}\frac{m^4}{t^2}+\frac{m^2}{3t}-\frac{1}{6}\right)\frac{2}{\sqrt{1-\frac{4m^2}{t}}}ln\left|\frac{1-\sqrt{1-\frac{4m^2}{t}}}{1+\sqrt{1-\frac{4m^2}{t}}}\right|$$

- We use $\Delta\alpha_{lep}$ as input in MESMER, our Monte Carlo event generator, and a fast simulation for the modelisation of the detector effects.

- The ratio R_{lep} is used to visualize easily the effect of an error in the estimation of a systematic, on the extraction of the leptonic running of α

$$R_{lep} = \frac{d\sigma(\Delta\alpha_{lep})}{d\sigma(\Delta\alpha_{lep}=0)} \sim 1+2\Delta\alpha_{lep}$$

Mean Beam Energy shift ± 1GeV

- For the beam energy, a shift (here ±1 GeV) can be easily identified from the data in both $R_{lep}(\theta_e)$ and $R_{lep}(\theta_{muon})$

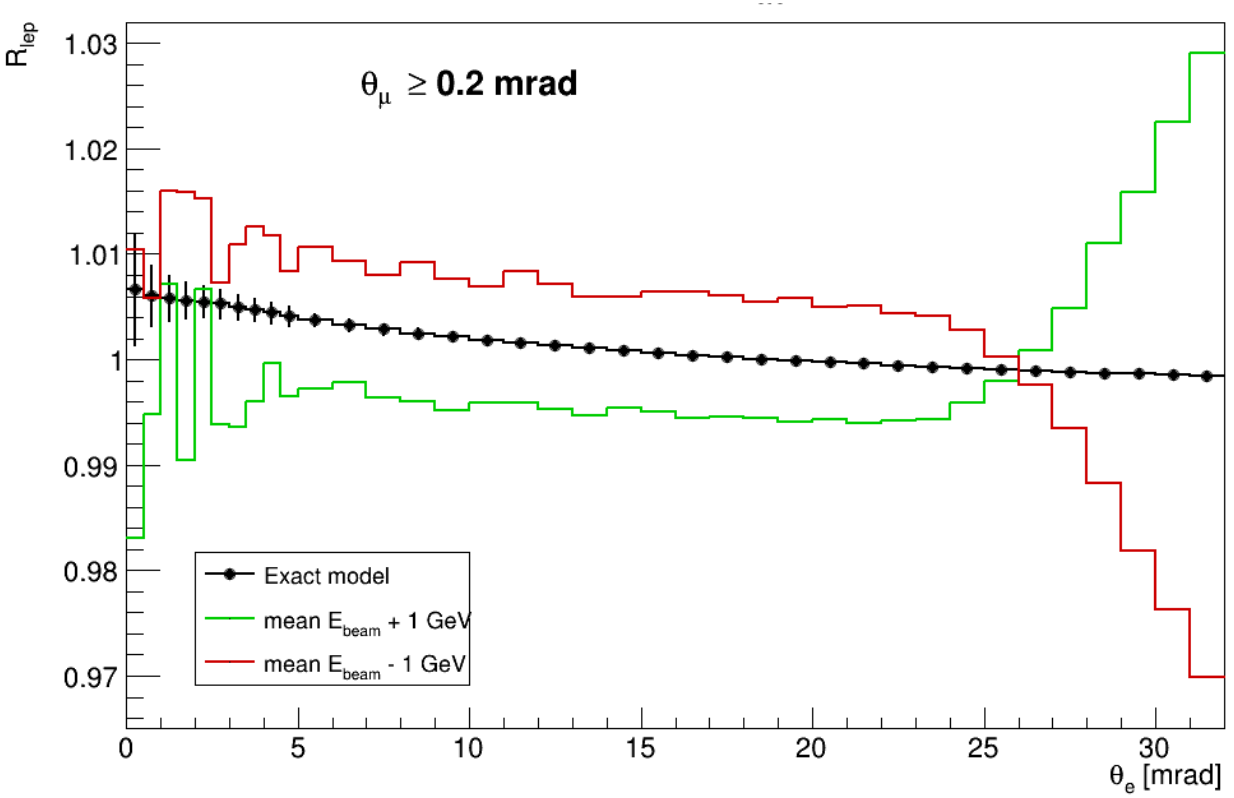

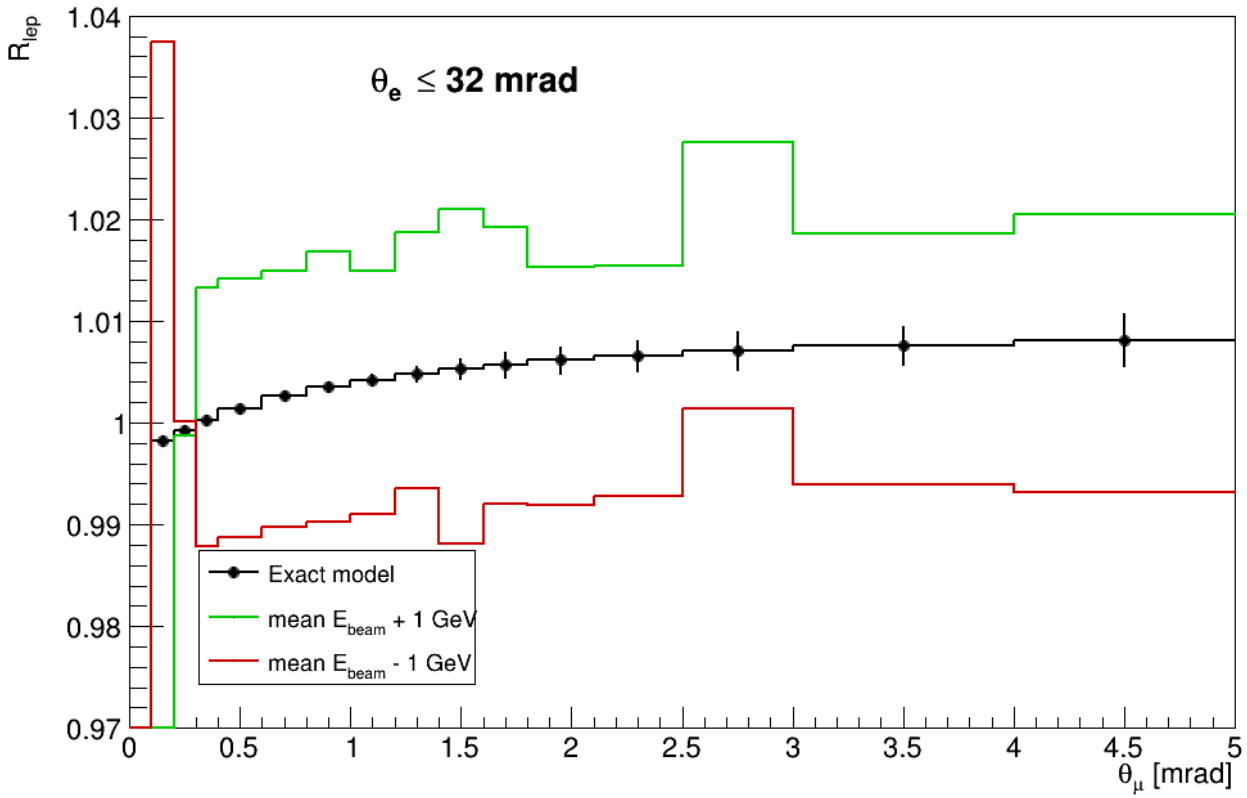

- *Lumi = 1pb^{-1}*

Data – MC comparison

Procedure

We produce histograms from data (test run summer 2023) and Monte Carlo samples, and apply some selection cuts:

- Golden event (1 track in, 2 tracks out)
- Vertex $\chi^2 < 150$
- $\theta_e < 32$ mrad
- $\theta_\mu > 0.2$ mrad
- $|Z_{vertex} - Z_{target}| < 3$ cm
- |Acoplanarity| < 1 rad (the cut is needed because the elastic events are expected to be planar)

Data

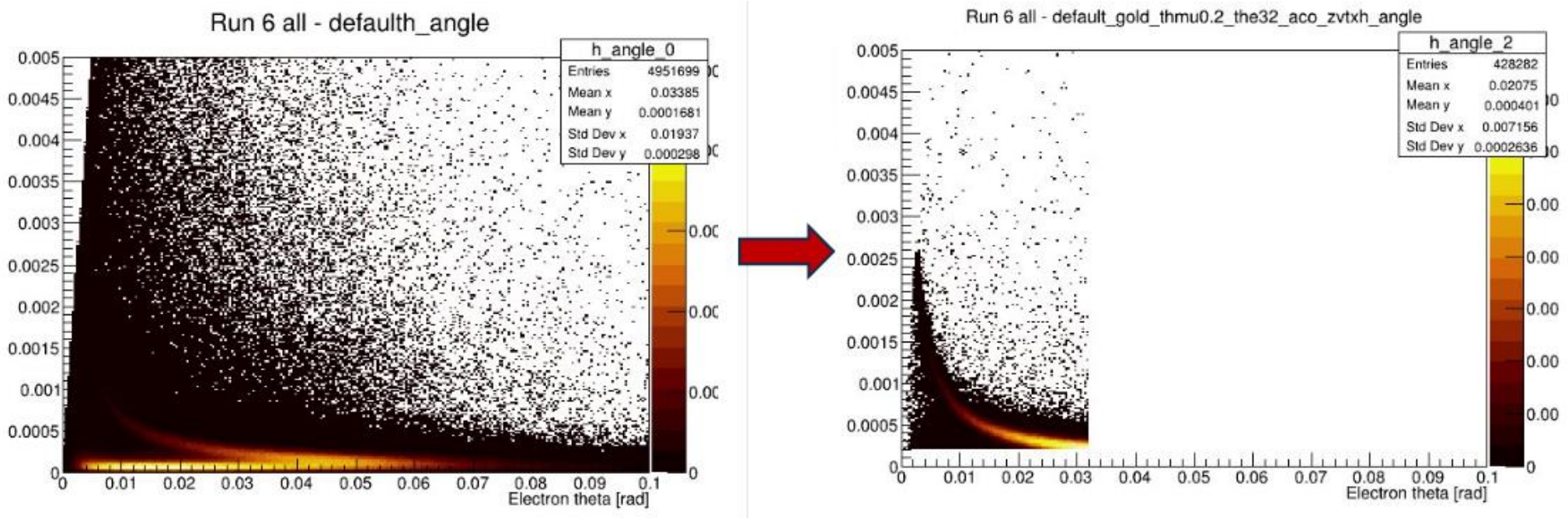

Comparison

We then compare the ratio R = MC/data for some quantities,

We are doing a **shape** analysis, to do so we use the intergral of the histograms and normalize them

Muon angle

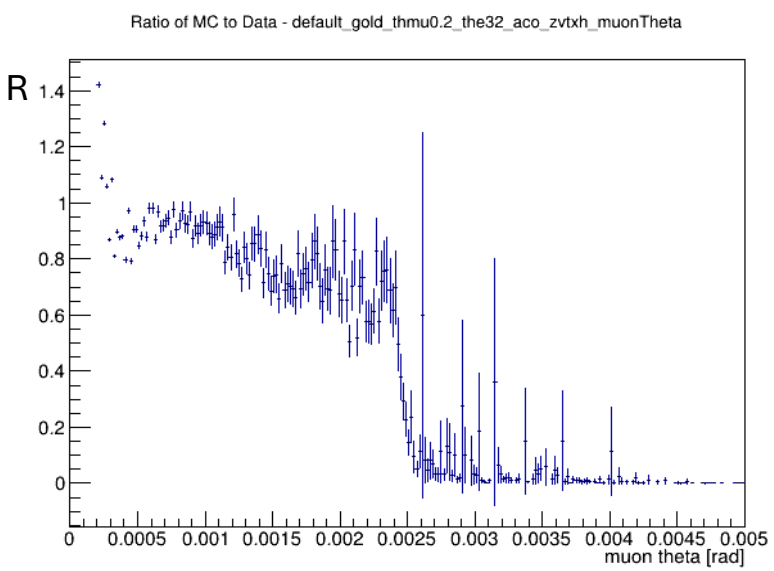

Electron Angle

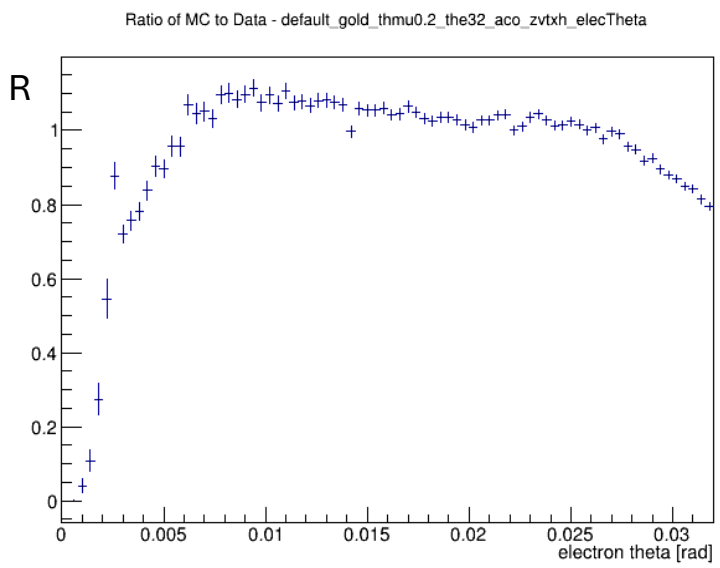

Opening Angle

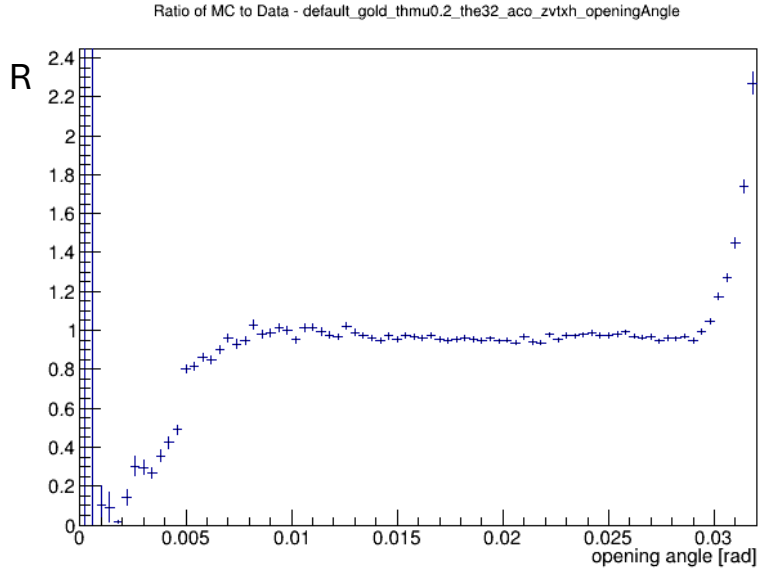

Comparison

We then compare the ratio R = MC/data for some quantities,

We are doing a **shape** analysis, to do so we use the Intergral of the histograms and renormalise them

Muon angle

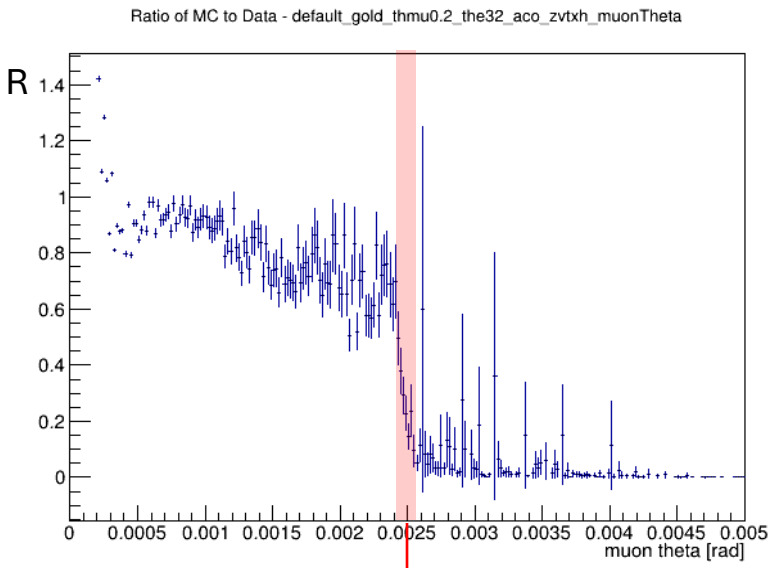

Electron Angle

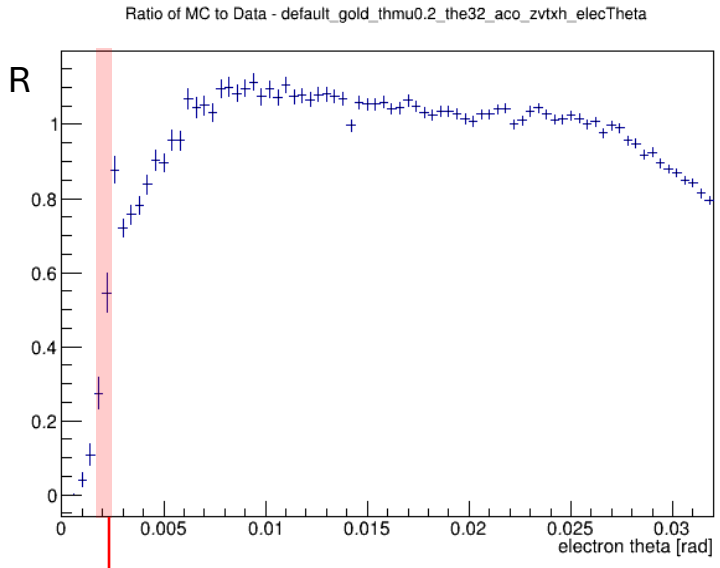

Opening Angle

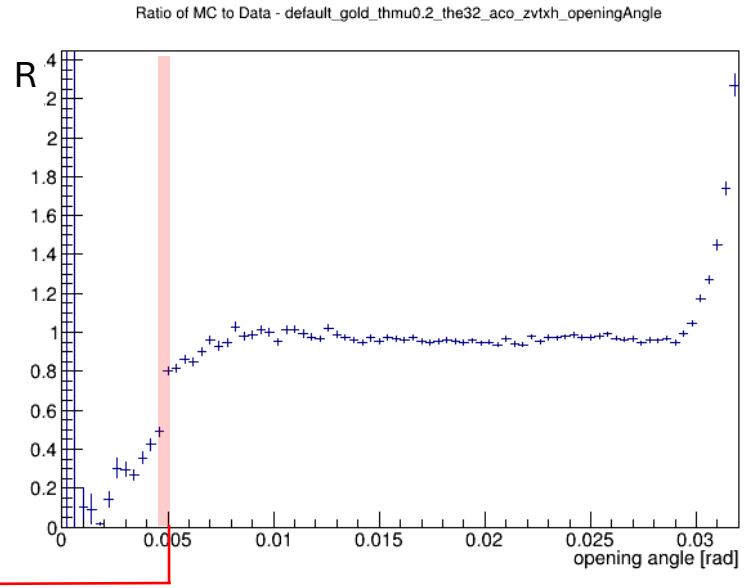

Drop around 2.5mrad for both muon and electron angle (5 for opening angle) because we don't have a proper particle identification.

Here we assume the track with the biggest scattered angle is always the electron and the smallest the muon. This is not true for this region

Comparison

We then compare the ratio R = MC/data for some quantities,

We are doing a **shape** analysis, to do so we use the Intergral of the histograms and renormalise them

Muon angle

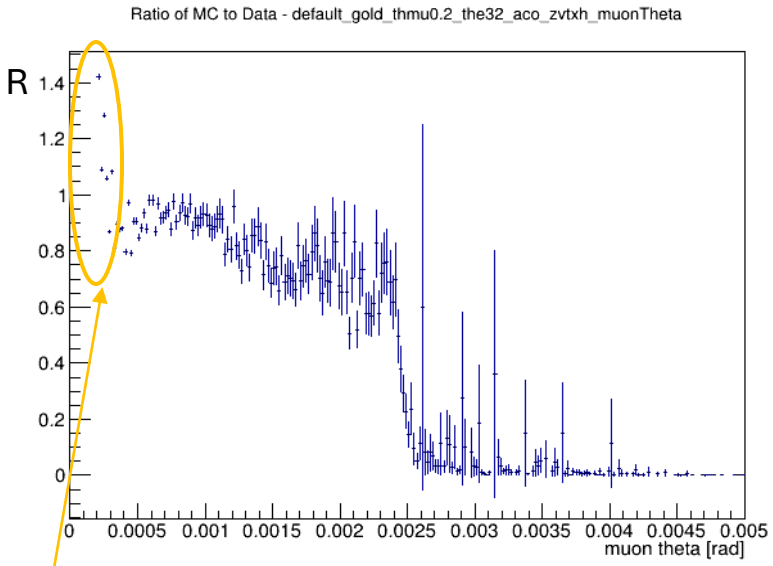

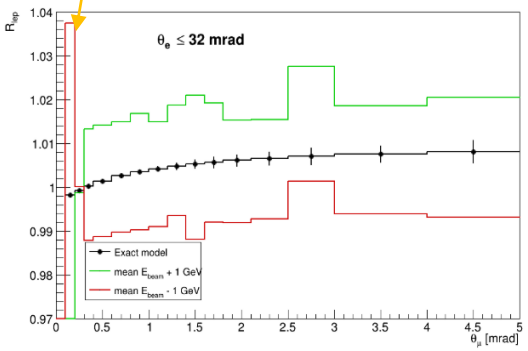

Electron Angle

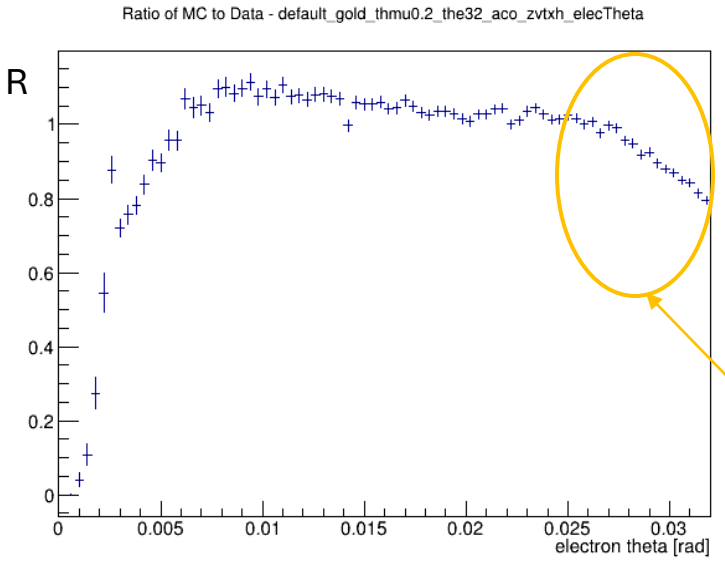

Opening Angle

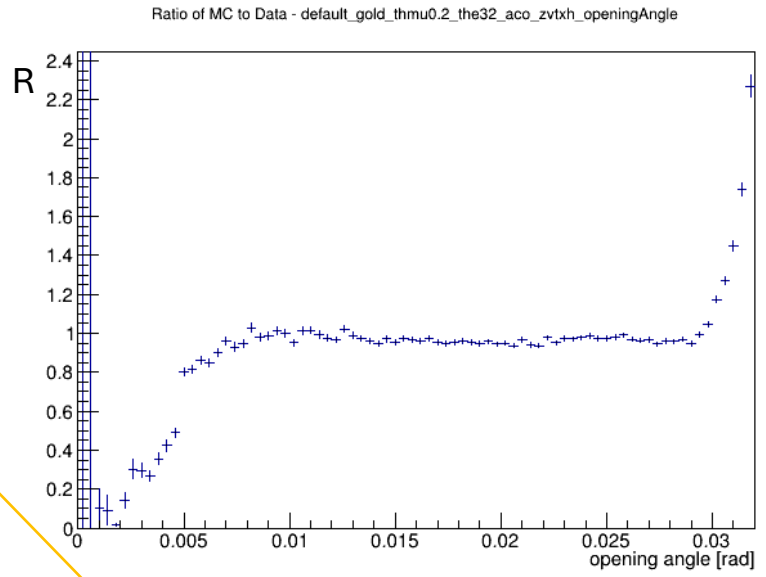

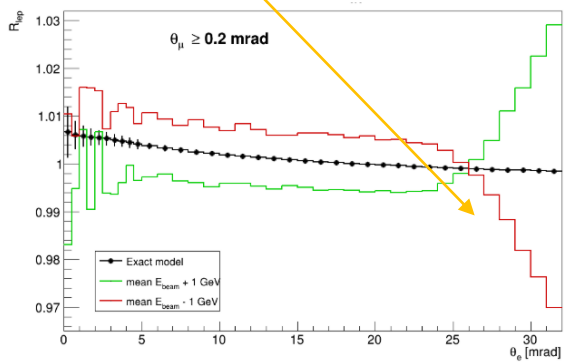

The large slopes at the very low muon angle and large electron angle are compatible with some systematics effect.

Here we compare with a shift in the Energy beam from fastSim *(care the black slope in fastSim is due to the running of alpha leptonic, not in our data)*

Comparison

We then compare the ratio R = MC/data for some quantities,

We are doing a **shape** analysis, to do so we use the Intergral of the histograms and renormalise them

Muon angle

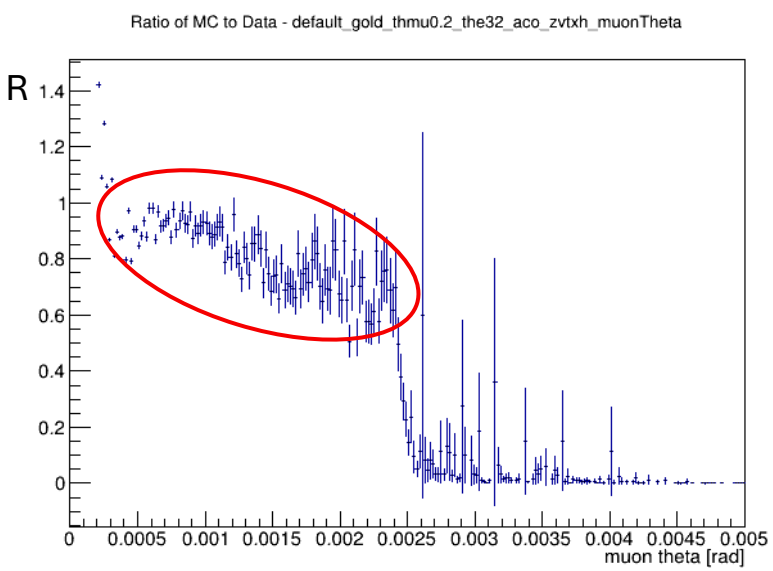

Electron Angle

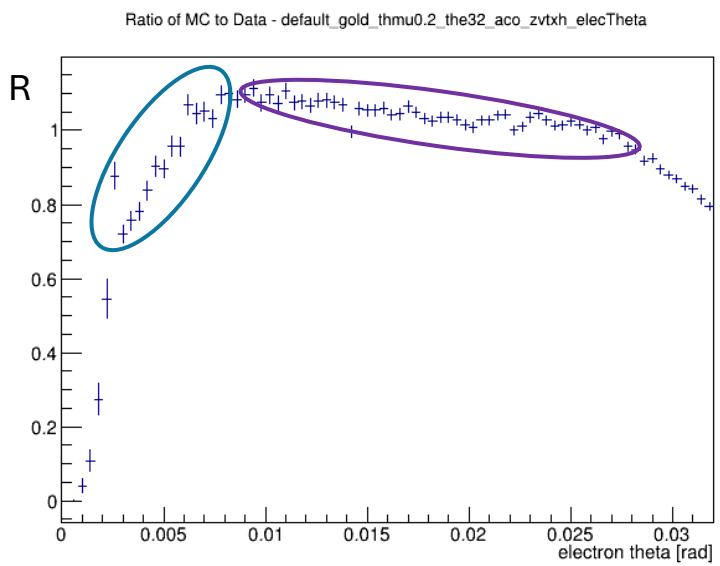

Opening Angle

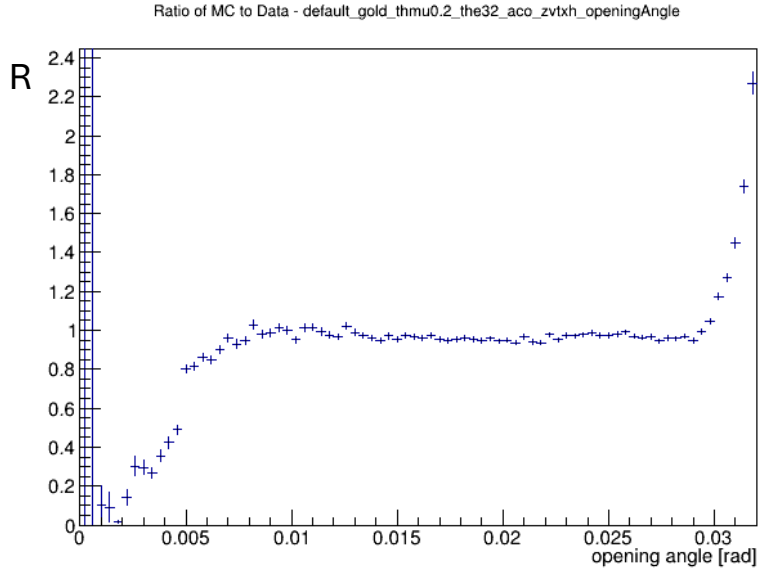

But there is some unexplain behavior:

- what is the downward slope for muon angle in ~[0.25 ; 2.5] mrad ?
- what is this large upward slope for electron in ~[2.5 ; 7] mrad ?
- what is the slight downward slope for electron in ~[7 ; 25] mrad ?

Conclusion

- The data-Monte Carlo comparison needs improvement and progress are made:
    - Adding background to Monte Carlo
    - Improving the reconstruction algorithm
    - Analysis on the selection criteria

- I am currently working on the selection criteria

Quantum Error Correction and Applications

Supervisors: Prof. Costas Andreopoulos, Dr. Gabriel Perdue and Dr. Doğa Murat Kürkçüoğlu

Sam Godwood
sgsgodwo@liverpool.ac.uk
21/06/24

LIV.INNO

SQMS

UNIVERSITY OF LIVERPOOL

Quantum Computing Fundamentals

- A two-level quantum system (qubit) is the basic unit of information:
  - N qubits → 2^N Hilbert space $|0\rangle = \begin{pmatrix}1\\0\end{pmatrix}, |1\rangle = \begin{pmatrix}0\\1\end{pmatrix}$
  - $\alpha|0\rangle + \beta|1\rangle,\ \alpha, \beta \in \mathbb{C},\ |\alpha|^2 + |\beta|^2 = 1$

- Unitary operators (gates) manipulate states:

$$X = \begin{pmatrix}0 & 1\\1 & 0\end{pmatrix},\ \text{e.g. } \mathrm{X}|0\rangle = |1\rangle, \qquad Z = \begin{pmatrix}1 & 0\\0 & -1\end{pmatrix},\ \text{e.g. } \mathrm{Z}|1\rangle = -|1\rangle, \qquad \mathrm{R_y}(\theta) = \begin{pmatrix}\cos(\frac{\theta}{2}) & -\sin(\frac{\theta}{2})\\ \sin(\frac{\theta}{2}) & \cos(\frac{\theta}{2})\end{pmatrix}$$

- Measurements give 1 bit of information:
  - Described a set of $\{M_i\}$ operators $\sum_i M_i^\dagger M_i = I$
  - Probability of outcome i, $p_i = \langle\psi|M_i^\dagger M_i|\psi\rangle$, post measurement state $\frac{M_i|\psi\rangle}{\sqrt{p_i}}$
  - E.g. $M_0 = |0\rangle\langle 0|, M_1 = |1\rangle\langle 1|$

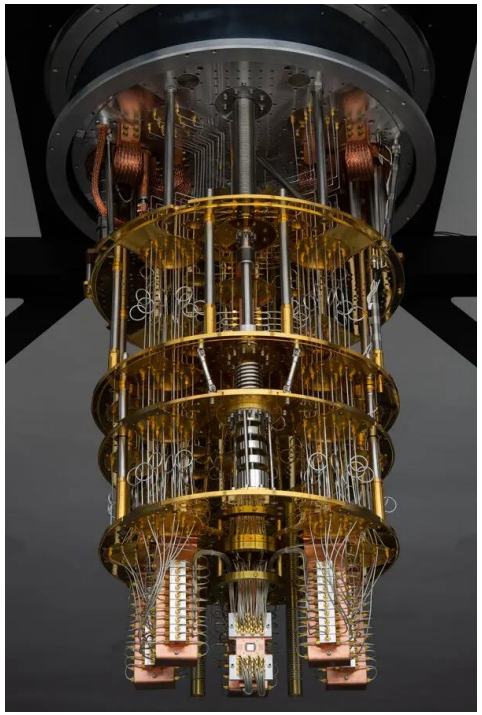

- Quantum computers are well suited for simulating quantum systems
  - But… Quantum Computers are inherently noisy
  - Qubits are subject to continuous errors **AND** decoherence
  - For problems of interest, quantum error correction (QEC) is needed

Sam Godwood
sgsgodwo@liverpool.ac.uk
21/06/24

LIV.INNO SQMS UNIVERSITY OF LIVERPOOL

Quantum Error Correction

- Goal:
  - Correct against errors without destroying encoded information
- How?
  - Encode redundancy, combining physical qubits to create logical qubits
  - Use ancilla qubits to detect errors

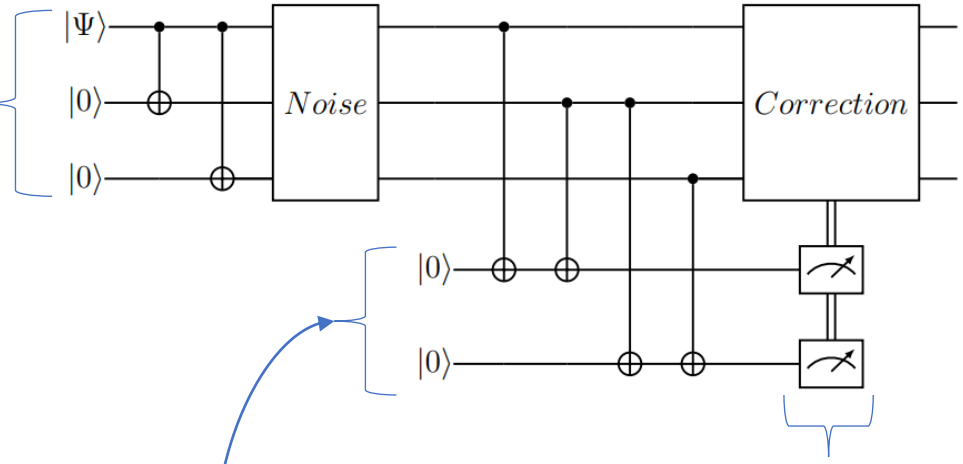

Toy Example: 3 qubit code

- Encode 3 physical qubits into a logical qubit → $|0\rangle_L = |000\rangle, |1\rangle_L = |111\rangle$
- 2 ancilla qubits to detect bit flips (X errors)
- Measure ancilla qubits → Apply corrections based on most likely error

We simulate for error set $\{X_1, X_2, X_3\}$, each error occurs with probability p:

- Final state fidelity ($F = |\langle\psi'|\psi\rangle|^2$) improved provided $p < \frac{1}{2}$
- But this is **VERY** unrealistic
- Break even: Logical error rate lower than physical error rate

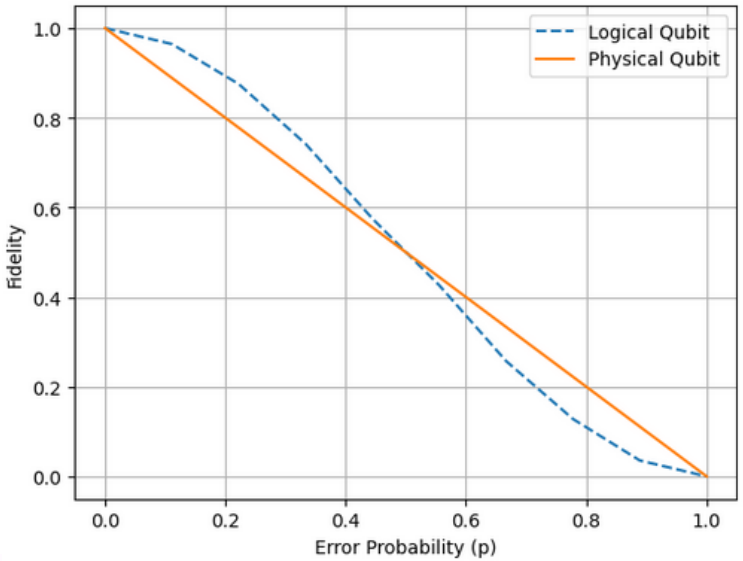

Sam Godwood
sgsgodwo@liverpool.ac.uk
21/06/24

LIV.INNO SQMS UNIVERSITY OF LIVERPOOL

Quantum Noise

- Noise modelled by Kraus operators K_i, $\sum_i K_i^\dagger K_i = 1$
- Density matrix $\rho = |\psi\rangle\langle\psi|$ → States evolve via $\rho' = \sum_i K_i^\dagger \rho K_i$,
- Main noise channels:
  - Depolarizing Channel:

$$K_0 = \sqrt{1-p_1}\,I, \qquad K_i = \sqrt{\frac{p_1}{3}} \sum_{\sigma \in \{X,Y,Z\}} \sigma$$

  - SPAM Channel:

$$K_0 = \sqrt{1-p_2}\,I, \qquad K_i = \sqrt{p_2}\,X$$

  - Thermal Decoherence:

$$K_0 = |0\rangle\langle 0| + \sqrt{1-p_{T_1}}\,|1\rangle\langle 1|, \qquad K_1 = \sqrt{P_{T_1}}\,|0\rangle\langle 1|$$

  - Phase Damping:

$$K_0 = \sqrt{1-2p_{T_2}}\,I, \quad K_1 = \sqrt{p_{T_2}}\,|0\rangle\langle 0|, \quad K_2 = \sqrt{p_{T_2}}\,|1\rangle\langle 1|$$

- We simulate the 3 qubit code under these noise models
  - Performance becomes severely degraded
  - We need codes that protect against **ALL** errors

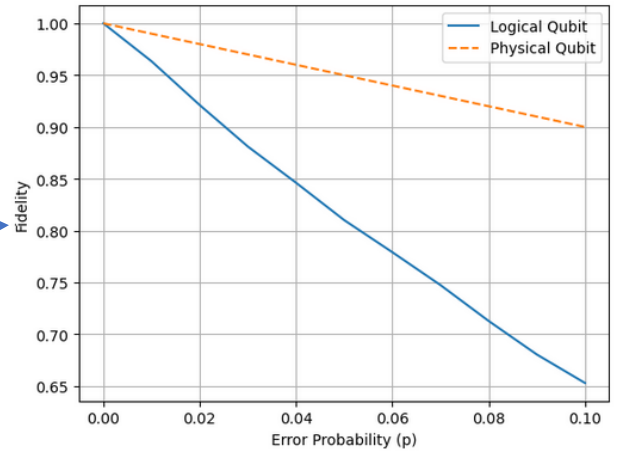

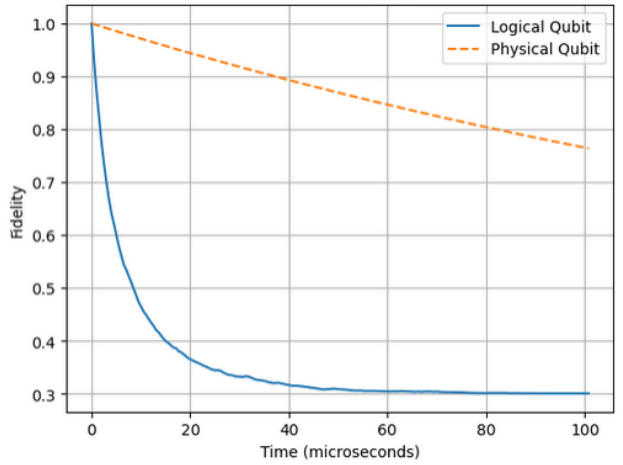

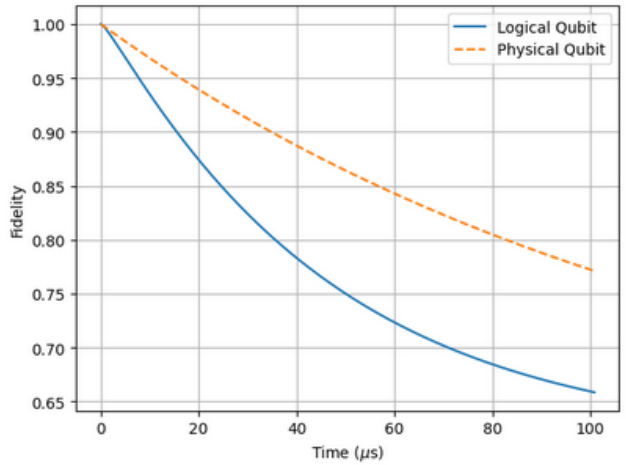

Sam Godwood
sgsgodwo@liverpool.ac.uk
21/06/24

LIV.INNO SQMS UNIVERSITY OF LIVERPOOL

Surface Code

- Logical qubit on a lattice
  - Qubits are placed at each lattice site
  - Qubits classified as physical, X ancilla or Z ancilla
  - Error correction 'cycle' → One round of ancilla measurements
  - Z ancilla forces neighbouring qubits into a ± 1 eigenstate of $Z_a Z_b Z_c Z_d$
  - X ancilla forces neighbouring qubits into a ± 1 eigenstate of $X_a X_b X_c X_d$
  - Errors cause change in measurement outcomes, e.g.

$$(Z_a Z_b Z_c Z_d) X_a |\psi\rangle = -X_a (Z_a Z_b Z_c Z_d) |\psi\rangle = -X_a |\psi\rangle$$

7 Qubit Surface Code

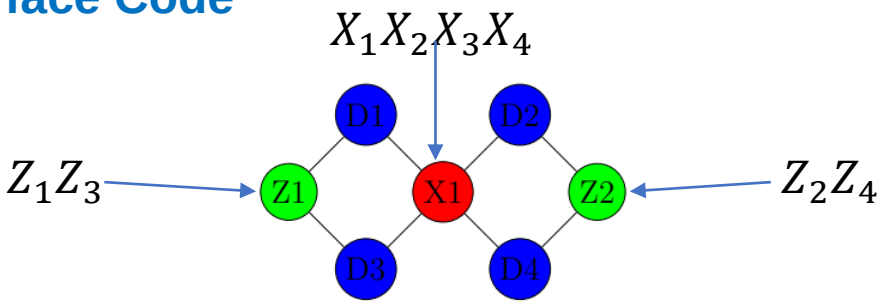

$$|0\rangle_L = \frac{1}{\sqrt{2}}(|0000\rangle + |1111\rangle), \; |1\rangle_L = \frac{1}{\sqrt{2}}(|0101\rangle + |1010\rangle)$$

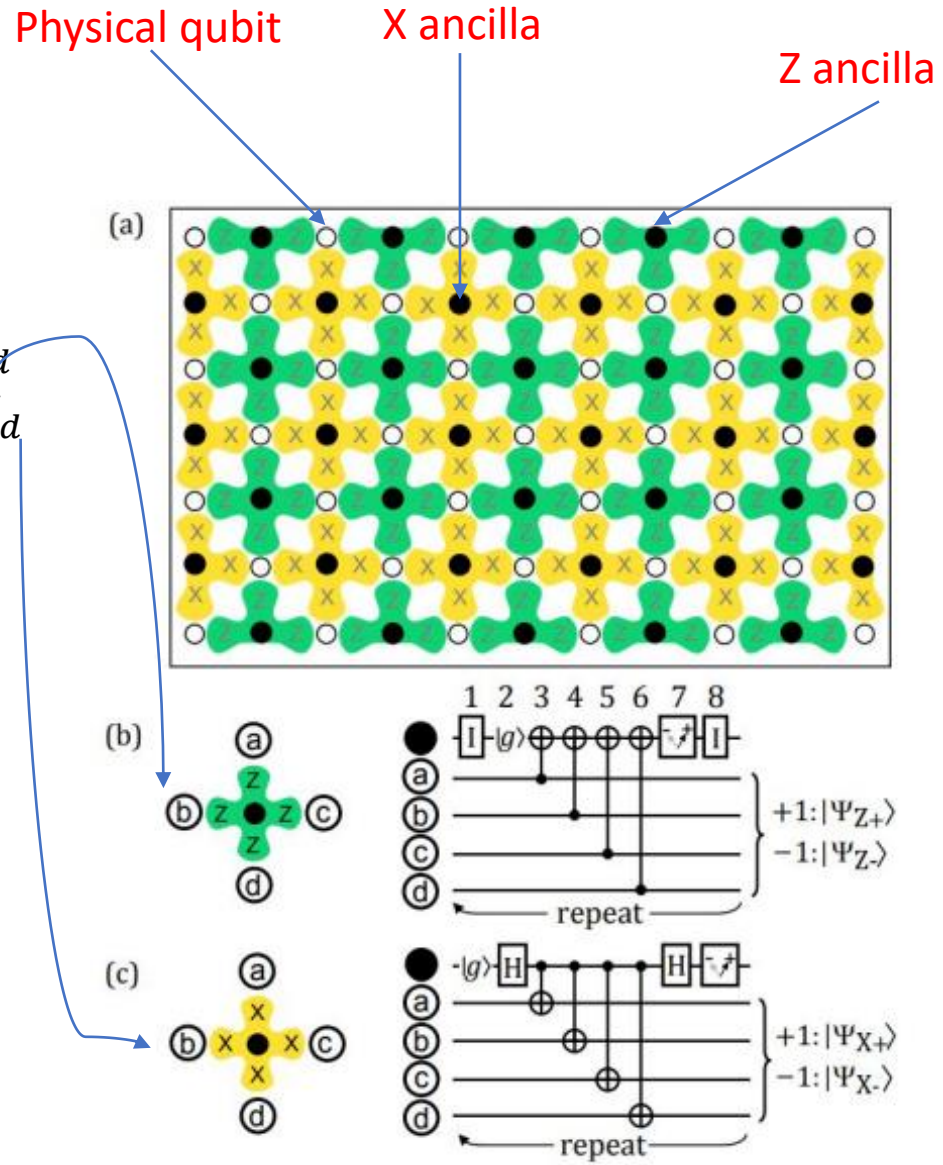

arxiv:1208.0928

Sam Godwood
sgsgodwo@liverpool.ac.uk
21/06/24

LIV.INNO SQMS UNIVERSITY OF LIVERPOOL

7 Qubit Surface Code

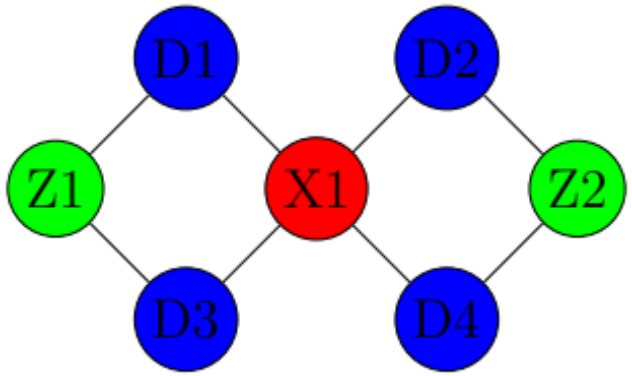

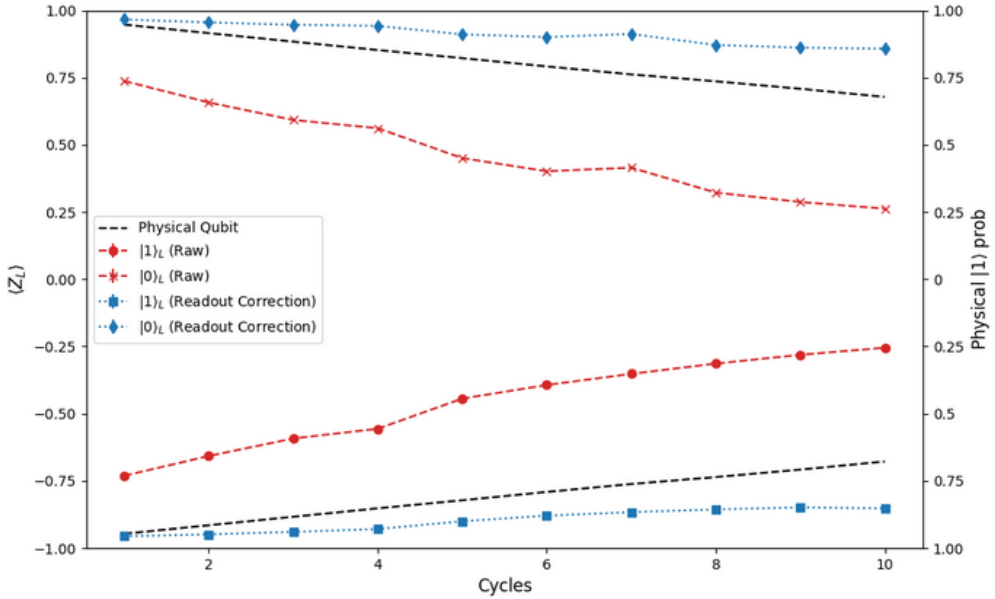

- We simulate repeated error correction cycles on IBM's 'FakeOslo'
- Perform readout error correction → Discard shots where errors are detected, or results lie outside of code space
- Calculate $\langle Z_L \rangle$ → Compare to physical $|1\rangle$ probaility
- We show improved lifetime of logical qubit vs physical qubit
- But… the probability of detecting no errors decreases exponentially

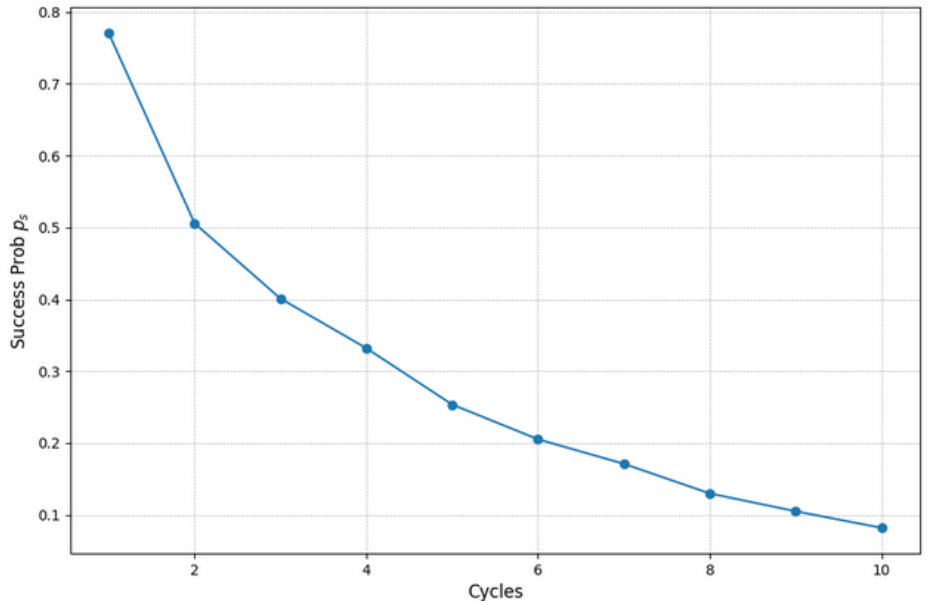

Sam Godwood
sgsgodwo@liverpool.ac.uk
21/06/24

LIV.INNO SQMS UNIVERSITY OF LIVERPOOL

Variational Methods as a Proof of Principle

➢ Variational Methods:

- Consider a Hamiltonian $H|\phi\rangle = E|\phi\rangle$ … we know $\langle\psi|H|\psi\rangle \geq E$
- Aim is to minimize $\langle\psi|H|\psi\rangle$
- Use a parameterized quantum circuit to compute $\langle\psi(\theta)|H|\psi(\theta)\rangle$
- Optimize θ classically

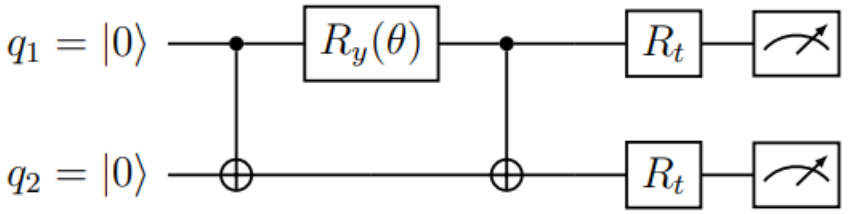

Logical Circuit

➢ Hydrogen molecule Hamiltonian:

$$H = g_0 I_1 I_2 + g_1 Z_1 I_2 + g_2 I_1 Z_2 + g_3 Z_1 Z_2 + g_4 X_1 X_2$$

➢ The [4,2,2] code:

$$|00\rangle_L = \frac{1}{2}(|0000\rangle + |1111\rangle)\,,\ |01\rangle_L = \frac{1}{2}(|0011\rangle + |1100\rangle),$$

$$|10\rangle_L = \frac{1}{2}(|0101\rangle + |1010\rangle),\ \ |11\rangle_L = \frac{1}{\sqrt{2}}(|0110\rangle + |1001\rangle)$$

➢ Trial ansatz $|\psi(\theta)\rangle = e^{-\frac{i\theta Y_1 X_2}{2}}|00\rangle$

Physical Circuit

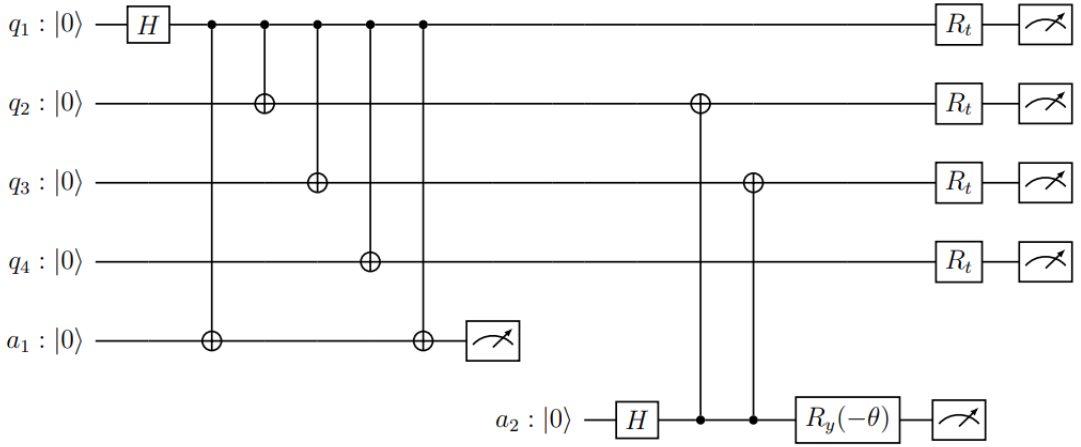

Sam Godwood
sgsgodwo@liverpool.ac.uk
21/06/24

LIV.INNO SQMS UNIVERSITY OF LIVERPOOL

Variational Methods as a Proof of Principle

- → Readout error correction
- → Calculate expectation value of each term in H
- → Minimize each term in H

- ➢ Sample $\theta \in \{-\pi, \pi)$:
  - Encoding improves accuracy for each term
- ➢ Minimization procedure for θ:
  - Encoding improves accuracy for every internuclear separation

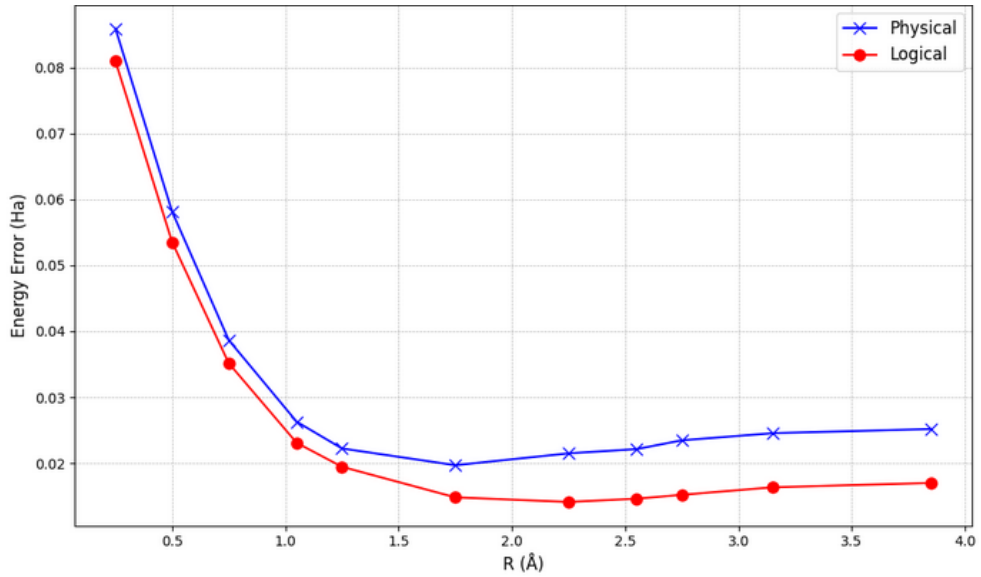

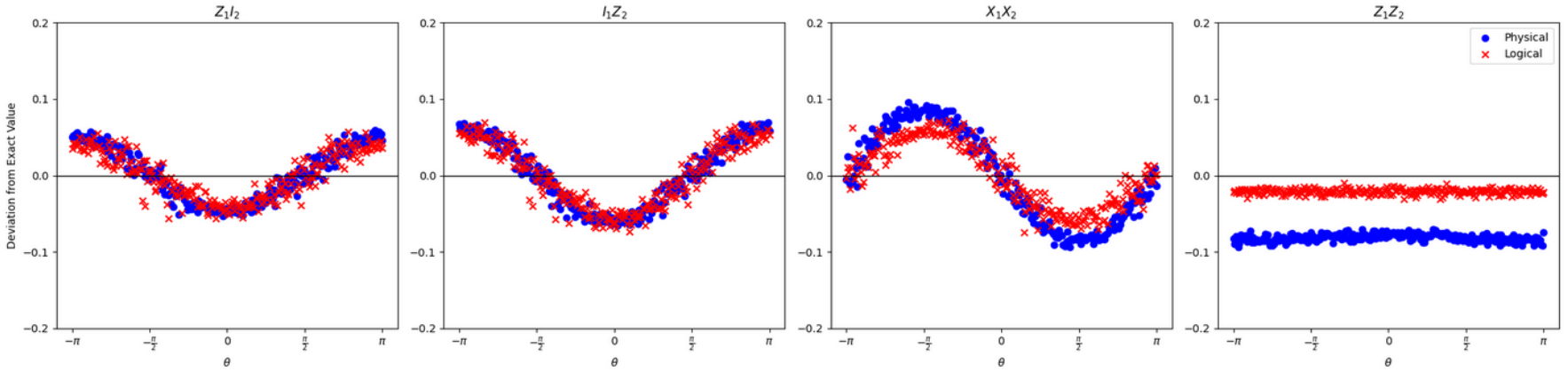

Sam Godwood
sgsgodwo@liverpool.ac.uk
21/06/24

LIV.INNO SQMS UNIVERSITY OF LIVERPOOL

Summary and Future Work

- Quantum Computers offer powerful ways to tackle classically intractable problems in physics
  - But… QEC is needed for problems of interest
- We have shown small QEC codes can increase life time and improve accuracy on current devices
  - But… these codes are very limited

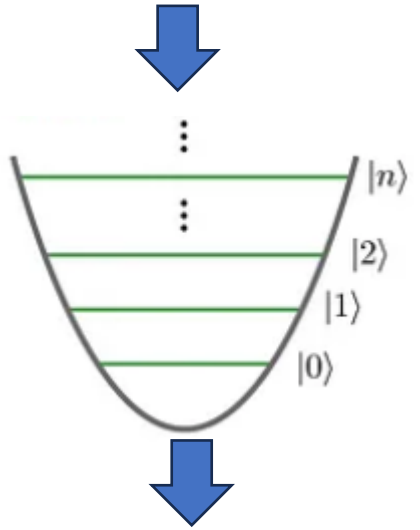

- What are the most promising options?
  - Encoding a logical qubit into a single continuous variable (CV) system (Harmonic oscillator)
  - Can be realised with long lifetime SRF Cavities (Fermilab SQMS)
  - E.g. GKP codes → Already achieved break even experimentally

- There are many open questions:
  - How feasible is combining CV codes with discrete variable codes?
  - Which discrete variable codes should be used? → Analysis of noise propagation and thresholds
  - Can we improve the accuracy of simulations with these codes?
  - Possible analysis of multi-mode, oscillator-oscillator codes etc…

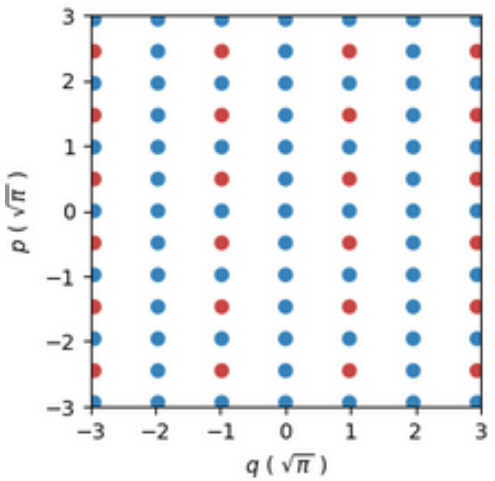

Sam Godwood
sgsgodwo@liverpool.ac.uk
21/06/24

LIV.INNO SQMS UNIVERSITY OF LIVERPOOL

BACKUP

Sam Godwood
sgsgodwo@liverpool.ac.uk

Neutrino Interaction Modelling

- Uncertainties in modelling neutrino interactions are one of the main limiting factors for precision neutrino oscillation measurements (CP, mass ordering, searches for steriles) and other BSM searches at neutrino experiments
- **Difficult** problem at the GeV scale (e.g. Dune)
  - Multiple reaction mechanisms and transitions from non-perturbative to perturbative regimes.
  - Dense nuclear environment impacts: Binding, nucleon-nucleon correlations, intranuclear rescattering.
- Limitations of Current Models:
  - No comprehensive theory to fully explain neutrino interactions
  - Dependence on simulations blending theoretical inputs with limited experimental data
  - Classically, exact treatments of scattering scale exponentially in the nucleon number due to the Fermion sign problem.

We need event generators to realise events, so that we can perform the same analysis on simulation as experimental data.

‘Overarching’ aim:
Can utilize quantum advantage and interface between quantum processors and GENIE?

Genie
UNIVERSAL NEUTRINO GENERATOR & GLOBAL FIT

Sam Godwood
sgsgodwo@liverpool.ac.uk
21/06/24

LIV.INNO SQMS UNIVERSITY OF LIVERPOOL

Superconducting Qubits

- SQMS qubits use superconducting technologies:
  - "2D": arrays of superconducting transmons
  - "3D": superconducting transmons coupled to a resonator cavity (main focus)

Taken from Anna Grassellino - SQMS

1. LC circuit with Josephson junction

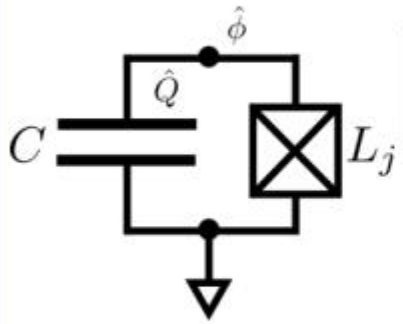

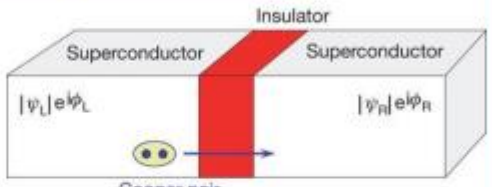

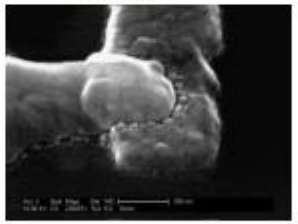

"Transmon" qubits

J. Koch et al, Phys. Rev. **A** 76, 042319 (2007)

+

2. Resonators (cavities)

2D

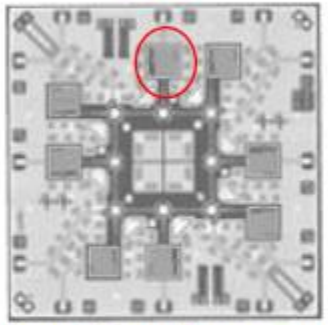

Rigetti 8-qubit processor

$Q \sim 10^5$

$T_{coherence} \sim 0.000001$ s

M. Reagor et al, Science Advances, Vol.4, no. 2, (2018)

3D

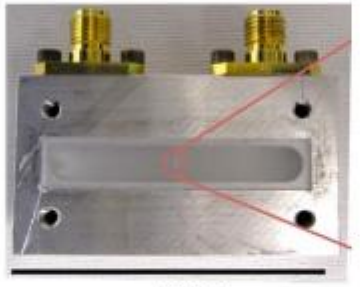

3D transmon

$Q \sim 10^8$

$T_{coherence} \sim 0.001$ s

H. Paik et al, Phys. Rev. Lett. 107, 240501 (2011)

Fermilab SRF resonators

$Q > 10^{10}$

$T_{coherence} > 1$ s

A. Romanenko et al, Phys. Rev. Appl. 13, 134052 (2020)

Sam Godwood
sgsgodwo@liverpool.ac.uk
21/06/24

LIV.INNO SQMS UNIVERSITY OF LIVERPOOL

Determination of the Dipion Contribution to the Muon g-2 with the KLOE Detector

Supervised by:
Graziano Venanzoni
Fedor Ignatov
Paolo Beltrame

UNIVERSITY OF LIVERPOOL

LEVERHULME TRUST

Determine a_μ^{HLO} by relating HLO contribution to cross section of $\pi\pi\gamma$

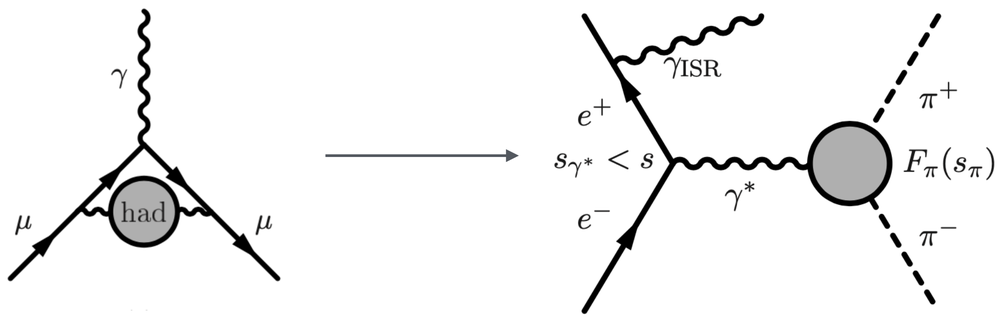

$$a_\mu^{\mathrm{HLO}} = \frac{\alpha^2}{3\pi^2}\int_{M_\pi^2}^{\infty}\frac{K(s)}{s}R(s)ds$$

$$\sigma_{\pi\pi(\gamma)} = \sigma_{\mu\mu(\gamma)}\frac{d\sigma_{\pi\pi\gamma}/ds'}{d\sigma_{\mu\mu\gamma}/ds'} = \frac{4\pi\alpha^2}{3s'}(1+2m_\mu^2/s')\beta_\mu\frac{d\sigma_{\pi\pi\gamma}/ds'}{d\sigma_{\mu\mu\gamma}/ds'}$$

$$R(s) = \frac{\sigma^0(e^+e^- \to \text{hadrons}(+\gamma))}{\sigma_{\text{pt}}}$$

- At 73%, $\pi^+\pi^-$ dominate the lowest order hadronic contribution at low energy, where pQCD is not applicable
- Scan over an energy range from the pion threshold and up to $\sqrt{s} \sim 1$ GeV by using ISR events
- Ongoing KLOE analysis plans to reduce the total uncertainty on a_μ^{HLO} by approximately a factor of 2 by using full available dataset

Blinding

- Reduce bias towards the expected value of a_μ on behalf of the team
- First KLOE analysis to be performed blinded and must be done on software level
- Change the cross section slightly by removing a small amount (few %) of random events based on the momentum transfer Q^2, whilst leaving other distributions unchanged. Done by generating random efficiencies, ε_i , that determines the percentage of events to remain in a specific bin of $Q^2_{\pi\pi}$ or $Q^2_{\mu\mu}$
- A check was performed on $\pi\pi\gamma$ and $\mu\mu\gamma$ events to see whether or not blinding can be undone by exploiting the properties of the blinding strategy and check the relative difference between a_μ and the blinded value α_μ
-

$$\frac{d\sigma_{\pi\pi\gamma}/dQ^2_{\pi\pi}\Big|_{\pi\pi\text{ blind}}}{d\sigma_{\mu\mu\gamma}/dQ^2_{\mu\mu}\Big|_{\mu\mu\text{ blind}}}$$

Correct value

$$\frac{\alpha_\mu - a_\mu}{a_\mu} \approx 6\,\%$$

$$\frac{d\sigma_{\pi\pi\gamma}/dQ^2_{\pi\pi}}{d\sigma_{\mu\mu\gamma}/dQ^2_{\pi\pi}}\Bigg|_{\pi\pi\text{ blind}}$$

Wrong ratio
Same ROOT-file

$$\frac{\alpha_\mu - a_\mu}{a_\mu} \approx 15\,\%$$

$$\frac{d\sigma_{\pi\pi\gamma}/dQ^2_{\pi\pi}}{d\sigma_{\mu\mu\gamma}/dQ^2_{\mu\mu}}\Bigg|_{\pi\pi\text{ blind}}$$

Correct ratio
Same ROOT-file

$$\frac{\alpha_\mu - a_\mu}{a_\mu} < 1\,\%$$

- A solution to this problem is to have blinded rootfiles only be available at the very end after all analysis steps have been signed off. This way, corrections are found with working (unblinded) rootfiles but only applied on blinded rootfiles
- Approach requires honesty from the group, like with other experiments

Detector tuning

- Agreement between data and Monte Carlo is important for precision measurements
- Compare various data and MC variables relating to momentum, position, tracks and clusters and group distributions into three preliminary categories based on the agreement
- Performed on 7 pb^{-1} of $\pi^+\pi^-\pi^0$ data collected in 2005 ~3.5 million events, chosen due to having pions in the final state and being a background
- Investigations are still underway to determine the cause of the discrepancies

STENTU Variables Overview

Variable	Consistent	Inconsistent	V.Inconsistent
Momentum			
p_x	•		
p_y	•		
p_z		•	
$p_t = \sqrt{p_x^2 + p_y^2}$:		•	
$p_{tot} = \lvert\boldsymbol{p}_+\rvert + \lvert\boldsymbol{p}_-\rvert$:		•	
Position			
x_{first}		•	
y_{first}	•		
z_{first}		•	
x_{last}		•	
y_{last}	•		
z_{last}	•		
x_{pca}			•
y_{pca}			•
z_{pca}		•	
θ (polar)		•	
ϕ (azimuth)	•		
x_{clu}	•		
y_{clu}	•		
z_{clu}		•	
Tracks			
M_{trk}			•
n_{hits}			•
n_{vtx}	•		
Clusters			
n_{prompt}		•	
E_{clu}			•
T_{clu}		•	
$E_{\text{total,clu}}$			•
$Q^2_{\pi\pi}$		•	
Trgtype	•		

Examples of consistent variables

Variables in the transverse plane were generally found to be consistent between data and MC

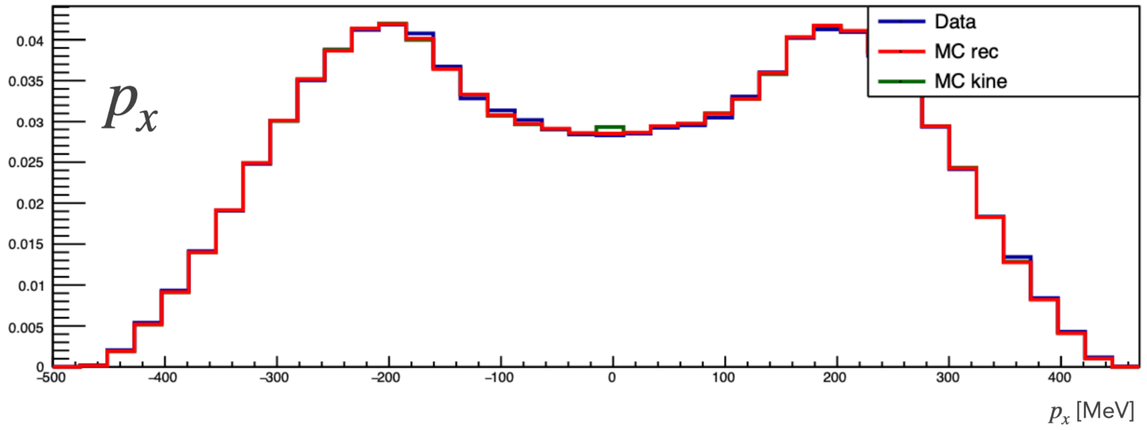

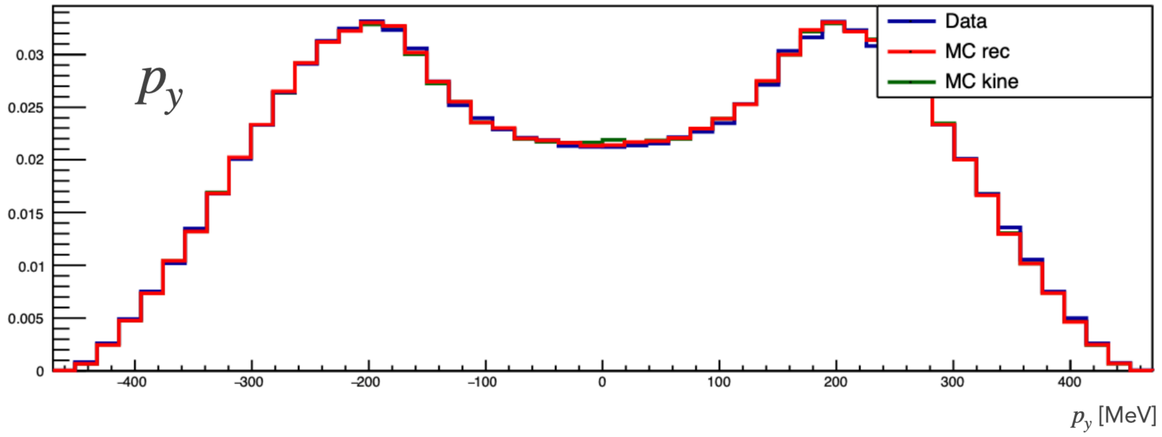

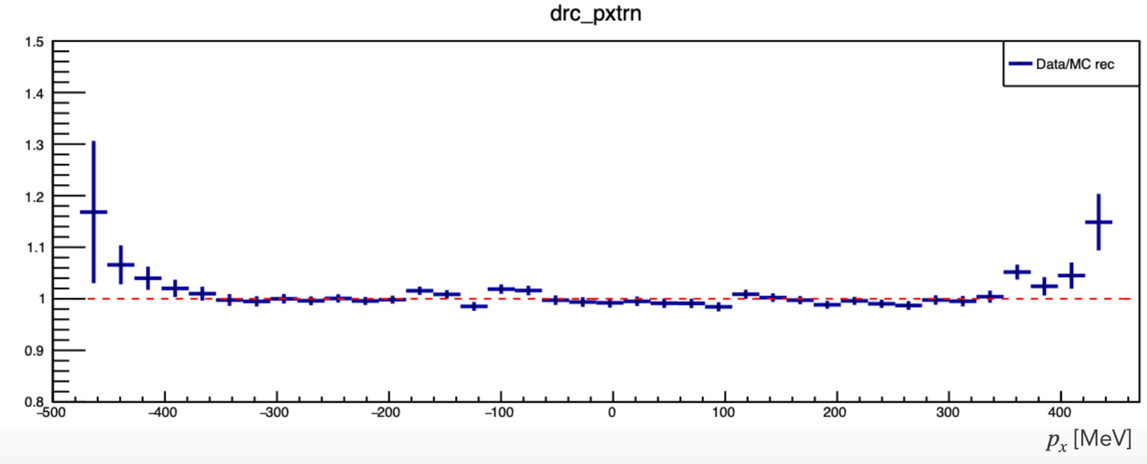

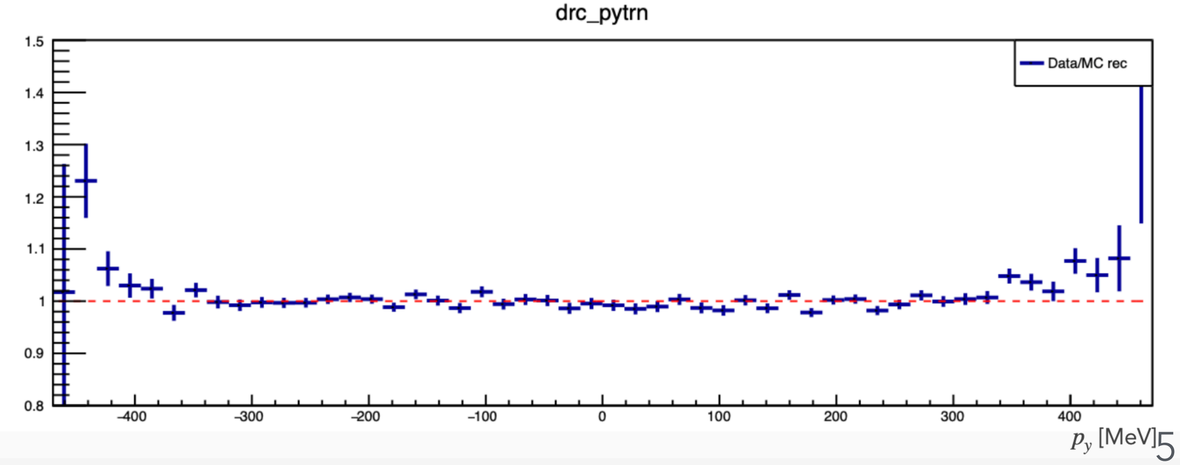

Examples of inconsistent variables

Variables along the z-axis were generally found to be inconsistent

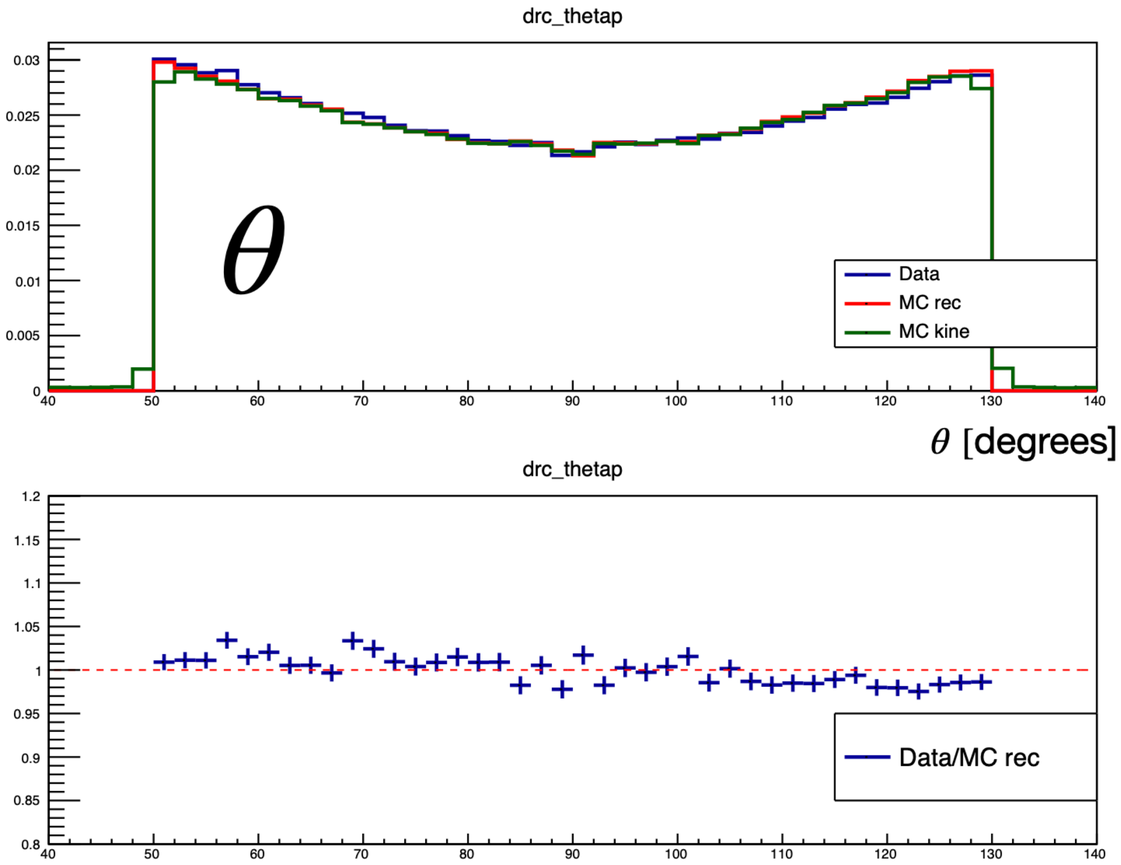

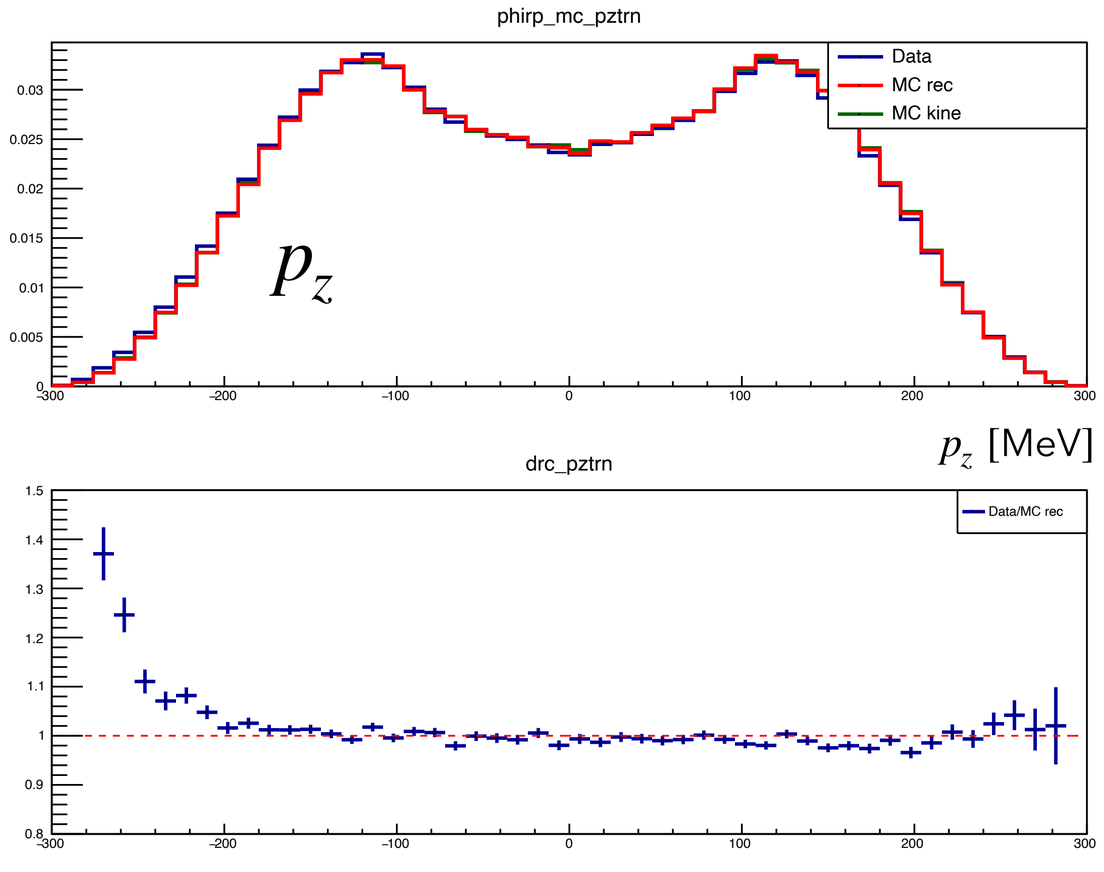

Examples of very inconsistent variables

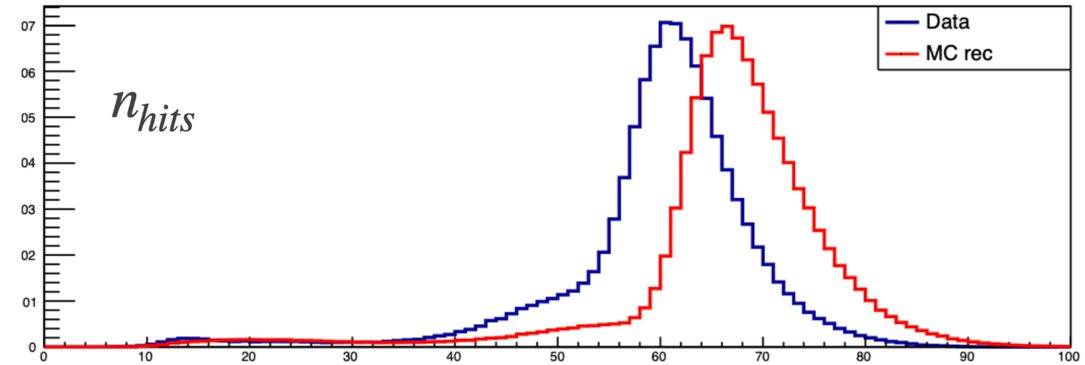

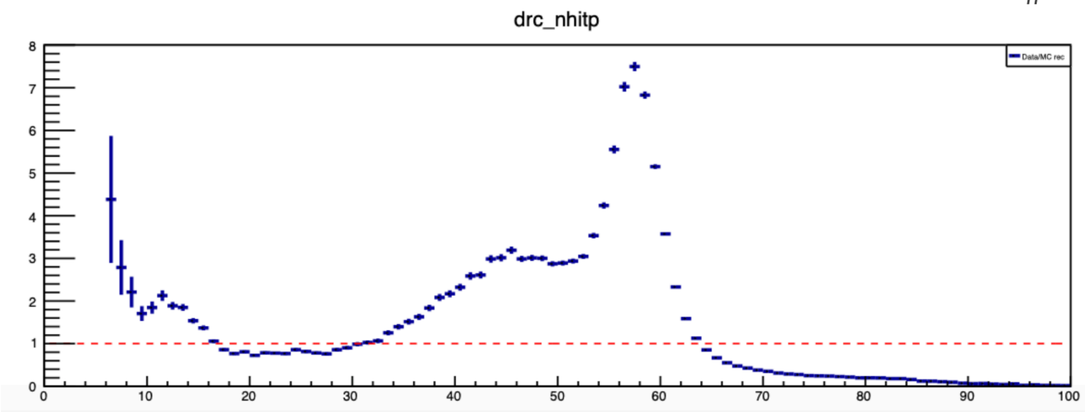

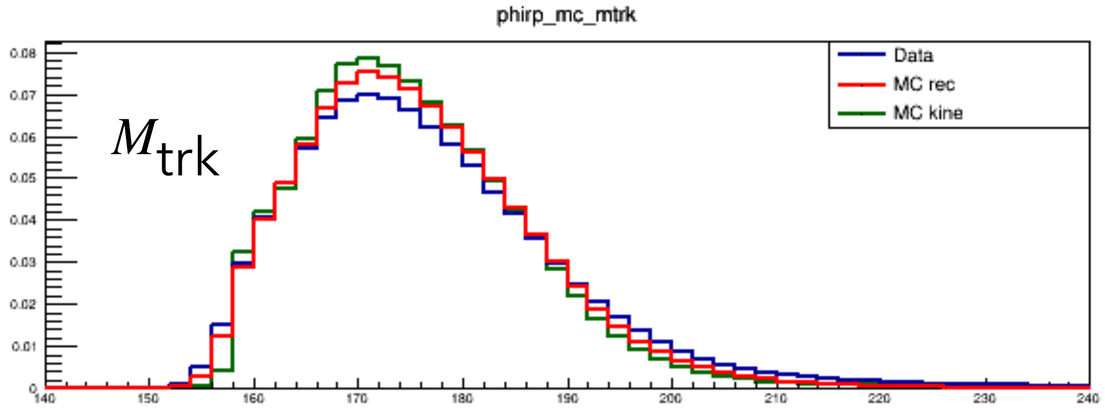

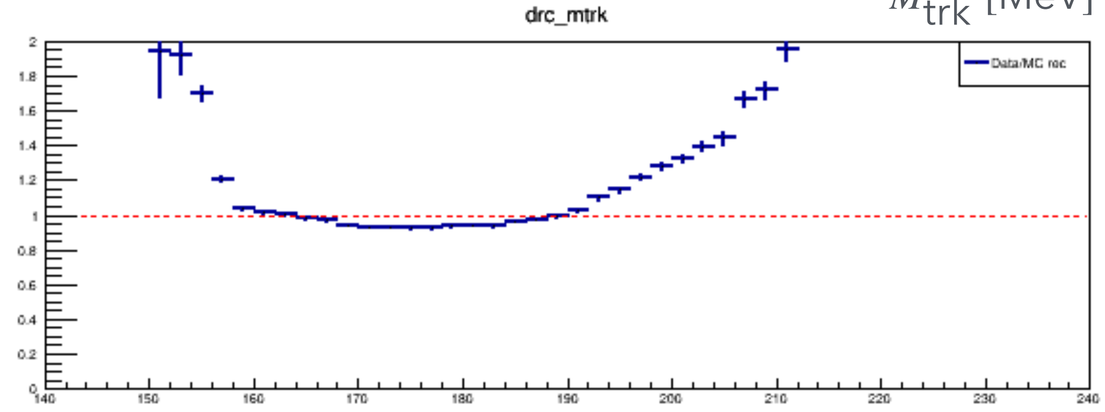

$$\left(\sqrt{s}-\sqrt{|p_+|^2+M_{\mathrm{trk}}^2}-\sqrt{|p_-|^2+M_{\mathrm{trk}}^2}\right)^2-(p_++p_-)^2=0$$

Discrepancy between positive and negative tracks

Discrepancies were found between positive and negative tracks in the data, but <u>not</u> in MC

Again found in variables calculated along the z-axis

Discrepancies also found in previous analyses in collinear $\pi^+\pi^-$ and $\mu^+\mu^-$ events

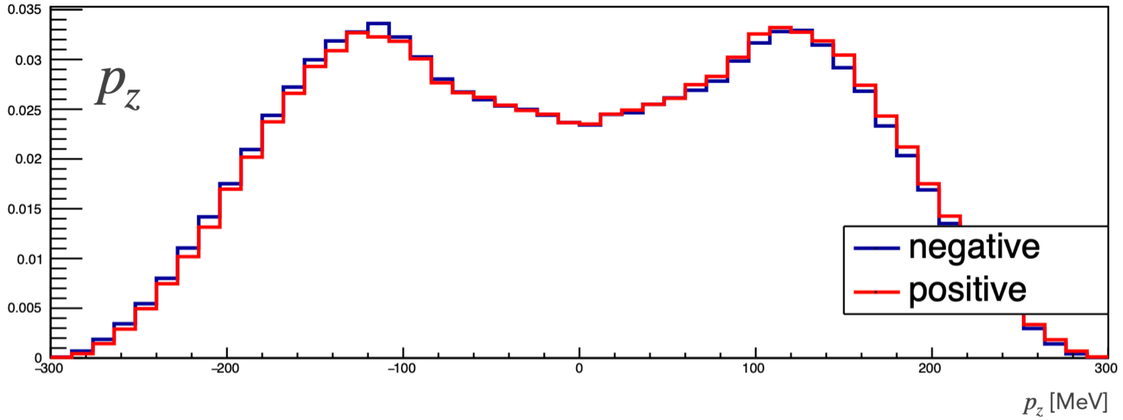

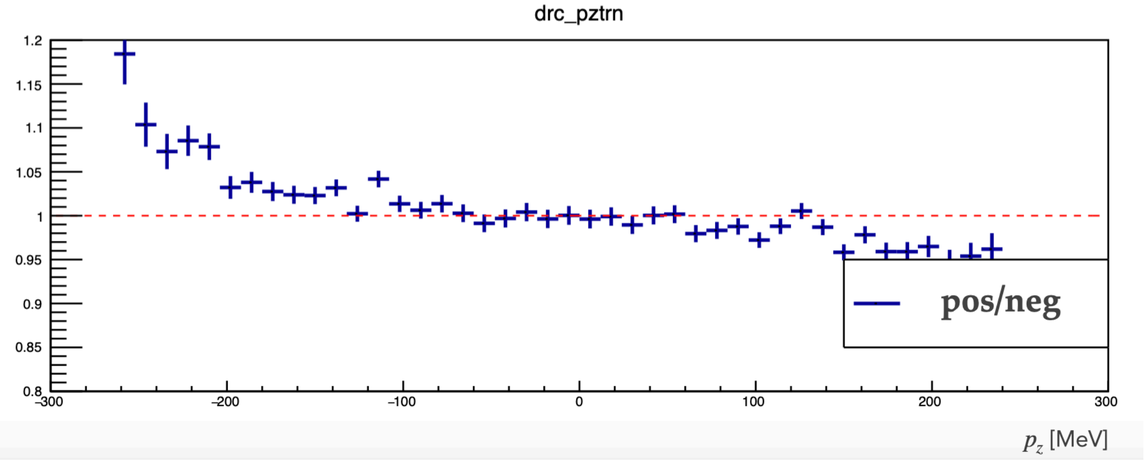

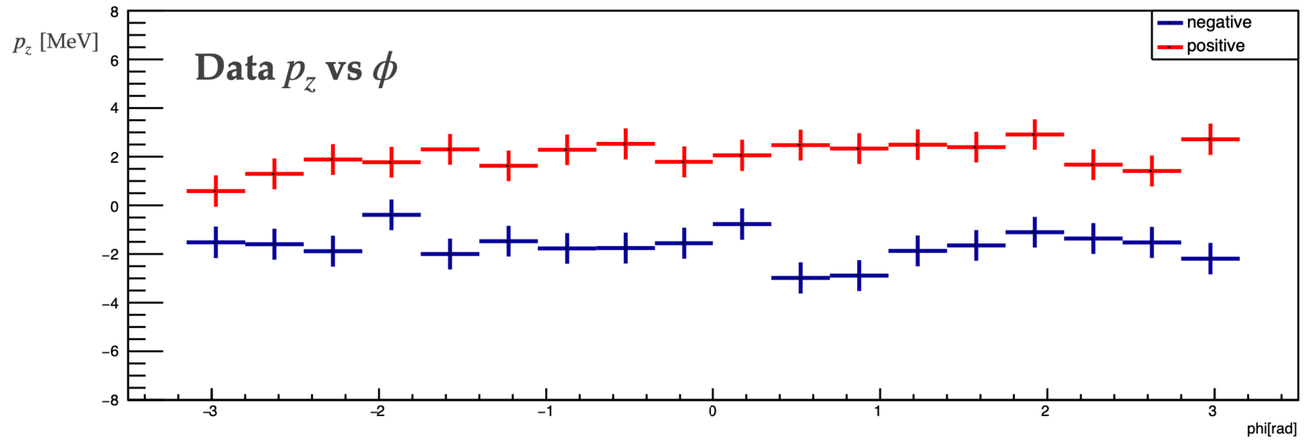

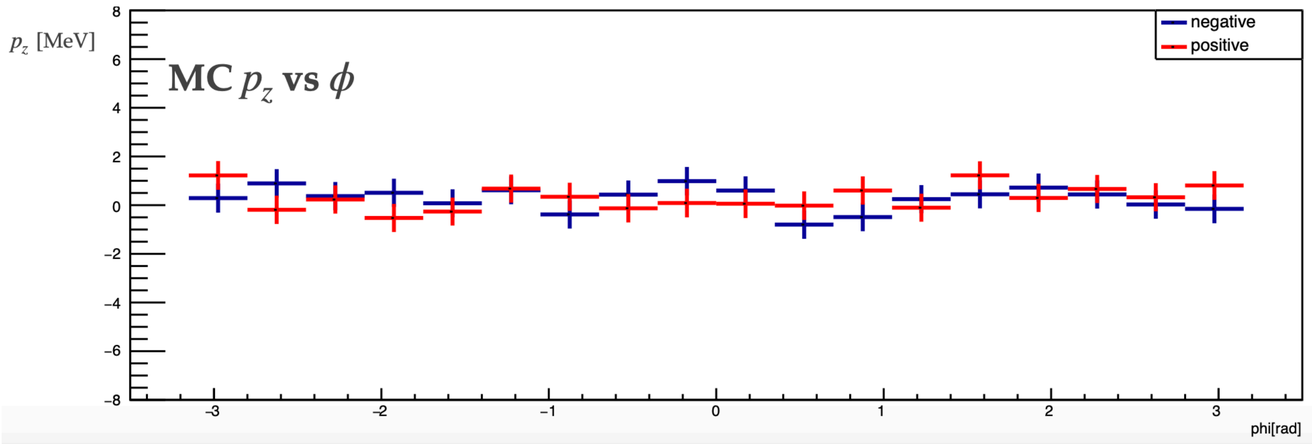

Conclusion

- Blinding code ready to be implemented as needed
- Discrepancies found between data and MC
- Discrepancies found between positive and negative tracks in data but not in MC
- Source of the discrepancies are yet to be determined and will be the focus of future investigation

LEVERHULME TRUST

UNIVERSITY OF LIVERPOOL

MUonE : a novel way to measure the hadronic contribution to the muon g-2

Giorgia Cacciola

21/06/2024

The anomalous magnetic moment of the muon

The anomalous magnetic moment of the muon is a low energy observable

$$a_\mu = \frac{(g_\mu - 2)}{2}$$

The standard model calculation :

$$a_\mu^{SM} = a_\mu^{QED} + a_\mu^{EW} + a_\mu^{HAD}$$

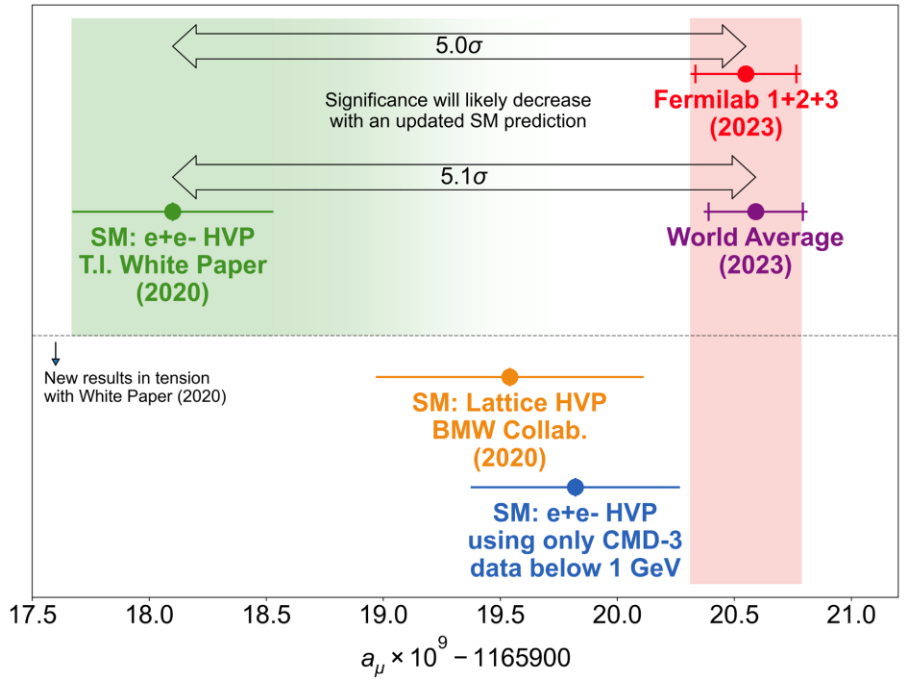

The hadronic contribution has the largest uncertainty:

$$a_\mu^{HAD} = a_\mu^{HLO} + a_\mu^{HVP,NLO} + a_\mu^{HVP,NNLO} + a_\mu^{HLbL}$$

There is a long-standing discrepancy between experimental measurements and theoretical predictions of the anomalous magnetic moment of the muon.

The aim of MUonE

The aim of the MUonE experiment is to measure a_μ^{HLO} independently of other experiments by using accurate measurements of $\mu - e$ elastic scattering on a low z target. The goal is to have a statistical uncertainty of 0.3% and a similar systematic uncertainty.

$$a_\mu^{HLO} = \frac{\alpha}{\pi}\int_0^1 dx(1-x)\Delta\alpha_{had}[t(x)]$$

$$t(x) = \frac{x^2 m_\mu^2}{x-1} < 0$$

The measurement of $\Delta\alpha_{had}$ can be obtained from the shape of the differential cross section of the $\mu - e$ elastic scattering.

The plot of the integrand is a smooth function this means that the calculation of the integral is simplified in the space-like region.

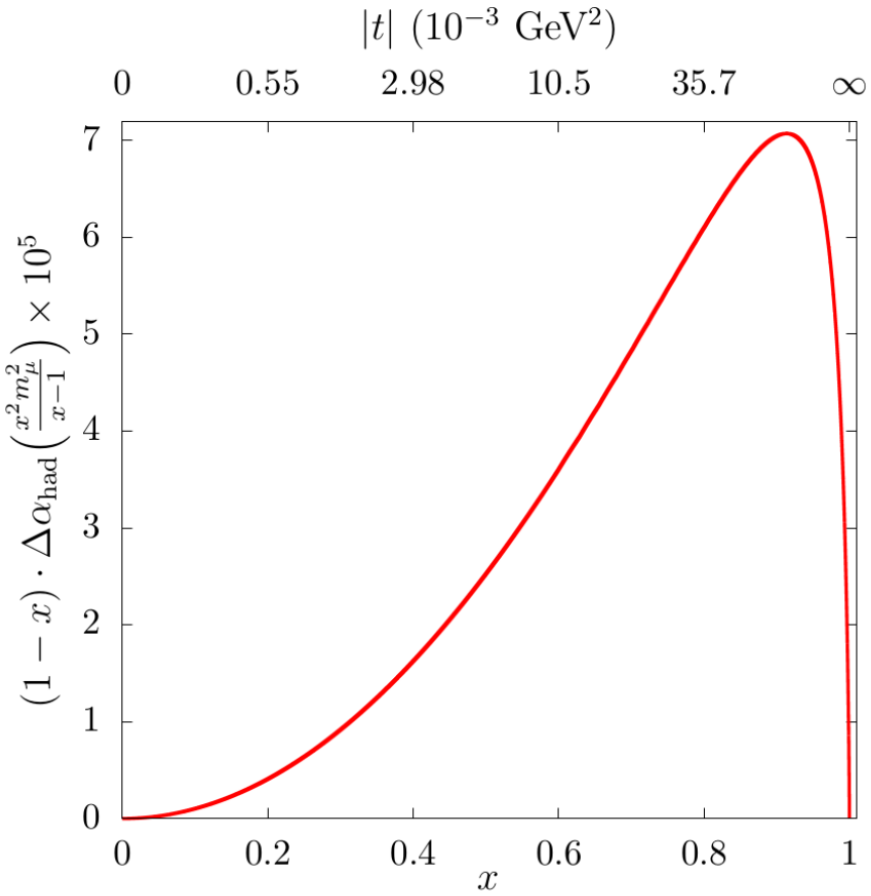

The MUonE experiment will have access to 88% of the integrand and the rest will be extrapolated.

$\mu - e$ elastic scattering

$$\Delta\alpha(t) = \Delta\alpha_{\mathrm{lep}}(t) + \Delta\alpha_{\mathrm{had}}(t) + \Delta\alpha_{\mathrm{top}}(t)$$

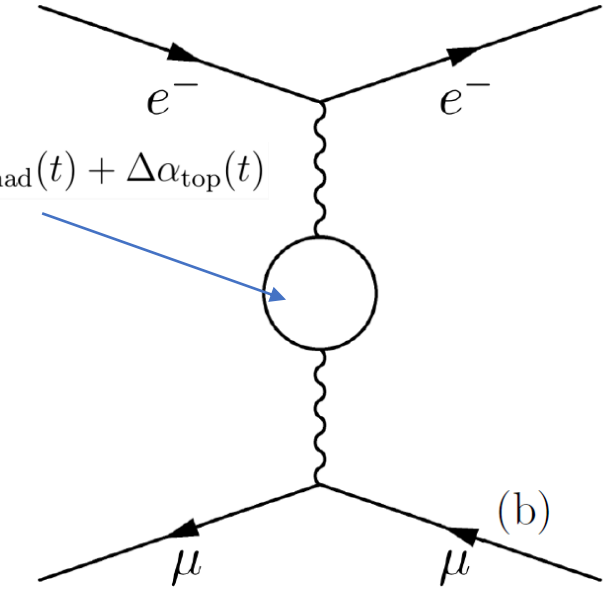

An advantage of this elastic process is its simple kinematics.

The correlation of the electron and muon scattering angles enables the rejection of a significant fraction of the background events.

$$\sin(\theta_\mu) = \sin(\theta_e)\sqrt{\frac{E_e^2(\theta_e) - m_e^2}{[E_\mu + m_e - E_e(\theta_e)]^2 - m_\mu^2}}$$

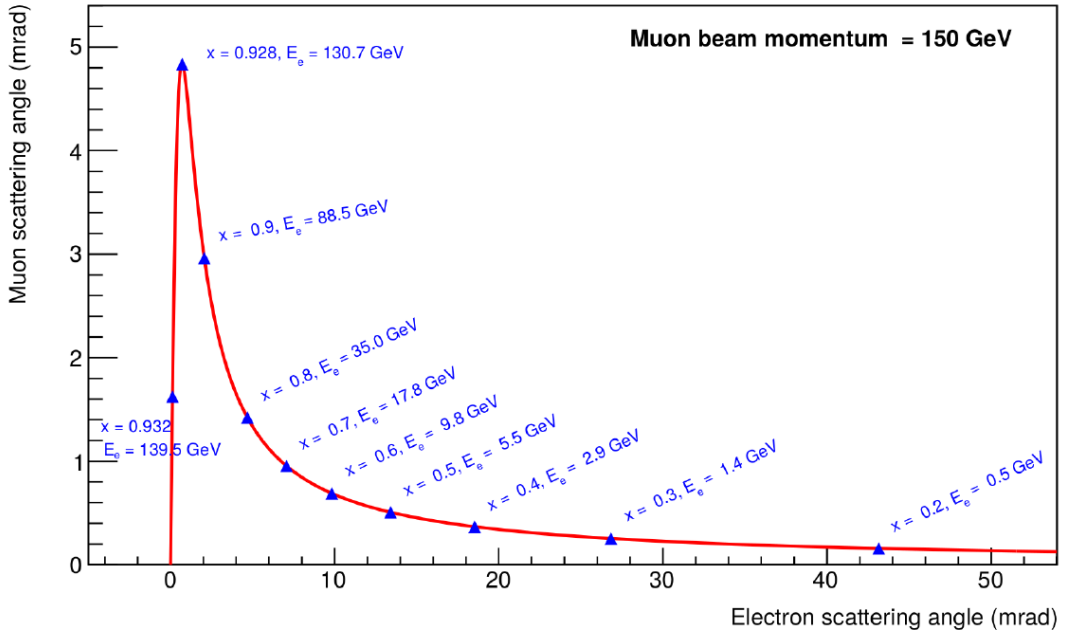

Experimental Setup

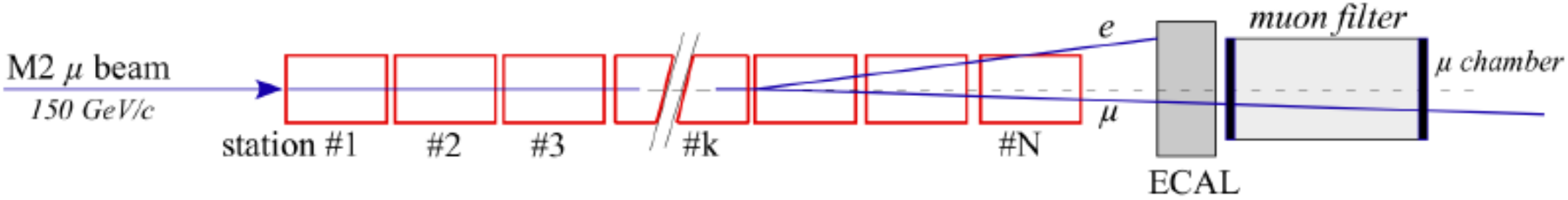

- The MUonE experiment has a modular structure, it will be made up of 40 identical station that all behave as independent detectors.
- The location for the experiment is the M2 muon beam at CERN that provides 160 GeV muons.
- Before the stations there is the beam momentum station , this gives information on the momentum of the muons that are coming from the beam.
- Downstream of the stations is an electromagnetic calorimeter and along side the muon filter these are used for particle identification .

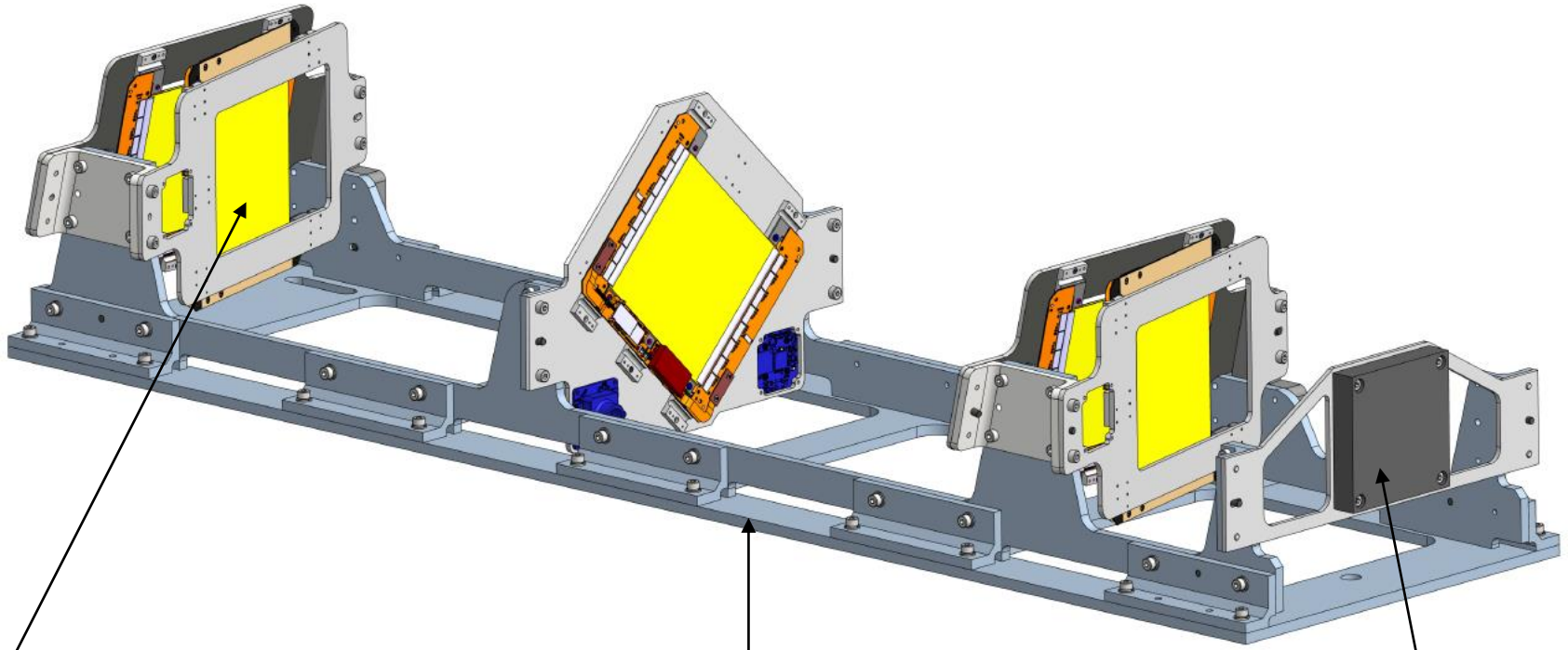

Each MUonE station has 3 pairs of 2S modules, these are silicon strip sensors that were developed for the phase 2 upgrade of CMS .

A MUonE station has a support structure that is approximately 1m in length, the current material being used is Invar.
Invar is a material that is made of 64% iron and 36% nickel.

Each station has an individual target of carbon that is 2 cm thick.

Carbon-Fibre Frames

The aim of this study : to find a material that would be able to replace invar as the material for the support structure of the MUonE stations.

- Invar has a low CTE of 1.2ppm/K
- However, it is difficult to machine as well as being expensive and heavy.

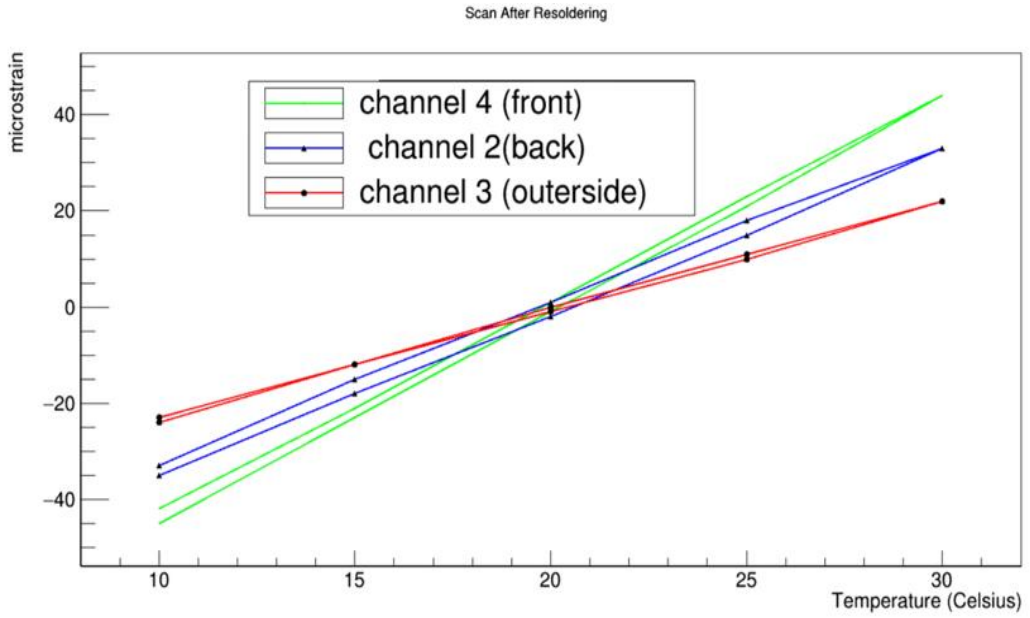

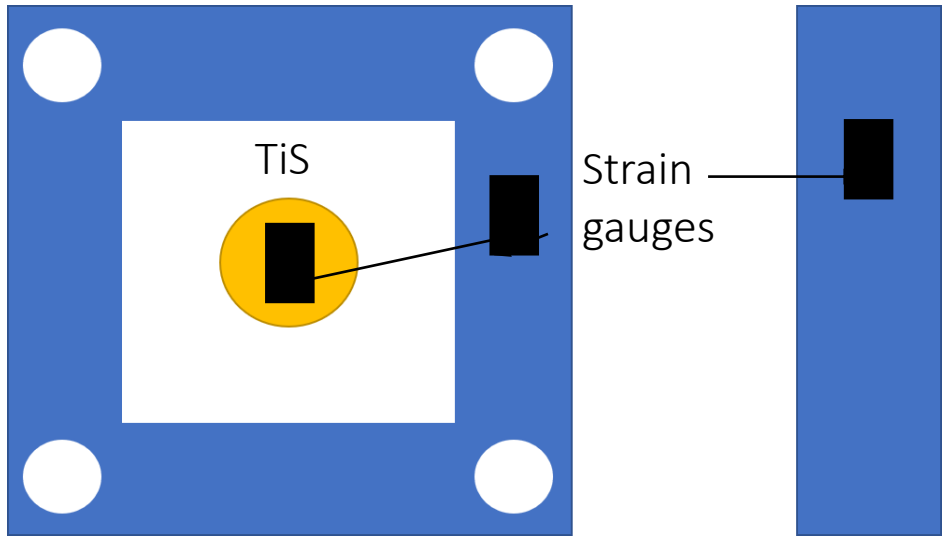

Front view of carbon fibre frame

Side view of carbon fibre frame

- 3 strain gauges were attached to the carbon fibre frame and one was attached to a sample of Titanium silicate.
- Measurements of the strain were taken in 5 degree intervals.
- From this we can determine the CTE as well as observe any bending
- The result here was of 3ppm/K.
- The next material that is currently being looked at is M55J which is a carbon-fibre and cyanate ester composite.

Alignment

The aim of the alignment is to align the position and orientation of each module in each tracking station.
The process is to align the measurement direction and the rotation around the beam axis for each module. This is done by introducing alignment parameters and is carried out through an iterative process.
The two plots of module 0 show the effect of the alignment algorithm.

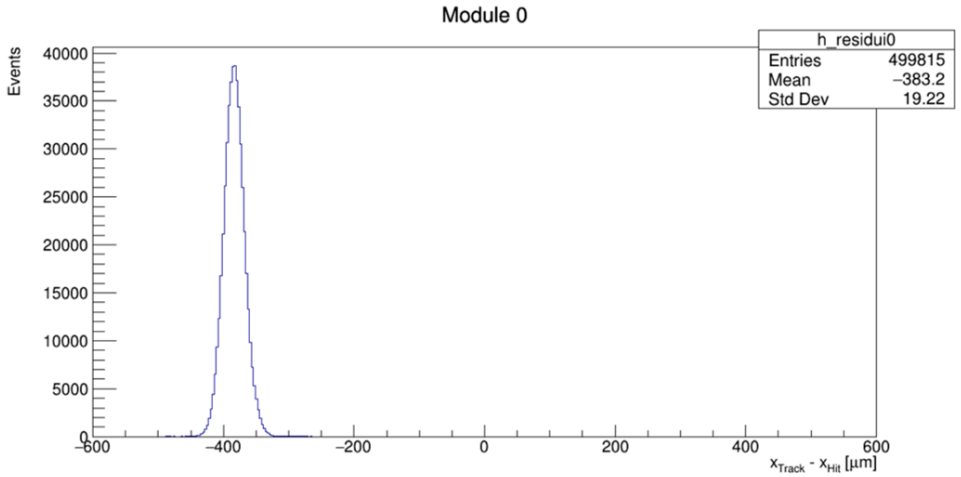

Before alignment

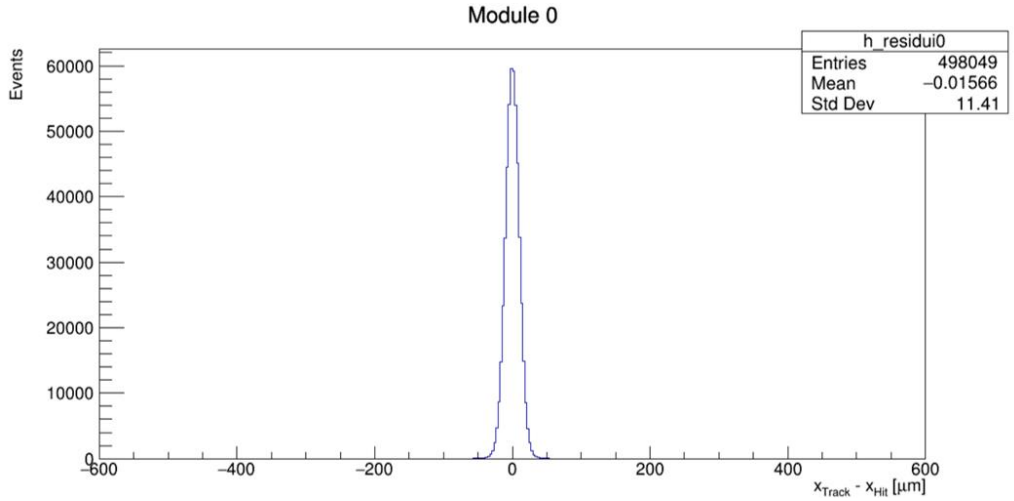

After alignment

Simulations Studies

The aim of this study is to determine the optimal pitch and thickness for a future silicon strip sensor.

- The first set of simulations show how much charge is deposited into the silicon strips of a sensor with different silicon thicknesses.
- The second set of simulation shows the charge deposited with varying strip pitches for sensors of 320 micron thickness
- The plots shown represent sensors that are perpendicular to a 160 GeV muon beam.

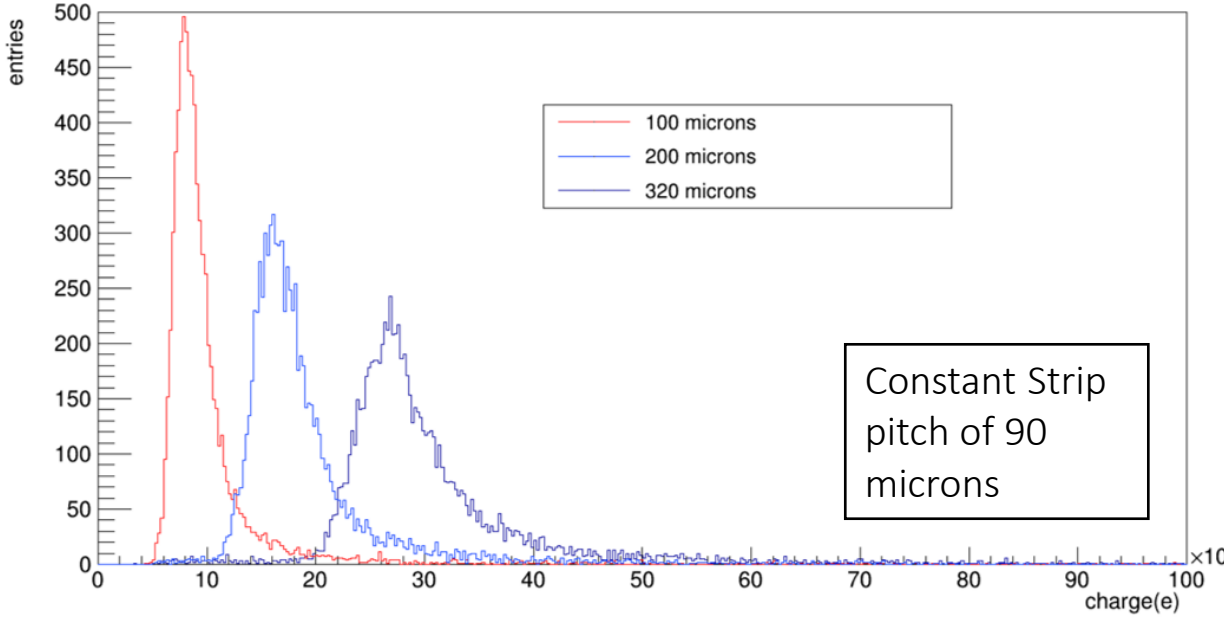

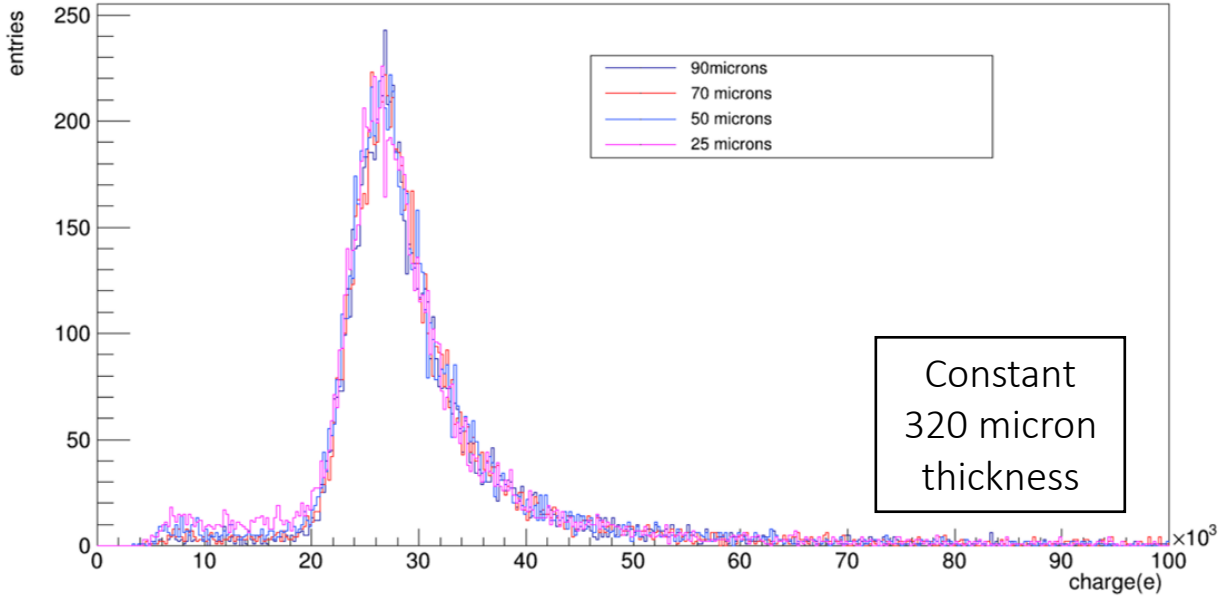

Future plans

MUonE has submitted a proposal for a first run with a small scale version of the final apparatus in 2025.
One of the main aims of this test run would be to get a preliminary result of
Δαhad with a 20% statistical uncertainty and a comparable systematic uncertainty.

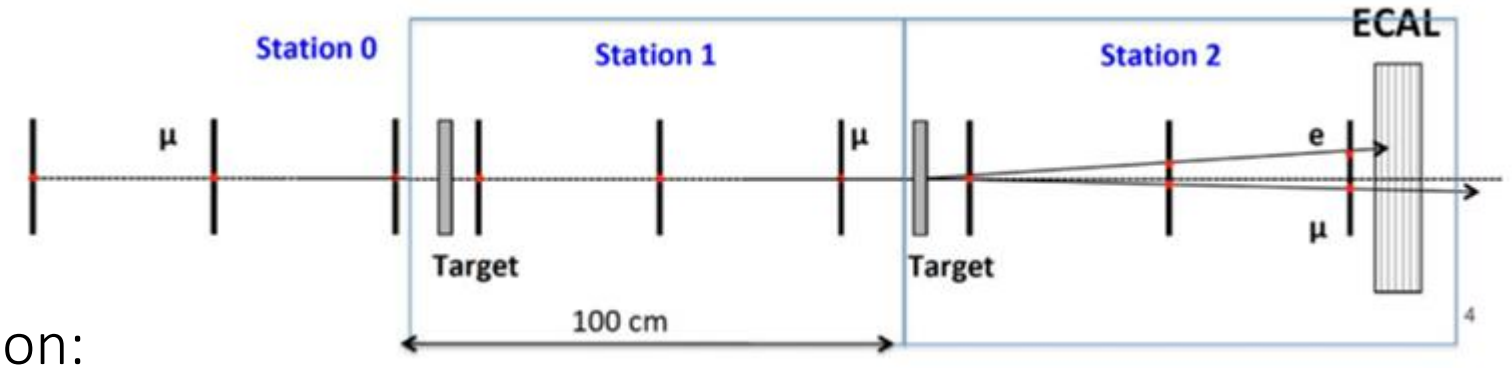

I will be continuing to work on:

- the carbon fibre structure studies
- continuing alignment studies
- will be making further contributions to the data analysis, through the simulation tuning of the intrinsic resolution.

Thank you for listening